MASTERARBEIT | MASTER'S THESIS

Titel | Title

Effect of endocrine disruptors on cell morphology: focus on tight junction

verfasst von | submitted by

Joshua Lukas Rieger B.Sc.

angestrebter akademischer Grad | in partial fulfilment of the requirements for the degree of

Master of Science (MSc)

Wien | Vienna, 2025

Studienkennzahl lt. Studienblatt | Degree programme code as it appears on the student record sheet:	UA 066 659
Studienrichtung lt. Studienblatt | Degree programme as it appears on the student record sheet:	Masterstudium Lebensmittelchemie
Betreut von | Supervisor:	Ass.-Prof. Dott. ric. Giorgia Del Favero Privatdoz.

Abstract English

Endocrine active chemicals (EACs) and endocrine disruptive chemicals (EDCs) are substance groups that interfere with hormone signaling and binding pathways. Exposure to the latter results in a negative impact on health, while first ensures no long-lasting effect on physiological homeostasis. EACs and EDCs are omnipresent in the environment and occur in an abundance of chemical groups. This work investigates the impact of selected EDCs including mycoestrogens alternariol (AOH), plasticizers bisphenol A (BPA), bisphenol F (BPF), diisodecyl phthalate (DiDP), and EACs, including prescription drug and environmental contaminant levonorgestrel (LNG) and the endogenous hormone 17-beta-estradiol (E2) on the morphology of tight junctions and barrier integrity of human gastrointestinal epithelial cells. Due to the recently described effect of AOH and BPA on adhesion molecules like integrins, it would be expected that EDCs could also alter tight junction proteins. The specific focus is on morphology of scaffolding and tight junction protein Zonula occludens 1 (ZO-1) and tight junction protein Claudin 4 (CLDN4). We applied the EDCs and EACs on a Caco-2 and HT29-MTX-E12 coculture, which mimics the intestinal tract. This coculture produces mucus, forms previously mentioned tight junctions and villi, thereby simulating the gastrointestinal barrier. Through reduction of mucus a multitude of conditions can be mimicked such as Irritable Bowel Syndrome. After proven absence of cytotoxicity for the concentration range of chosen EDCs, verified by CellTiter-Blue® cell viability assay, several other experiments were performed. This includes first a characterization of the coculture, following the application of different nanoparticles (NPs) and immunofluorescence staining of tight junction proteins. Additionally, measurements of transepithelial electrical resistance (TEER) and paracellular permeability via Lucifer yellow assays were performed to support our hypothesis. Treatment of BPA and BPF altered tight junction morphology, which led to increased permeability and a decreased barrier function. AOH and E2 likewise induced significant changes in tight junction morphology. DiDP and LNG exhibited less distinct but detectable effects on tight junctions, suggesting an alternate interaction with tight junctions compared to the other substances. This work highlights the need for assessment of the potential health risks associated with exposure to orally derived EDCs. Through this knowledge we could gain a deeper understanding of the toxicological impact of EDCs on intestinal barrier function.

Abstract Deutsch

Endokrin aktive Chemikalien (EACs) und endokrin disruptive Chemikalien (EDCs) sind Substanzen, welche Hormon-Signalwege und -Bindungssellen stören. Jedoch verursachen nur EDCs damit einen negativen Einfluss auf die Gesundheit. EDCs und EACs sind in der Umwelt allgegenwärtig und kommen in heterogen verteilten chemischen Gruppen vor. Diese Masterarbeit untersucht den Einfluss von EDCs, darunter Mykotoxin Alternariol (AOH), Weichmacher, Bisphenol A (BPA), Bisphenol F (BPF) und Diisodecyl Phthalate (DiDP), und EACs, darunter das Verhütungsmedikament Levonorgestrel (LNG) und das endogene Hormon 17-beta-Östradiol, auf die Barriere Integrität von menschlichen Magen-Darm-Epithel Zellen, mit einem gewissen Fokus auf die Morphologie der Tight Junctions (TJ). Kürzlich wurde in der Literatur aufgedeckt, dass AOH und BPA Adhäsionsmoleküle, wie Integrine, beeinflussen können. Um diese These weiter zu unterstützen haben wir vorgeschlagen, dass andere endokrine aktive Subtanzen diese und ähnlich Strukturen, wie TJs, auch beeinflussen können. In dieser Arbeit war der spezielle Fokus auf den TJ-Proteinen Claudin 4 (CLDN4) und Zonula occludens 1 (ZO-1). Dabei haben wir EDCs und EACs mit einer Caco-2 und HT29-MTX-E12 Kokultur inkubiert. Diese Kokultur ahmt den Darmtrakt nach, indem sie Schleim produziert und TJs und Zotten ausbildet, und damit die Magen-Darm-Barriere simuliert. Wir simulierten Erkrankungen, wie das Reizdarmsyndrom durch Reduzierung von Schleim. Erst wurden nicht-zytotoxische Konzentrationsbereiche, durch den CellTiter-Blue®-Zellviabilitätsassay, festgestellt. Danach wurde in mehrere Experimente die Kokultur charakterisiert, zum Beispiel durch die Anwendung von Nanopartikeln (NP) und Immunofloureszenzfärbung von TJ-Proteinen. Des Weiteren wurden auch Transepithelische elektrische Widerstandsmessungen (TEER) und die Zell-Permeabilität, durch den Lucifer-yellow assay, gemessen. Dabei veränderte die Behandlung mit BPA und BPF die Morphologie der TJs, dies führte zu einer erhöhten Permeabilität und einer verminderten Barrierefunktion. AOH und E2 haben auch signifikante Veränderungen der TJ Morphologie verursacht. Jedoch hatten DiDP und LNG den geringsten Einfluss auf die Morphologie von TJs. Diese Arbeit unterstreicht die Notwendigkeit einer Bewertung der potenziellen Gesundheitsrisiken, die mit der Exposition gegenüber oral aufgenommenen EDCs verbunden sind. Durch diese Erkenntnisse könnten wir ein tieferes Verständnis der toxikologischen Auswirkungen von EDCs auf die Darmbarrierefunktion gewinnen.

Acknowledgements

Zuerst will ich Prof. Freddy Kleitz und Dr. Claudia Iriarte-Mesa für die Entwicklung, Synthese und das Teilen der Nanopartikel und Prof. Doris Marko, dass ich die Einrichtungen und Ressourcen des Departments Lebensmittelchemie und -toxikologie verwenden durfte, danken. Zusätzlich will ich der ganzen Arbeitsgruppe danke, dass sie mich immer unterstützt haben und mich eingelernt haben. Zuletzt danke ich meiner Betreuerin Giorgia Del Favero, welche mich immer unterstützt hat und mir diese großartige Chance der Masterarbeit gegeben hat.

.

Abbreviations

AOH: Alternariol

bacNPs: Rod-shaped bacteria-like nanoparticles

bacNPs -CH_3: Methylated rod-shaped bacteria-like nanoparticles

bacNPs -PO_3: Phosphonated rod-shaped bacteria-like nanoparticles

BPA: Bisphenol A

BPF: Bisphenol F

bw: body weight

CLDN 4: Claudin 4

CTB: CellTiter Blue®

DiDP: Diisodecyl phthalate

DMEM: Dulbecco's Modified Eagle Medium

DMSO: Dimethylsulfoxide

EACs: Endocrine active chemicals

EDCs: Endocrine disruptive chemicals

ER: Estrogen receptor

ERα: Estrogen receptor alpha

ERβ: Estrogen receptor beta

E2: 17-beta-Estradiol

FITC: Fluorescein isothiocyanate

FBS: Fetal bovine serum

GFP: Green fluorescent protein

HBSS: Hanks' Balanced Salt Solution

ICE: Integrated Chemical Environment

JAMs: Junctional adhesion molecules

LNG: Levonorgestrel

MAGUKs: Membrane-associated guanylate kinase-like homologues

NAMs: New approach methodologies

NPs: Nanoparticles

PBPK: Physiological based pharmacokinetic

PBS: Phosphate buffered saline

PBS-A: Phosphate buffered saline (variation A)

P/S: Penicillin-Streptomycin

srNPs: Small rod nanoparticles

srNPs -CH_3: Methylated small rod Nanoparticles

srNPs -PO_3: Phosphonated small rod Nanoparticles

TJ: Tight junction

ZO-1: Zonula Occludens 1

Contents

List of figures

1. Introduction

1.1. Endocrine active chemicals

Endocrine active substances (EACs) and Endocrine disruptive chemicals (EDCs) are chemicals that affect receptor binding or hormone synthesis by altering the hormone balance of the endocrine system, however only EDCs impact human health negatively.[1,2] This change in homeostasis can have various severe symptoms, for example reproductive, developmental and sexual behavior dysfunctions.[3] Most EDCs have similar structures to endogenous steroid hormones, 17-beta-estradiol (E2) or androgen, yet this does not necessarily need to be the case. Through structural similarities EDCs tend to mimic the steroid hormones and can therefore elicit non-genomic effects.[4] Another mechanism of action can be their interference with the actions of steroid hormones by agonistic or antagonistic binding to the corresponding receptors.[5] Exposure to EDCs can be dermal, oral or through inhalation. Orally derived EDCs can appear through various groups of chemicals. These groups range from plasticizers, containing for example bisphenol A (BPA), bisphenol F (BPF) and diisodecyl phthalate (DiDP) to substances of natural origin.[5,6] Relevant substances in this context include isoflavones, like genistein, but also mycoestrogens, such as alternariol (AOH) and zearalenone.[7] Other man-made chemicals such as female contraceptive medication, implementing progestins as active components, can obviously act as EACs. One of these contraceptives is the second generation progestin levonorgestrel (LNG), which can be used as emergency or for daily contraceptive use.[5,6]

1.2. Human gastrointestinal epithelial cells

To protect the human body the gastrointestinal tract is layered with a single-cell-thick coating of intestinal epithelium cells, composed of various specialized cells that play multiple unique and essential roles. Their main tasks include nutrient absorption, immune defense and creation and up-keep of the intestinal barrier function. The major types of gastrointestinal epithelial cell types are enterocytes, goblet cells, paneth cells, enteroendocrine cells, stem cells and others.[8,9]

The most frequent gut epithelium cell types are enterocytes, which are responsible for the absorption of nutrients, electrolytes and water. They form a brush border of microvilli on their apical surface, to increase their surface area and make nutrient update more efficient.

Additionally they house important digestive enzymes, which are essential to breakdown most food matrixes.[10,11] Another cell type are Goblet cells, these secrete mucus, forming a layer that lubricates the intestinal surface and acts protectively, shielding it from digestive enzymes and microbial invasion.[8,9] This mucus layer, is primarily composed of mucins such as gel-forming mucin 2.[12] It provides an extra physical protection limiting direct contact between the gut microbiota and epithelial cells. This mucus layer furthermore leads to a reduction of inflammation and helps to sustain barrier integrity.[13] Another important cell type are paneth cells, which are located at the base of the crypts in the small intestine. In these crypts they secrete peptides and proteins that regulate the gut microbiota.[8,9] Enteroendocrine cells are essential for the release of endogenous hormones and peptides to regulate gut motility, mucus secretion, and appetite. In contrast, tuft cells and M cells are involved in the immune system of the gut. They sample antigens and can thereby protect the gut from exogenous microorganisms.[8,9]

The integrity of the intestinal epithelial barrier is maintained by specialized intercellular junctions, particularly tight junctions (TJs), which interconnect epithelial cells at particular positions in the membrane. They also regulate paracellular transport of ions. These functions are also referred as barrier, gate and fence function in literature.[13,14] Disruption of these junctions can lead to increased intestinal permeability, lack of nutrient absorption, triggering of inflammation and contribution to conditions such as inflammatory bowel disease.[13,14] The intestinal epithelium is continuously renewed every three to five days by stem cells located at the base of the crypts, ensuring constant repair, up-keep and adaptation to various challenges.[8] This dynamic renewal system is essential for keeping up a balanced gut, especially given the constant exposure to dietary dangers, microorganisms, and potentially harmful contaminants in the gut lumen.[13,14]

1.3. Aim of this study

The gastrointestinal barrier is a key protective system in the human body. Gastrointestinal epithelial cells are in constant contact with various amounts of exogenous substances, while most do not harm them, some can potentially pose a threat to gut homeostasis. This consistent stress on the cells, due constant exposure to not only dietary components and microbial metabolites but also to environmental contaminants, is a pivotal subject in the field of toxicology. Many different substances can come into contact with the epithelium. One of these groups are EDCs, which we centered this work on, based on previous research. Firstly, the

findings of Dr. Crudo and colleagues 2022[15], they found that human feces have estrogen-like activity after anaerobic digestion, i.e. digestion as in the intestine. This results in constant exposure to estrogen-like active substances in the gut epithelium. Secondly, Groestlinger J *et al.* 2022[16] demonstrated mycotoxin with described endocrine disruptive potential like AOH have an impact on the structure of colon epithelial cells. Furthermore, Del Favero *et al.* 2024[17] elucidated another aspect of the molecular mechanism of xenoestrogens. In this work it was observed that short term exposure to mycoestrogens impacts cell morphology and motility. They suggested that xenoestrogens could induce changes in the cell cytoskeleton and act as binding partners for integrins, which is an essential adhesion molecule. These findings lead us to believe that not only mycoestrogens, but that potentially other EDCs or EACs can have an impact on the morphology of epithelial cells. Through this we decided to investigate this phenomenon more in depth, focusing on a variety of EDCs and EACs from different origins. We hypothesize that EDCs and EACs could have a broader impact on adhesion molecules as described until now and with this impact TJs in expression and in their morphology, thereby impacting barrier function on different levels. Elaborating on this, another aim of this thesis was the further extension of the technical tools available to evaluate barrier integrity at the nanoscale, to accompany observation on cell morphology with functional performance. Building on the knowledge of Bergen *et al*. 2025[18] namely that nanoparticle size impacts the penetration depth and the intercellular distance of cells after incubation, while Iriarte-Mesa *et al.* 2024[19] established the impact of functionalization on the earlier mentioned parameters. Our goal was to test, already developed nano-scaled materials in different sizes and in functionalization states, on our coculture model as sensors of the intestinal barrier integrity. In summary, the goal of this study was to investigate the impact of selected endocrine-disrupting compounds on the morphology of human epithelial cells, with a specific focus on the organization and expression of the TJs proteins ZO-1 and CLDN4. Additionally, we wanted to test the performance of tools of evaluation on barrier integrity at the nanoscale.

2. Theoretical background

2.1. Substances of use

2.1.1. Alternariol

Alternariol is a mycotoxin produced by mold of the genus *Alternaria alternata*. These fungi are common contaminants in a wide variety of food products, including grains, fruits, vegetables, tomato products, nuts and oilseeds. Main exposure to alternariol is dietary, with fruits, tomatoes, oilseeds and cereal-based foods in their fresh and processed forms being the major sources of exposure.[20] AOH is most known for its strand breaking effects and mutagenicity. *In vitro* experiments have shown that AOH induces DNA strand breaks in multiple human cell lines.[21–23] AOH also exhibits a concentration dependent increase of mutagenicity.[22] Biomonitoring studies have detected AOH metabolites in urine of the general population in western countries, indicating widespread exposure. The estimated daily intakes across dietary surveys reach up to 1.9 to 39 ng/kg bw per day.[24] These frequently exceed the threshold of toxicological, of 2,5 ng/kg bw/day, concern set by regulatory agencies, highlighting its relevance for public health risk assessment.[25–27]

As a result of AOH being in the spotlight of toxicologist for a while, discussion has arisen if it still should be considered an “emerging” mycotoxin, though it still belongs in the definition, with it being frequently detected in food and feed but lacks comprehensive regulatory limits due to insufficient toxicological data.[28,29] AOH is notable for its genotoxic and mutagenic properties, as well as its ability to interfere with cell cycle regulation, DNA repair, and induce oxidative stress and autophagy.[30] More relevant to this thesis is the lesser known effect of alternariol exhibiting an endocrine disrupting activity. *In vitro* studies have demonstrated that AOH can act as a weak estrogen agonist, binding preferentially to estrogen receptor β (ERβ), though with much lower affinity than the endogenous hormone 17-beta-estradiol.[31,32] Another suggested interaction was the possibility of AOH being a possible antagonist effect on the androgen receptor.[33] To further support this data from literature we used the online simulation tool SwissTargetPrediction.[34] Here an algorithm predicts potential binding sites of AOH in the human body, based on the similarity principle, through reverse screening.[34–36] The results can be seen in figure 1, where the estrogen receptor alpha (ERα) and ERβ, were predicted to have the highest affinity of binding for AOH. The relatively low binding probability can be attributed to the low binding affinity of AOH compared to E2. Higher concentrations of AOH have shown to increase E2 and progesterone production. The mycoestrogen can also modulate the

transcriptional activity of various nuclear hormone receptors, including those for estrogens and progestogens. This endocrine activity in the human can be explained by its similar structure to natural hormone E2, as AOH is also a diphenolic compound.[27,31]

Another aspect is the interaction of AOH with the gastrointestinal barrier function. AOH can activate the nuclear translocation of the aryl hydrocarbon receptor, which regulates the homeostasis of cell integrity and can thereby impact intestinal barrier function.[37] Additionally, AOH can decreased zonula occludens 1 (ZO-1) expression and thereby increase the permeability of a monolayer.[16,38]

A

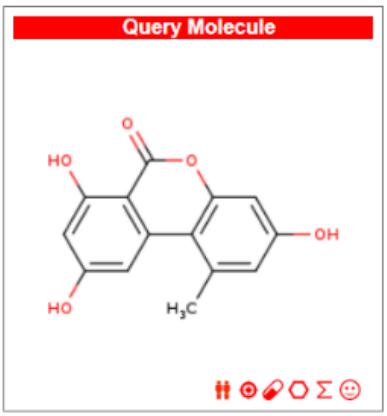

B

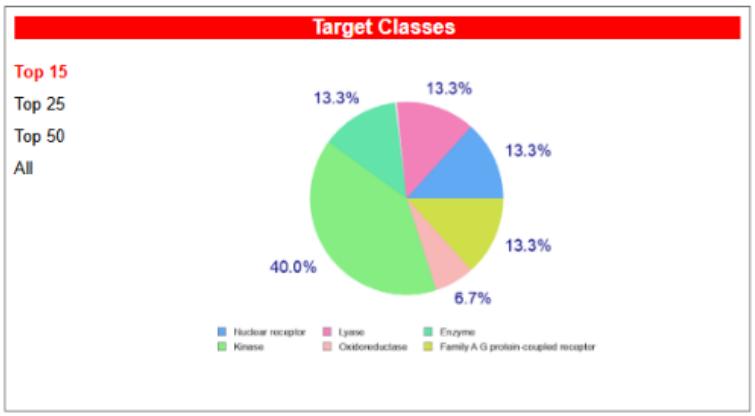

C

Target	Common name	Uniprot ID	ChEMBL ID	Target Class	Probability*	Known actives (3D/2D)
Estrogen receptor alpha	ESR1	P03372	CHEMBL206	Nuclear receptor		75 / 47
Estrogen receptor beta	ESR2	Q92731	CHEMBL242	Nuclear receptor		73 / 65
Carbonic anhydrase XII	CA12	O43570	CHEMBL3242	Lyase		18 / 60
Carbonic anhydrase IX	CA9	Q16790	CHEMBL3594	Lyase		20 / 72
Estradiol 17-beta-dehydrogenase 3	HSD17B3	P37058	CHEMBL4234	Enzyme		6 / 29
Serine/threonine-protein kinase PIM1	PIM1	P11309	CHEMBL2147	Kinase		3 / 5

Figure 1: (A) Structure of Alternariol (B) Pie chart of prediction divided into color coded subgroups (C) Prediction of targets with common name, ID´s and probability of binding. Smiles: "CC1=CC(=CC2=C1C3=C(C(=CC(=C3)O)O)C(=O)O2)O".[39] Created with SwissTargetPrediction.[34–36]

2.1.2. Bisphenol A

Bisphenol A is a synthetic chemical in use primarily as a plasticizer. There it is used as an additive during manufacturing of polycarbonates and epoxy resins, to ensure more flexible properties. These materials are found in a wide range of consumer products, including food contact materials and beverage coatings and containers, for example water bottles, baby bottles, the internal coatings of metal cans, and even in the linings of drinking water pipes. Due to its extensive use in industry and its environmental persistence, BPA is considered an omnipresent contaminant.[40] Many regulatory actions have been taken throughout the years to regulate BPA. Very recently, additional regulatory actions have been taken by the EU, banning Bisphenol A in certain food contact materials in December 2024.[41]

The primary source of BPA exposure for the general population is dietary intake. As it is used in food contact materials and thereby can migrate into food, especially when these items are heated, for example in a microwave.[42] Other lower exposure risks include contaminated drinking water, dermal absorption from handling thermal paper receipts and other consumer products.[40,43] Human biomonitoring studies demonstrated that the vast majority of people, have detectable levels of BPA in their bodies.[42] The EFSA suggested a dietary exposure to BPA at 1,5 µg/kg bw per day for the average adult, for 18 month old children they demonstrate an even higher level at 5,3 µg/kg bw per day.[44]

Due to BPAs widespread exposure many risks have been well characterized. The main toxicological endpoint of BPA is its function as an endocrine disruptor. The contaminant can bind to and activate or antagonize several nuclear hormone receptors, including estrogen receptors (ERα, ERβ), estrogen-related receptors, androgen receptors, and peroxisome proliferator-activated receptors.[45] To confirm with previously published data we evaluated BPA by using the online tool SwissTargetPrediction. The results of this screening can be seen in figure 2. There the predicted binding sites with the highest affinity were the earlier mentioned ERα and ERβ and the androgen receptor. Through all this data multiple symptoms were established from exposure to BPA, these can range from alteration in gene expression to reproductive and developmental disorders, metabolic disturbances, immune system modulation, and increased risk of certain cancers. [46] Particularly sensitive periods for all EDCs include fetal and early postnatal development. Where natural hormones play an essential role for growth and organ formation. BPA exposure can disrupt these by interfering with hormone-regulated pathways.[42,40,43]

An additional aspect of BPA is its effect on the intestinal barrier function. Occurrence of BPA in the gut is not uncommon, due to its main exposure-pathway being as a food contaminant. In colonic tissue BPA can down regulate expression of claudin-1, ZO-1 and occludin.[47] This downregulation of key tight junction protein leads to inhibition of barrier function and increased intestinal permeability. *In vivo* studies also found that dietary concentrations of BPA can induce intestinal injuries.[48]

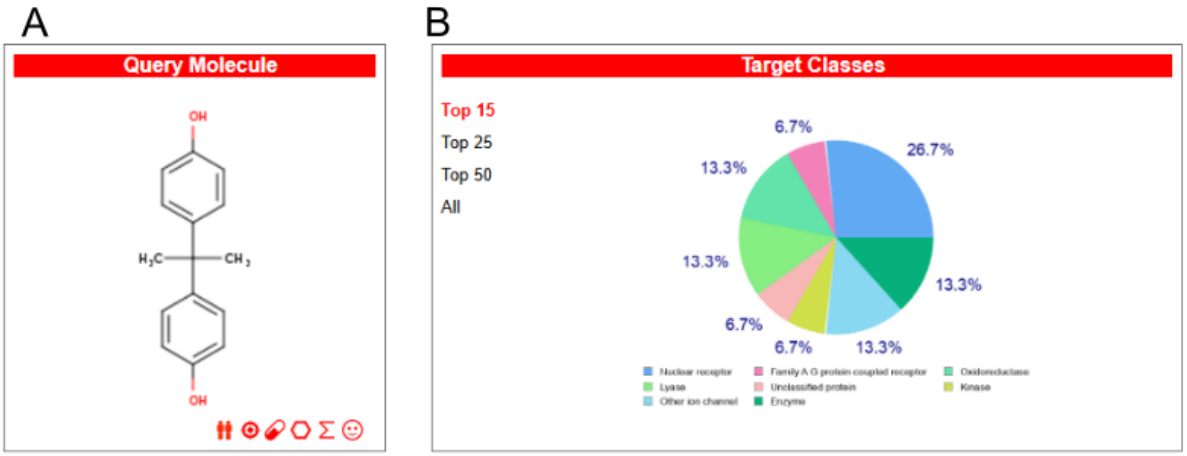

C

Target	Common name	Uniprot ID	ChEMBL ID	Target Class	Probability*	Known actives (3D/2D)
Androgen Receptor	AR	P10275	CHEMBL1871	Nuclear receptor		20 / 11
Estrogen receptor alpha	ESR1	P03372	CHEMBL206	Nuclear receptor		237 / 84
Estrogen receptor beta	ESR2	Q92731	CHEMBL242	Nuclear receptor		235 / 82
Serotonin 6 (5-HT6) receptor	HTR6	P50406	CHEMBL3371	Family A G protein-coupled receptor		4 / 2
Estrogen-related receptor gamma	ESRRG	P62508	CHEMBL4245	Nuclear receptor		2 / 1
Arachidonate 5-lipoxygenase	ALOX5	P09917	CHEMBL215	Oxidoreductase		29 / 10

Figure 2: (A) Structure of Bisphenol A (B) Pie chart of prediction divided into color coded subgroups (C) Prediction of targets with common name, ID´s and probability of binding. Smiles "CC(C)(C1=CC=C(O)C=C1)C1=CC=C(O)C=C1".[49] *Created with SwissTargetPrediction.*[34–36]

2.1.3. Bisphenol F

Bisphenol F is a synthetic compound structurally and functionally similar to bisphenol A. Due to the restriction to bisphenol A in food contact materials substitutes like BPF are and will be increasingly used in the production of polycarbonate plastics, epoxy resins, and other consumer products.[50] BPF can be found in food packaging, personal care products, baby

bottles, and other materials that come into contact with food and beverages, leading to human exposure through dietary intake as well as dermal and possibly inhalational routes.[51] Biomonitoring studies have detected BPF in urine, serum, and breast milk from various populations in Europe, indicating widespread and ongoing exposure.[52] The dietary exposure to BPF can vary dramatically, some studies found 25 ng/kg bw per day, while a later conducted study found 0,485 ng/kg bw per day.[53]

Literature demonstrates BPFs hormonal mimicry activity is of similar magnitude and character to that of BPA. These studies found that BPF exhibits estrogenic, antiestrogenic, androgenic, and antiandrogenic effects in both *in vitro* and *in vivo* systems.[52] This proves that BPF is not only structurally similar to BPA, but also functionally. BPF exhibits multiple different endocrine disruptive effects, like binding to nuclear estrogen receptors and furthermore it has been shown that exposure to BPF can alter organ weights, reproductive endpoints, and enzyme expression in experimental models. Aligning with the literature data we used the online tool SwissTargetPrediction, which results can be seen in figure 3. The top two predicted binding spots for BPF were the endocrine receptors ERα and ERβ.

Considering the ban of BPA in food contact materials in December 2024 an increase in usage, but also exposure to humans is unavoidable. As it has mostly been used as a BPA substitute, underlining the toxicological relevance of BPF.[50,54]

Furthermore, BPF can disrupt intestinal homeostasis, leading to dysregulation of mucosal barrier and intestinal inflammation. This effect is hypothesized through disruption of the Notch/Wnt signaling pathway.[48] BPF can also impact the gut microbiota composition. Gut microbial composition is tightly related with the their own metabolite profiles, which indirectly regulate the gut barrier.[48]

A

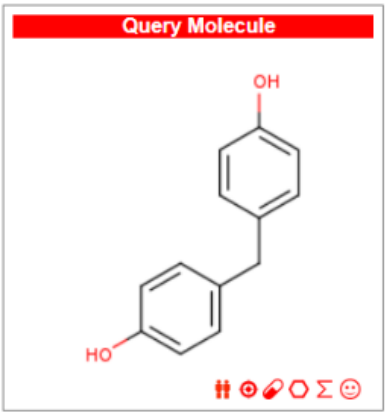

B

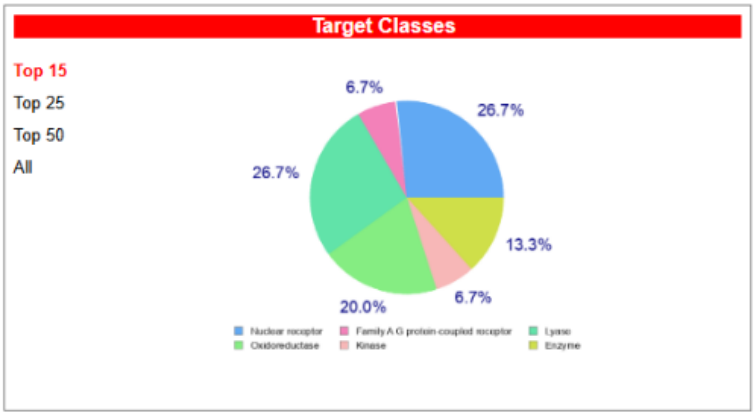

C

Target	Common name	Uniprot ID	ChEMBL ID	Target Class	Probability*	Known actives (3D/2D)
Estrogen receptor alpha	ESR1	P03372	CHEMBL206	Nuclear receptor		249 / 84
Estrogen receptor beta	ESR2	Q92731	CHEMBL242	Nuclear receptor		251 / 82
Androgen Receptor	AR	P10275	CHEMBL1871	Nuclear receptor		16 / 11
Serotonin 6 (5-HT6) receptor	HTR6	P50406	CHEMBL3371	Family A G protein-coupled receptor		4 / 2
Estrogen-related receptor gamma	ESRRG	P62508	CHEMBL4245	Nuclear receptor		1 / 1
Carbonic anhydrase II	CA2	P00918	CHEMBL205	Lyase		79 / 12
Carbonic anhydrase IV	CA4	P22748	CHEMBL3729	Lyase		5 / 2

Figure 3: (A) Structure of Bisphenol F (B) Pie chart of prediction divided into color coded subgroups (C) Prediction of targets with common name, ID´s and probability of binding. Smiles: "OC1=CC=C(CC2=CC=C(O)C=C2)C=C1".[55] *Created with SwissTargetPrediction.*[34–36]

2.1.4. Diisodecyl phthalate

Diisodecyl phthalate is widely used as a plasticizer in the production of flexible polyvinyl chloride products, including floor materials, cables, car parts and food contact materials. Due to its extensive use in manufacturing, DiDP is released into the environment during both production and through consumer products, which means exposure can take place via contamination of food or migration into it.[56,57] Kransler *et al*. 2013[58] calculated estimated exposure values as high as 1 µg/kg bw per day.

Experimental studies have demonstrated endocrine disruptive features, showing that DiDP induces transcriptional changes in genes regulating steroid hormone balance and estrogen receptors, even at relatively low concentrations in zebra fish models. DiDP exposure led to

significant changes in the expression of genes involved in steroidogenesis and hormone signaling.[59] Repeated dose toxicity studies in animals have shown that DiDP can cause increased liver weights and changes in lipid metabolism, although the relevance of these effects to humans may be limited due interspecies differences.[60,61] Importantly, developmental toxicity has been observed in animal studies at doses lower than those causing overt parental toxicity, with effects including reduced fetal survival and developmental abnormalities.[62] Interestingly when DiDP was checked with the online tool SwissTargetPrediction no binding prediction to the estrogen receptors could be seen, as shown in figure 4, coinciding with literature. This might have several reasons, first the lack of evidence from *in silico* and *in vitro* binding experiments, on which the website is partly based on. Another part could be due to the chemical structure, with its two long chains DiDP might not be binding to the estrogen receptors but might be blocking the entrance to the binding pocket.

Phthalates endocrine mechanism of action is not related to binding of a hormone receptor, but different interference with the endocrine system. One of these mechanisms is the, phthalate induced, blockage of the androgen pathway, thereby inhibiting testosterone synthesis and impaired androgen receptor signaling.[63] Phthalates have also shown to impact expression of epithelial markers, like ZO-1 and mesenchymal markers. These changes could be due to the impact of phthalates on the TGF-β/Smad signaling pathway.[63,64] Though it is also hypothesized that an exposure to phthalate induce a decreased AR expression and increased ERα expression, which could lead to these epithelial markers.[65]

A

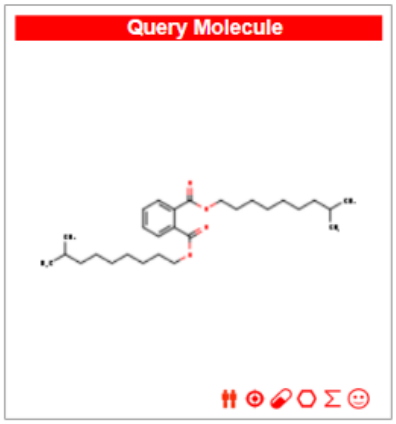

B

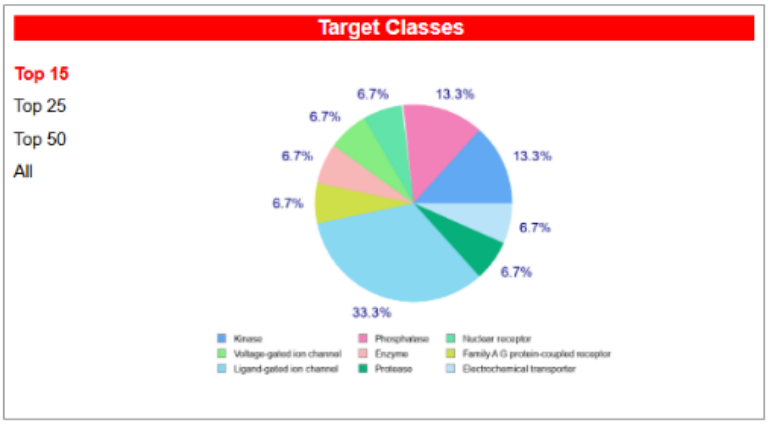

C

Target	Common name	Uniprot ID	ChEMBL ID	Target Class	Probability*	Known actives (3D/2D)
Protein kinase C delta	PRKCD	Q05655	CHEMBL2996	Kinase		0 / 8
Protein kinase C alpha	PRKCA	P17252	CHEMBL299	Kinase		0 / 9
Protein-tyrosine phosphatase 1B	PTPN1	P18031	CHEMBL335	Phosphatase		0 / 10
T-cell protein-tyrosine phosphatase	PTPN2	P17706	CHEMBL3807	Phosphatase		0 / 7
Androgen Receptor *(by homology)*	AR	P10275	CHEMBL1871	Nuclear receptor		0 / 1
Potassium channel subfamily K member 2 *(by homology)*	KCNK2	O95069	CHEMBL2321615	Voltage-gated ion channel		0 / 1

Figure 4: (A) Structure of Diisodecyl Phthalate (B) Pie chart of prediction divided into color coded subgroups (C) Prediction of targets with common name, ID´s and probability of binding. Smiles: "CC(C)CCCCCCCOC(=O)C1=CC=CC=C1C(=O)OCCCCCCCC(C)C".[66] *Created with SwissTargetPrediction.*[34–36]

2.1.5. Levonorgestrel

Levonorgestrel is a synthetic second generation progestin widely used in various contraceptive formulations, including combined oral contraceptives, progestin only pills and emergency contraceptives.[67,68] It exerts its primary contraceptive effect by acting as an agonist of the progesterone receptor, thereby inhibiting ovulation and altering cervical mucus to prevent sperm penetration.[69] Due to its widespread use, levonorgestrel is excreted in significant quantities and has been detected in water bodies worldwide, where it persists because it is not fully removed by conventional wastewater treatment processes.[70,71] Therefore exposure to LNG can vary drastically, when taking it as the mini pill the concentration of LNG is usually 30 µg per pill, while consumption of contaminated water can lead to an exposure of up to 0,7 ng/kg bw per day.[71,72]

Levonorgestrel elicits its endocrine active function as an interaction with both androgen and estrogen receptors in addition to its primary progestogenic action. Studies have demonstrated that LNG can induce both androgenic and estrogenic activities *in vitro* and *in vivo*, leading to complex effects on reproductive development and function.[73] In figure 5 the results of the SwissTargetPrediction can be seen. In contrast to several experimental studies, the probability of binding to the estrogen receptor is low compared to other endocrine receptors. One of these studied was in aquatic organisms such as fish, where exposure to environmentally relevant concentrations of levonorgestrel caused both masculinization and feminization, depending on the dose and context, reflecting its dual activity on sex hormone pathways.[69,73] In human cell culture models, levonorgestrel and its degraded metabolites have been shown to significantly reduce the production of β-hCG, an essential hormone crucial for early pregnancy maintenance, suggesting probable risks to reproductive health even at low environmental concentrations.[69]

An additional aspect of LNG is its effect on key cell-cell adhesion molecules. *In vivo* exposure to LNG can lead to reduced expression of desmosomal cadherin desmoglein-1α and diminish the mucosal barrier thereby increasing mucosal epithelial permeability.[74] Combined oral contraceptives, such as LNG, can also alter the gut microbiome composition and the permeability of the gut.[75] This effect is suggested due to the estrogen-gut axis, a mechanism which suggests that there is an interaction between the gut microbiome composition and systematic estrogen concentration.[75–77]

A

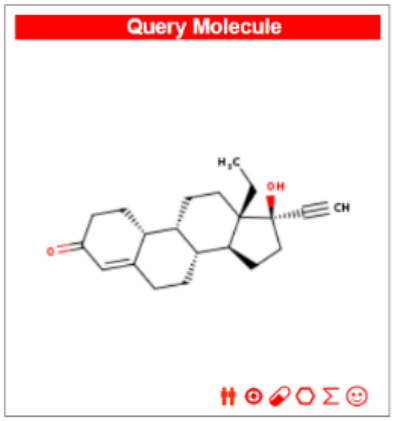

B

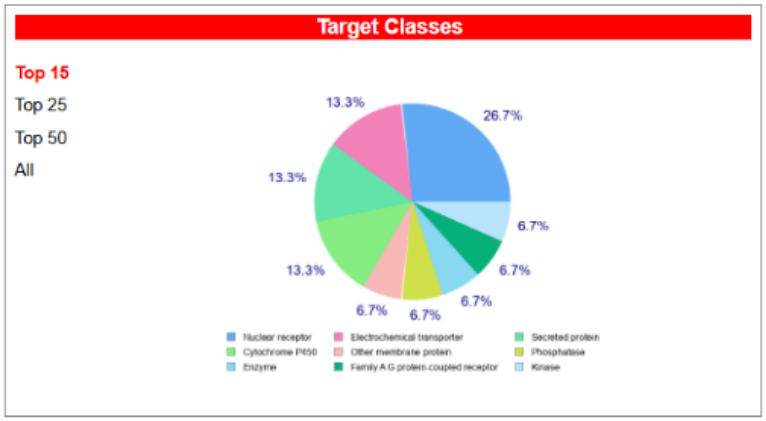

C

Target	Common name	Uniprot ID	ChEMBL ID	Target Class	Probability*	Known actives (3D/2D)
Androgen Receptor *(by homology)*	AR	P10275	CHEMBL1871	Nuclear receptor		104 / 124
Glucocorticoid receptor	NR3C1	P04150	CHEMBL2034	Nuclear receptor		63 / 41
Serotonin transporter	SLC6A4	P31645	CHEMBL228	Electrochemical transporter		22 / 5
Testis-specific androgen-binding protein	SHBG	P04278	CHEMBL3305	Secreted protein		39 / 47
Progesterone receptor	PGR	P06401	CHEMBL208	Nuclear receptor		52 / 51
Estrogen receptor alpha	ESR1	P03372	CHEMBL206	Nuclear receptor		23 / 36
Cytochrome P450 19A1	CYP19A1	P11511	CHEMBL1978	Cytochrome P450		82 / 312

Figure 5: (A) Structure of Levonorgestrel (B) Pie chart of prediction divided into color coded subgroups (C) Prediction of targets with common name, ID´s and probability of binding. Smiles: "CC[C@]12CC[C@@H]3[C@H]([C@@H]1CC[C@]2(C#C)O)CCC4=CC(=O)CC[C@H]34".[78] *Created with SwissTargetPrediction.*[34–36]

2.1.6. 17-beta-Estradiol

17-beta-Estradiol is the main endogenous estrogen in humans; it is primarily produced in the ovaries and in peripheral tissues. As a natural steroid hormone, E2 plays a managing function in controlling reproductive physiology, including stimulation of endometrial proliferation, and feedback inhibition of pituitary hormone release.[79] Beyond reproduction, E2 exerts broad systemic effects, influencing cardiovascular, skeletal, metabolic, and neural functions through both genomic and non-genomic signaling pathways mediated by ERα and ERβ located in the nucleus, cytoplasm, and at the cell membrane.[80,81]

To evaluate the ability of the online tool, E2 was also analyzed in SwissTargetPrediction, which produced the anticipated result. The highest binding affinities were to endocrine receptors such as ERα and ERβ, but also to androgen or serotonin receptors. These results can be seen in figure 6.

The use of E2 in experimental systems is deliberately set and controlled, to differentiate it from endocrine disruptors whose environmental or dietary exposure levels can be highly variable by compound. By providing a consistent and physiologically relevant standard, 17-beta-estradiol ensures the validity of assay systems and enables the quantification of relative potencies for other substances under investigation.[80–82]

Zhou et al. 2017[83] demonstrated E2 can reduce the expression of tight junction protein ZO-1 in human primary gut tissue and human gut epithelial cell line.[83] Contrary to this Choi *et al*. 2018[84] established that estrogen reinforces barrier formation. In their study, TEER values and tight junction expression increased dose dependent, with the addition of E2. They additionally found that E2 can inhibits TNFα-induced nuclear translocation of NF-κB.[84]

A

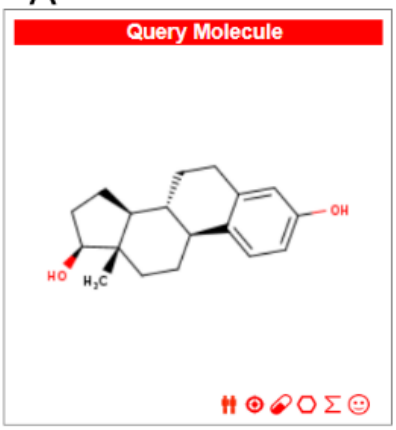

B

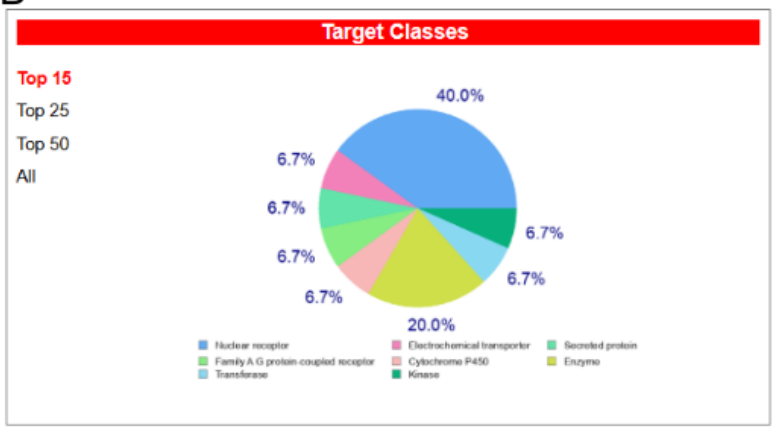

C

Target	Common name	Uniprot ID	ChEMBL ID	Target Class	Probability*	Known actives (3D/2D)
Androgen Receptor	AR	P10275	CHEMBL1871	Nuclear receptor		40 / 38
Estrogen receptor alpha	ESR1	P03372	CHEMBL206	Nuclear receptor		48 / 107
Serotonin transporter	SLC6A4	P31645	CHEMBL228	Electrochemical transporter		9 / 80
Estrogen receptor beta	ESR2	Q92731	CHEMBL242	Nuclear receptor		45 / 93
Testis-specific androgen-binding protein	SHBG	P04278	CHEMBL3305	Secreted protein		21 / 18
Estrogen-related receptor alpha	ESRRA	P11474	CHEMBL3429	Nuclear receptor		1 / 8
Estrogen-related receptor beta	ESRRB	O95718	CHEMBL3751	Nuclear receptor		1 / 7
G-protein coupled estrogen receptor 1	GPER1	Q99527	CHEMBL5872	Family A G protein-coupled receptor		1 / 1
Cytochrome P450 19A1	CYP19A1	P11511	CHEMBL1978	Cytochrome P450		13 / 56
Adenylate cyclase type 10	ADCY10	Q96PN6	CHEMBL5854	Enzyme		1 / 1

Figure 6: (A) Structure of 17-beta-estradiol (B) Pie chart of prediction divided into color coded subgroups (C)Prediction of targets with common name, ID´s and probability of binding. Smiles: "C[C@]12CC[C@H]3[C@H]([C@@H]1CC[C@@H]2O)CCC4=C3C=CC(=C4)O".[85] *Created with SwissTargetPrediction.*[34–36]

2.2. Tight junctions

TJs are intercellular junction proteins that occur in between epithelial cells. Their primary localization is at the apical region of cell–cell contact. Here TJs seal contacts, which connect epithelial cells and control the passage of fluid and substances between the cells to the basolateral side. TJs consist of special sealing proteins (i.e. occludins, claudins), which bind to each other at the most apical region of the cells, where adjacent plasma membranes appear to partially fuse with each other, as can be seen in figure 7, and of anchor proteins that retain these special sealing proteins and bind to more extensive structural sound scaffold, like the actin cytoskeleton.[86] The inter connection of two membranes happens through two complementary TJ strands, they create a natural seal as a result of a tight coupling of the TJs. In this way, they also form a natural barrier for the lateral diffusion of membrane proteins. Through this apical and basolateral membrane regions are separated from each other and each have their own characteristic composition of membrane proteins.[10]

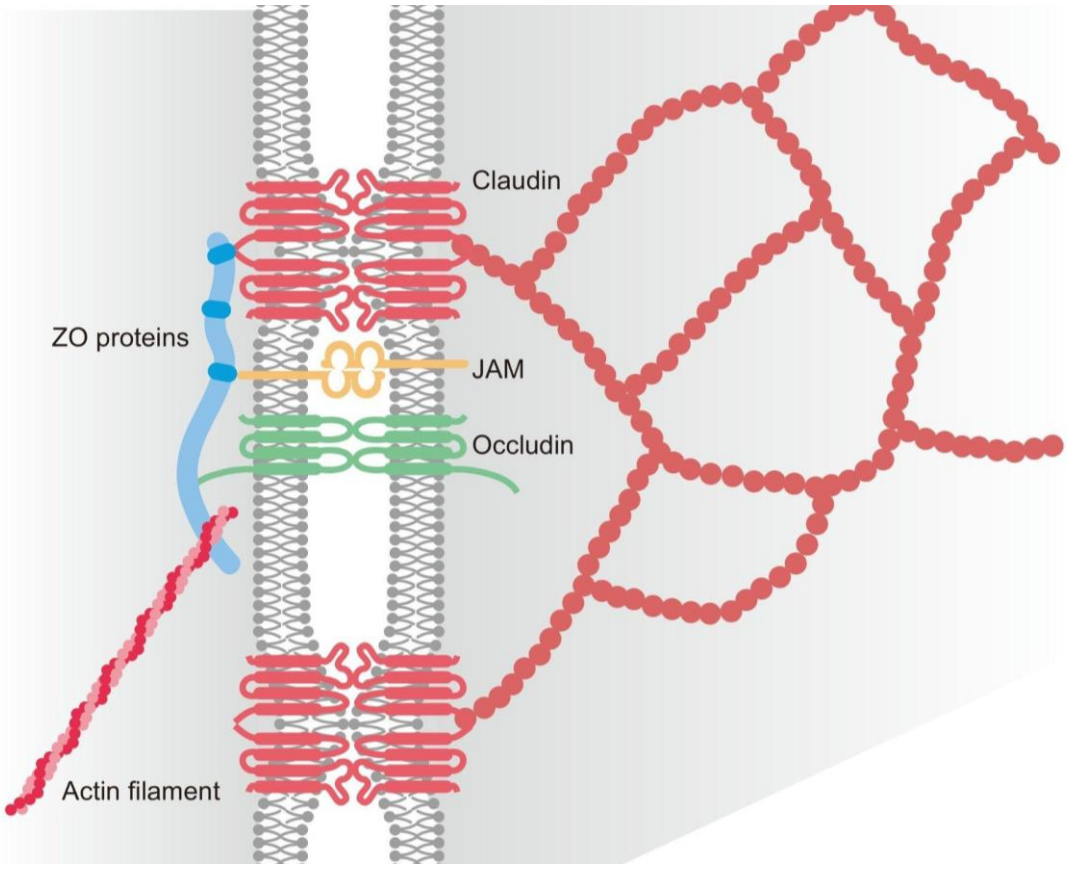

Figure 7: Schematic structure of the two cell membrane connections through tight junctions highlighting: zonula occludens; claudins and actin cytoskeleton and other tight junction proteins; cropped and taken from Otani et al. 2020[86]

There are several groups of tight junctions or associated proteins like membrane proteins, claudins[87], scaffolding protein family of ZO-1[88], membrane proteins like TJ-associated MARVEL domain-containing proteins[89] and junctional adhesion molecules[90] within the immunoglobulin superfamily that localize to TJs.

2.2.1. Zonula occludens 1

The scaffolding protein ZO-1 is located at the cytoplasmic membrane surface of intercellular TJs in epithelial and endothelial cells. The encoding of the 220 kDA protein is done via the TJP1 gene. It also was the first discovered tight junction protein. ZO-1 main physiological task is the crosslinking of other TJs strands such as claudins, occludin, and junctional adhesion molecules to the actin cytoskeleton. ZO-1 does through acting as a scaffold and containing multiple binding domains. Through this the whole TJs complex maintains its structural integrity and can sustain the epithelial barrier.[91,92]

ZO-1 is an membrane-associated guanylate kinase-like homologues (MAGUKs), these play an essential role in maintaining and creating specialized membrane domains in various types of cells.[93] ZO-1 holds various interactions domains, to which many essential membrane proteins can bind. One of these domains is the PDZ binding site, whereby other domains like SH_3- and GUK-domains also play an essential role. Through these binding sites it allows ZO-1 to work as a scaffold, interconnecting TJs proteins with the actin cytoskeleton.[94] McNeil *et al*. 2006[94] demonstrated that silencing or knocking out ZO-1 protein in kidney epithelial cells causes a three hour delay in TJs formation. Though even in ZO-1 silenced cells fully mature and working TJs formation can form. This highlights ZO-1's essential role in effectively creating the TJs complex.[94]

A further activity of ZO-1 is the involvement in the signal transduction at cell–cell junctions. Thereby it assists important cellular processes such as migration, proliferation and wound healing. ZO-1 can aid in the regulation of epithelial proliferation and repair. Through multiple conditions, like Inflammatory Bowel Disease, ZO-1 can be down-regulated. This down-regulation can lead to an increased intestinal permeability and defective mucosal repair.[95]

2.2.2. Claudin 4

Claudins are a group of TJs proteins in the family of adhesion molecules. Their weight can range from 21 to 28 kDa. Claudins have short cytosolic N- and C-terminal domains, to bind to different kinds of binding sites. The C-terminal contains a PDZ motif, which binds to homologous sites in scaffolding proteins, like ZO-1. The critical role of claudins is creating the selectivity of the paracellular transport mechanism, in between epithelial cells. This makes claudins essential for the upkeep of the barrier function. [96,97]

The previously mentioned terminals contain two extracellular loops and two cytoplasmic domains- one being an amino and one being a carboxyl terminal domain.[98] One of the most important proteins of this family is claudin 4 (CLDN4). This transmembrane protein is found in the gaps of epithelial and endothelial cells, where membranes come close to each other and interconnection via TJs strands happens.[99] Claudin 4 plays a crucial function in increasing the complexity of TJs and assisting paracellular permeability, which is vital for the physiological function of various organs and tissues.[100]

Inter-claudin interference is a special function, where one claudin protein disrupts higher order structures or channels formed by a different claudin.[101] Claudin 4 plays an essential role in assisting this special interference. This interference selectively inhibits the channel function of pore forming claudins, like claudin 2 or claudin 15. Furthermore, CLDN4 plays an essential function in regulating permeability and barrier function and is thereby considered a barrier-forming claudin. Through this the epithelial barrier permeability is being regulated by CLDN4. CLDN4's essential interactions with pore forming claudins is underscored, when the expression is experimentally removed, *via* knockout. Then overexpression of CLDN4 has minimal effect on TJs permeability, demonstrating its role in regulating pore-forming claudins.[101]

2.2.3. Barrier function

Maintenance of the barrier function, also distinguished as gate function and fence function, is one of the essential physiological functions of TJs. Pertaining the gate function, this regulates paracellular permeability by selective controlling of the passage of various small molecules and ions, such as water, these can then permeate through the intercellular space, thereby creating a tissue-specific barrier and special absorption properties.[102,103] This homeostasis is

achieved through transmembrane proteins such as claudins and occludin. These proteins can build special charge- and/or size-selective channels to make this permeability possible.[104] The fence maintains cell polarity by preventing the lateral diffusion of apical and basolateral membrane components and ensuring differential domain-specific distribution of proteins and lipids. Interactions between TJ, the actin cytoskeleton and intermediary proteins are the backbone of these functions, and the functions would not work without them. One of these intermediary proteins, ZO-1, is essential to stabilize the integrity of the junction complex. Interference of these proteins or functions is associated with multiple pathological conditions and could lead to inflammatory diseases and cancer.[104,105]

3. Materials and Methods

3.1. Materials

The list of the materials is all noted in the supplementary tables s1-s5.

3.2. Methods

3.2.1. HT29; HT29-MTX-E12; Caco-2

HT29, HT29-MTX-E12 and Caco-2 cells were the only cells used in this thesis. They all grew in the same medium: Dulbecco's Modified Eagle Medium (DMEM) with addition of glucose (4,5 g/L), 10 % inactivated fetal bovine serum (FBS), 1 % non-essential amino acids, 1 % L-glutamine and 1 % penicillin-streptomycin (P/S). HT29 and HT29-MTX-E12 cells were cultivated in a T75 flask, while Caco-2 were grown in a T175 flask. Cells were subcultivated roughly every two to four days, depending on confluency. For HT29 and HT29-MTX-E12 first, the medium in the flask was aspirated before the cells were washed once with 5 mL of PBS-EDTA. Then 1 mL of trypsin-EDTA solution was added, and the cells were incubated for five to ten minutes in the incubator at 37°C, 5 % CO2. The flask was checked under a light microscope, to verify if cells detached. After detachment of cells 5 mL of medium were added to the flask, then homogenized and conveyed to a centrifuge tube and next cells were counted as described in section 3.2.3. After the determination of the concentration of the cell suspension 750.000 cells were added back into the T75 flasks or T175, topping it up to 10 mL in total with growing medium. Splitting for Caco-2 had the same procedure, though double the volumes were added for every step, due to usage of T175 flasks.

3.2.2. Cell cultivation

Passaging of the cells depends on confluency and cell type, to keep nutrient density and confluency in check, was carried out in general every two to four days. During non-working hours cells were stored in the incubator under humidified conditions at 37°C, 5 % CO_2. Only viable cells from passage number between five and 30 were used for experiments.

3.2.3. Cell counting

Cells need to be passaged regularly, to maintain reproducibility of assays, and to do this the cell numbers need to be determined. To count cells, we used a Neubauer counting chamber, as seen in figure 8. Neubauer counting chambers are hemocytometers, a multitude of lines forming 96 squares, with a bottom and a top compartment, making it possible to count two cell suspensions at one time. The grid is made of two three by three millimeter counting grids, these divide each other into nine large squares, in the outer corners. Each large square consists of 16 smaller squares, in which cells were counted.

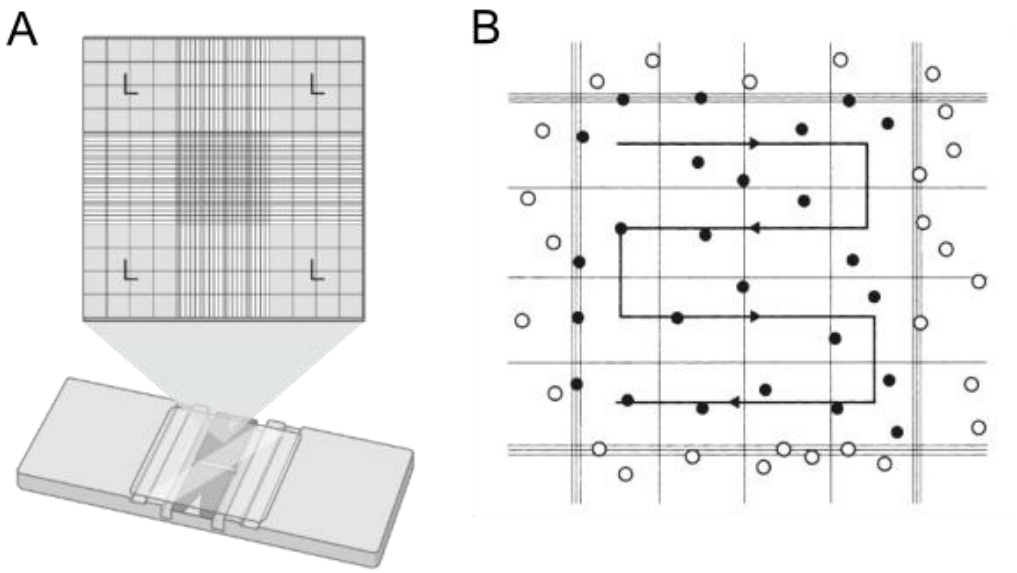

Figure 8: (A) Neubauer chamber, cover slip and the zoom onto the counting grid.[106] *(B) Illustration of one of the bigger squares with cells inside. Black cells were counted, while white cells were not counted. Black line as guideline on how to count cells in proper order*[107]

To count cells, they needed to be in a suspension. Firstly, adherent cells were detached with a trypsin-EDTA solution. This full process was described in detail in the cells' own sections 3.2.3-3.2.5. A small part of the cell suspension was diluted with a 1:10 solution of trypan blue and PBS. The dilution was dependent on cell line and confluency in the cells before, ranging from 1:2 to 1:10. First a cover slip was placed on the Neubauer counting chamber and then 10 µL of the stained cell suspension was pipetted between the cover slip and the Neubauer chamber. Afterwards the cells in the four large corner squares were counted, which are marked in figure 8 panel A with an "L". If cells happened to be on lines of the large squares not all of them were counted. A square contains four outer lines, of which two are chosen and only cells on these lines were seen as viable, as seen in figure 8 panel B. Trypan blue worked as a contrast agent, so dead cells are stained blue, while live ones appear with a black rim and white filling.

To calculate the concentration of the cell suspension, the average amount of cells per square was multiplied with the dilution factor from the trypan blue and the multiplication factor. The multiplication factor was 10^4 and was composed of the volume of the large squares in the Neubauer grid scaled to 1 mL. This calculation is shown in Equation 1.

$$concentration\ of\ cells\ [cells/ml] = cell\ average\ per\ 4\ big\ squares * dilution\ factor * 10^4 \quad (1)$$

3.2.4. Preparation of treatments

The effects treatments AOH, BPA, BPF, DiDP, LNG and was explored immunostaining, the Lucifer-yellow assay and the CellTiter-Blue® Cell Viability Assay. At the beginning of the experimental work, the substances were weighed in and then dissolved in Dimethylsulfoxide (DMSO) or in ethanol for E2 to get to a base stock with a concentration of 0,1 µM. This stock was then diluted to acquire further stocks. These stocks were diluted at least 1:1000 with medium before using them on the cells. Resulting in the highest concentration of solvent of 0,1 % in the treatments and solvent controls.

3.2.5. CellTiter-Blue®-Assay

To determine the cytotoxic effect of AOH, BPA, BPF, DiDP and LNG at different concentrations on the two cell lines Caco-2 and HT29, the CellTiter-Blue® (CTB)-assay was carried out. Viable cells reduced resazurin to fluorescent resorufin, non-viable cells on the

other hand cannot metabolize resazurin and thereby created no signal. First resazurin penetrated the cell, then the metabolic reduction happened. The fluorescent dye diffused out of cells and back into the surrounding medium, creating a fluorescent supernatant liquid. This liquid was then transferred to a black plate and measured in a plate reader. The overall activity of these redox enzymes in viable cells increased the amount of resorufin dye produced and can then be quantified through spectrophotometric methods.[108]

First cells were seeded into a 96-well plate and after 24 hours the treatment was added, this was then incubated for 24h at 1 h at 37°C, 5 % CO_2. First the Titer-Blue solution was created for this the cell Titer-blue dye was diluted 1:10 with DMEM without phenol red. Next the medium was aspirated and 100 µL of cell Titer-Blue solution, was added into the 96-well plate. The cells and the solution were incubated for 1 h at 37°C, 5 % CO_2. Afterwards 80 µL of the supernatant was pipetted into a 96 well black plate. The absorbance was then measured via plate reader at 560/590 nm against a background blank. Data was expressed as T/C [%] and the graphs were obtained after performance of n=3 biological experiments in technical triplicates.

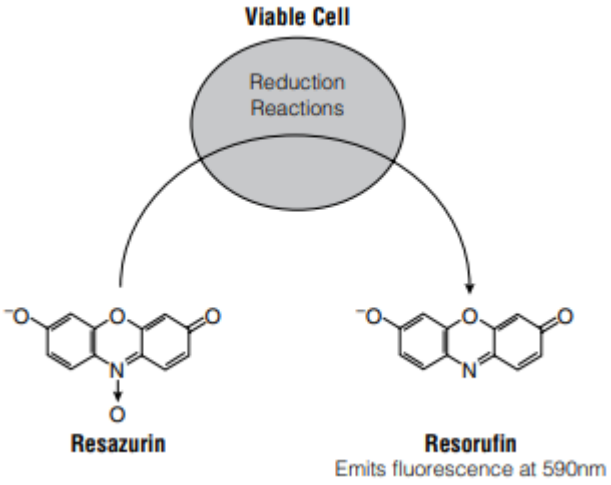

Figure 9: Visualization of the metabolic reduction of the cell from non-fluorescent resazurin to fluorescent resorufin[108]

3.2.6. Mucus removal/reduction

Mucus removal was adapted by a protocol established by Behrens *et al.*, 2002.[109] First the medium of the cells was aspirated, then 10 mM of N-acetyl-cysteine in cell culture medium was added. The volume was dependent on the plate/slide (500 µl for 24 well plate; 250 µl for µ-slide 8 well). Then the plate/slide is agitated at 220 rpm for 30 minutes at 37 °C, 5 % CO_2 (on MK3 control orbital shaker) afterwards the liquid was aspirated and the same volume of

10 mM N-acetyl-cysteine in medium was added and the process repeated. The liquid was aspirated, and the plate/slide was washed twice with medium, before treatments were applied.

3.2.7. Preparation of nanoparticle suspension

Mesoporous silica-based small-rod-nanoparticles (srNPs) and rod-shaped bacteria-like nano particles (bacNPs) and their functionalized variants methylated and phosphonated were kindly provided by Univ. Prof Freddy Kleitz and synthesized by Dr. Iriarte-Mesa. The functionalization groups can be seen in figure 11. These were first weighed in glass vials. Then FBS free cell culture medium was added to the containers to result in a concentration of 600 µg/mL. This suspension was first vortexed for 60 seconds, then sonicated in an ultrasound bath for 15 minutes and vortexed again for 60 seconds before application. The synthesis of the NPs was performed after the script from Yu *et al*. 2016[110], modifications to these directions were performed as in Bergen *et al.* 2025[18]. Additionally, the NPs were labeled with fluorescein isothiocyanate (FITC) as reported by Hohagen *et al*. 2022[111].

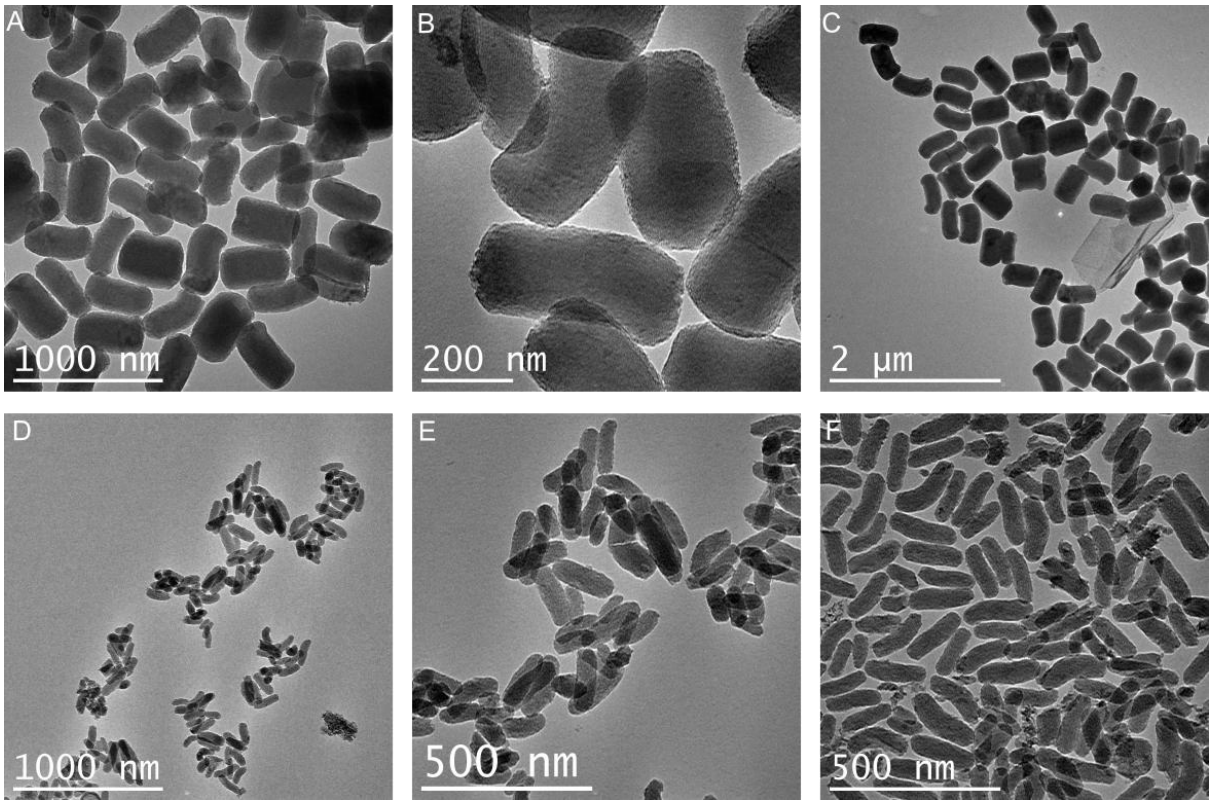

Figure 10: TEM-Images of non-functionalized silica-based mesoporous (A-C) big rod and (D-E) small rod nanoparticles, kindly provided by Prof. Freddy Kleitz and synthesized and imaged by Dr. Claudia Iriarte-Mesa after script from Yu et al. 2016[110].

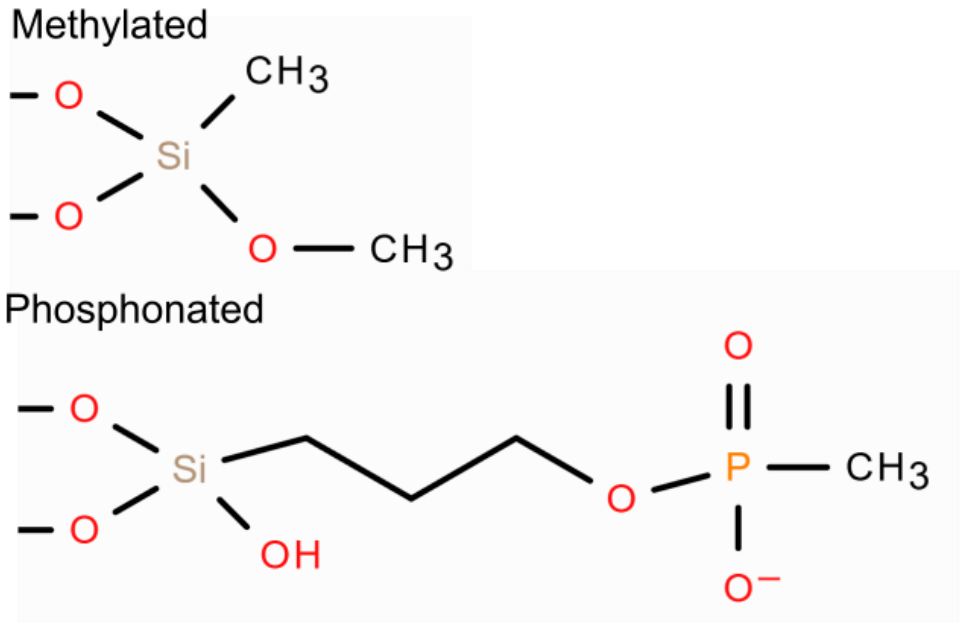

Figure 11: Functionalization groups of srNPs and bacNPs, methylated and phosphonated (created with webtool moldraw)[112]

3.2.8. Determination of penetration depth and intercellular distances

For penetration depth and intercellular distances a previously implemented protocol by Bergen *et al*. 2025[18] and Iriarte-Mesa *et al*. 2024[19] was adapted. First 85 000 cells/cm^2 of Caco2:HT29-MTX-E12 (9:1) were seeded into Sarstedt 24-well plates. These were differentiated either for 7 or for 21 days. Then mucus was either not reduced or reduced as described in section 3.2.8. Thereafter 500 µL of freshly prepared 600 µg/mL nanoparticle suspension was added, this suspension was prepared as detailed in section 3.2.9. After nanoparticle application the coculture was imaged in the Lionheart FX Automated microscope using the GEN5 Microplate Reader and Imager Software Version 3.05. Six 4x images per well were taken, one in phase contrast and in green fluorescent protein (GFP), per coordinates, where the focus plane (z-position) and coordinates, x,y-position were marked. After 6 hours of incubation under humidified conditions at 37 °C with 5 % CO_2, the cells were first washed twice with a 37 °C NES-buffer and then the 500 µL of 37 °C NES-buffer was added for further imaging. Cells were imaged again starting from the coordinates of the images taken at t=0. Then the new focal plane for phase contrast and for GFP was measured, additionally taking images in the old focal plane for GFP, showing that the nanoparticles have moved in the z-axis. The two new focus planes were also noted and through the difference between the old GFP focus and the new GFP focus the penetration depth arose. Furthermore, 20x images were taken in phase

contrast setting and distances between cells (intercellular distances) were measured manually in GEN5.

3.2.9. Lucifer yellow assay and TEER measurement

To determine the effect of Bisphenol F and Bisphenol A with and without srNPs on the permeability of a monolayer, TEER measurements and the Lucifer yellow assay were performed. The protocol was adapted from Beisl. *et al*. 2021[113]. First 85 000 cells/cm^2 of coculture (9:1, Caco-2:HT29-MTX-E12) were seeded into a 12 well plate with TC inserts. On the top the cells were seeded, while in the well THP-1 Medium was added to simulate the gastrointestinal tract. Then the cells were differentiated for 6 days, while medium was changed every two to three days. Afterwards the cells were treated with BPF (1 µM, 10 µM and 100 µM) and BPA (100 µM) for 24 h. After the treatment the media was suctioned off and the cells were washed with serum-free medium and then srNPs (600 µg/mL), as prepared in section 3.2.9, were added to half of the wells, resulting in one condition with NPs and one without. These NPs and the treatment with BPF and BPA were incubated for 6 h (37 °C, 5 % CO_2).

Before the end of the incubation the lucifer yellow solution was prepared. Here 0,1 mg/mL of Lucifer-Yellow CH-diLithium salt was dissolved in Hank's Balanced Saline Solution (HBSS). Then the medium was aspirated, and the cells were washed with HBSS twice, while 1,5 mL HBSS was added to the basolateral side, while on the apical side 500 µL lucifer yellow solution was applied. These solutions were incubated for 60 min at 37 °C, 5 % CO_2. 150 µL of the apical solution was taken and transferred in triplicates to a black plate, additionally 150 µL LY solution in triplicate and 150 µL HBSS (blank) was added to designated wells. Next the absorbance was measured with a plate reader (ex.485 nm; em.535 nm). Permeability was determined from n = 3 biological replicates in technical triplicates. Data was calculated as follows in equation 2:

$$permeability\,[\%] = samples - blank\,(LY) - blank * 100 \quad (2)$$

During the differentiation of the coculture the trans epithelial electrical resistance (TEER) was measured every two to three days. This was done as described by Srinivasan *et al*. 2015.[114] Additionally this measurement was done before the treatment with BPA and BPF before the addition of the NPs and 6 h afterwards. This was carried out using an Epithelial Voltohmmeter (EVOM2) coupled to STX4 EVOM Electrode with removable blades (World Precision

Instruments, Sarasota, FL, USA) with an adapter. Before measurement the electrode was washed with ethanol (70 %) and equilibrated first in PBS and then cell culture medium at room temperature.[113] TEER values were obtained from n = 3 independent biological replicates, in technical triplicates.

3.2.10. Immunostaining

Immunostaining Piezo1 Ion Channels

For immunofluorescence staining of Piezo1 ion channels, a previously implemented protocol by Del Favero *et al*. 2020[115] was adapted to be prepared in ibidi 8-well µ-slides. For this experiment two monocultures and a coculture (9:1, Caco-2:HT29) were seeded at a density of 85 000 cells/cm^2. Each µ-slide-half had two wells designated for the coculture, one for Caco-2 and one for HT29 cells for both differentiation periods. The first half was differentiated for 48 h and the second for 7 days. After the incubation time the medium was first aspirated, then the cells were fixed with ROTI Histofix Formaldehyde (4%) for 10 min in dark, washed with PBS-A twice, sealed and stored in the dark at 4 °C, until the staining procedure.

As a first step of the staining procedure, unspecific binding domains needed to be blocked. For this 250 µL/well 2% donkey serum in PBS-A was applied for 1 hour at room temperature. No permeabilization was done carried out, due to the staining being inside of the membrane. Then Piezo1 monoclonal antibody was diluted 1:400 in PBS-A and 200 µL of the antibody solution was added per well. The primary antibodies were incubated in the dark at 4°C overnight.

After incubation the cells were washed five times with PBS-A: twice for 10 min and thrice for 5 min. Next 200 µL of the secondary antibody, donkey anti-Mouse Alexa Fluor™ 647, solution per well was added. This solution was a dilution of 1:1000 in PBS-A. Thereafter 5x5 min of washing with PBS-A only was done. Then permeabilization with 0,2 % Triton-X in PBS-A was carried out for 15 min. Another blocking step with 250 µL/well 2% donkey serum in PBS-A was applied for 1 h at room temperature. To stain the actin cytoskeleton phalloidin Oregon green 488 was added in a 1:1000 dilution 200 µL per well. Then the slide was washed three times for 10 min with 0,05 % Triton-X in PBS-A and twice with PBS-A for 5 min. After the washing process, the slide was postfixated. For this step first 200 µL ROTI Histofix Formaldehyde (4%) was added and incubated for 10 minutes in the dark. Thereafter the slides were washed with

PBS-A twice, while collecting the residual formaldehyde. Then PBS-A glycine was added to inactivate the formaldehyde and incubated for 5 min. The slides were then washed twice with PBS-A. As a last step 2-3 drops of Roti-Mount FlourCare + DAPI (Mounting media) were added, then the slides were sealed with parafilm and wrapped in aluminum foil and put into the fridge (4 °C, dark), until imaging.

Images for Piezo1 were acquired with a confocal Zeiss microscope (LSM 800 equipped with ELYRA PS.1.5 system with a Plan Apochromat 63X/1.4 oil objective). Three 2D images were acquired from each well. The mean intensity was quantified from n = 3 biological replicates in technical quintuplicates; the data was analyzed in imageJ and evaluated in OriginPro.

Piezo1 channels were stained in a Caco-2/HT29, and not in the Caco-2/HT29-MTX-E12 coculture due to one important factor: It is important to fixate the cells with a 10:1 methanol/acetic acid combination, when staining a in a mucus producing coculture. The mixture would have fragmented the membrane and assisted in destroying the mucus layer for better antibody-antigen bindings. Though when staining a membrane protein this feature would have therefore distorted the localization of the Piezo1 ion channel. Instead 4% formaldehyde was used for the fixation process, which cannot penetrate the mucus, making a staining of a mucus producing culture obsolete. Hence, we choose not to include the goblet cells and substituting them for their origin cell line HT29.

Immunostaining ZO-1 & CLDN4

For immunofluorescence staining ZO-1 & CLDN4 TJ a previously implemented protocols by Iriarte-Mesa C *et al*., 2023[116] and Groestlinger *et al*., 2022[38] were adapted. First the coculture was seeded at a density of 85 000 cells/cm^2 (9:1, Caco-2:HT29-MTX-E12) in an 8-well ibidi µ-slide. Afterwards there was a 7-day differentiation period in the incubator at 37 °C and 5 % CO_2, exchanging medium every other day. Thereafter the medium was aspirated, and 200 µL of the different treatments were added and placed in humidified incubators at 37 °C and 5 % CO_2 for 24 h. After the 24 h passed, the treatments needed to be aspirated, then cells were fixed with a methanol and acetic acid mixture (9+1) overnight at 4 °C in the fridge. The next day the fixation mixture was aspirated, and the slides were washed with PBS-A twice, sealed and stored in a dark fridge at 4 °C, until the staining procedure.

As a first step the membrane was permeabilized. For this procedure 250 µL/well of 0,2 % Triton-X in PBS-A was added and incubated dark for 15 min. Afterwards unspecific binding domains were blocked with a 250 µL/well 2% donkey serum in PBS-A solution, which was applied for 1 h at room temperature. Then for ZO-1 Rabbit pAb was diluted 1:100 in PBS-A or Claudin 4 monoclonal antibody (3e2c1), conjugated Alexa Fluor 594 was diluted 1:500 in PBS-A, depending on the TJ was stained. Thereafter 200 µL of the antibody solution was added per well. The antibodies were incubated in a dark fridge at 4 °C overnight.

Then the slide was washed thrice for 10 min with 0,05 % Triton-X in PBS-A and twice with PBS-A for five min. Next only the secondary antibody for ZO-1 was added, since CLDN4 antibody was conjugated already, Donkey anti-Rabbit IgG (H+L) Alexa Fluor™ 488 was added 200 µL/well with a dilution of 1:1000 in PBS-A. Thereafter the slide was washed thrice for 10 min with 0,05 % Triton-X in PBS-A and twice with PBS-A for five min. After the washing steps the slide was postfixated. Postfixiation was done for ZO-1 and CLDN4, for this step, first 200 µL of the methanol and acetic acid (9+1) mixture was added and incubated for 10 min, dark. Thereafter the slides were washed with PBS-A twice, while collecting the mixture and the PBS-A. Then PBS-A glycine was added to inactivate the fixation step and incubated for five min. The slides were then washed twice with PBS-A. As a last step 2-3 drops of Roti-Mount FlourCare + DAPI (Mounting media) were added and the slides sealed with parafilm and wrapped in aluminum foil and put into the fridge (4 °C) until imaging.

Images for ZO-1 and CLDN4 and nuclei were acquired with a confocal Zeiss microscope (LSM 710 equipped with ELYRA PS.1 system with a Plan Apochromat 63X/1.4 oil objective (zoom 1.5)). Three 2D-images and one z-stack were acquired from each well. TJs thickness was manually measured in FIJI, there 15 TJ-strands were chosen randomly per image and then measured for area. To determine the analysis of the nuclei the 2D images with and without mucus were analyzed. To analyze the nuclei shape markers, first the shape markers analysis needed to be activated in FIJI. Thereafter five nuclei per image were chosen randomly and manually outlined and then measured via FIJI resulting in five shape markers: circularity, aspect ratio, roundness, solidity and the area. The area was calculated into relative area by dividing it by 100. For the z-stacks the z-distance was measured. For the z-distance the intensity of every quartered slice was measured and then plotted, the difference of the maxima from the DAPI signal and the ZO-1 signal was determined as the z-distance. Afterwards the height of the z-stacks was measured. For this the z-stacks were quartered. Thereafter the

slice with the first and the last signal was chosen manually; the difference of the slice number multiplied by the slice thickness resulted in the height of the z-stack.

For the expression of TJs the coculture was seeded the same as mentioned earlier and then differentiated for 3, 7, 14 or 21 days. Afterwards the staining procedure was done as mentioned above as a costaining, meaning both TJs were stained in one slide. Then confocal images were taken with a Zeiss LSM 800 with a 63 X oil objective. Three 2D images were acquired from each well. The mean intensity was quantified from n = 3 biological replicates in technical triplicates; the mean intensity of each image was measured and then the data was analyzed in FIJI and evaluated in OriginPro.

3.2.11. Integrated Chemical Environment PBPK-tool

To contextualize the tested concentrations during the *in vitro* experiments with real life scenario exposure, an overview about the pharmacokinetic profile of our chosen EDCs was obtained with the Integrated Chemical Environment (ICE) tool for Physiological based pharmacokinetic (PBPK) models. Even though this PBPK model is a simulation predicting how the substances would act in a proper PBPK model, based on chemical and structural properties, this does not necessarily include *in vivo* data, thus making it necessary to cautiously interpret the data being aware of potential limitations. Despite these considerations, this approach can provide a starting point for further analysis. At "https://ice.ntp.niehs.nih.gov/Tools", the tab PBPK and selected and the appropriate settings as can be seen in table 2. The selected concentrations were literature researched concentrations from exposure studies.[117]

Table 2: Settings of ICE_PBPK tool

Input description	Input
Species	human
Body weight	70 kg
ADME sources	Default

Exposure dose	AOH: 25 ng/kg[24] DiDP: 1 µg/kg[58] BPA: 1,5 µg/kg[44] BPF: 0,49 ng/kg[53] LNG1: 0,7 ng/kg[72] LNG2: 0,42 µg/kg[71]
Model	Solve_pbtk
Exposure route	oral
Exposure interval	24 h
Simulation length	3 days
Output concentration units	uM (µM)
Cas-numbers	AOH: 641-38-3 DiDP: 89-16-7 BPA: 80-05-7 BPF: 620-92-8 LNG: 797-63-7

4. Results

4.1. Characterization of the coculture

4.1.1. Tight junction protein expression in the coculture after 3, 7, 14 and 21 days

Before starting the analysis of the substances of interest, experiments were performed to better characterize the coculture model. For this the expression of the TJ proteins ZO-1 and CLDN4 were determined at four time points over a period of 21 days. Figure 12 illustrates representative images and the quantification of the expression of the TJs. Panel A shows representative images for ZO-1, and panel B CLDN4, at four different differentiation periods of the culture namely 3, 7, 14, and 21 days. It was expected that a longer differentiation would lead to an increase in intensity, due to the coculture regaining characteristic features, creating a strong barrier, which correlates with TJ expression. This data can be seen in panel C, first the intensity increases from 3 to 7 days. Though comparing prolonged differentiation of 14 days to the 7 days differentiated coculture, no significant change can be seen. When the

coculture was differentiated for 21 days the results for expression of ZO-1 were significantly lower than for the shorter differentiated coculture.

Panel D illustrates the fluorescence intensity of the TJ protein CLDN4. A different trend compared to panel C can be observed. Prolonged differentiation increased average intensity values. This resulted in the 21-day differentiated coculture having the highest intensity signal. Though like in panel C there was no significant difference between a 7-day and 14-day differentiation period in panel D.

4.1.2. Piezo1 ion channels

The expression of Piezo1 ion channels was determined to elicit the phenomenon of prolonged differentiation of the coculture and the impact on membrane proteins.[118,119] The immunofluorescence of Piezo1 ion channels was observed after a period of 48 h or 7 days of differentiation in gastrointestinal epithelial cell lines, to elucidate whether the density of cells or differentiation time would have an effect on the expression of the mechanosensitive Piezo1 ion channel. Figure 13 shows the measured intensities in three distinct intestinal cell culture models for two different differentiation periods. Panel A shows the intensity results for HT29 cells, showing a statistically significant decrease in fluorescence signal after the prolonged differentiation process. Panel B presents a similar trend for the fluorescence intensity in Caco-2 cells. In this graph the signal intensity decreased significantly after the longer differentiation period. Panel C illustrates the measured intensities of the Piezo1 ion channel in the Caco-2/HT29 coculture. In the coculture the most significant reduction was observed. This trend suggests a consistent time-dependent effect in this culture mode.

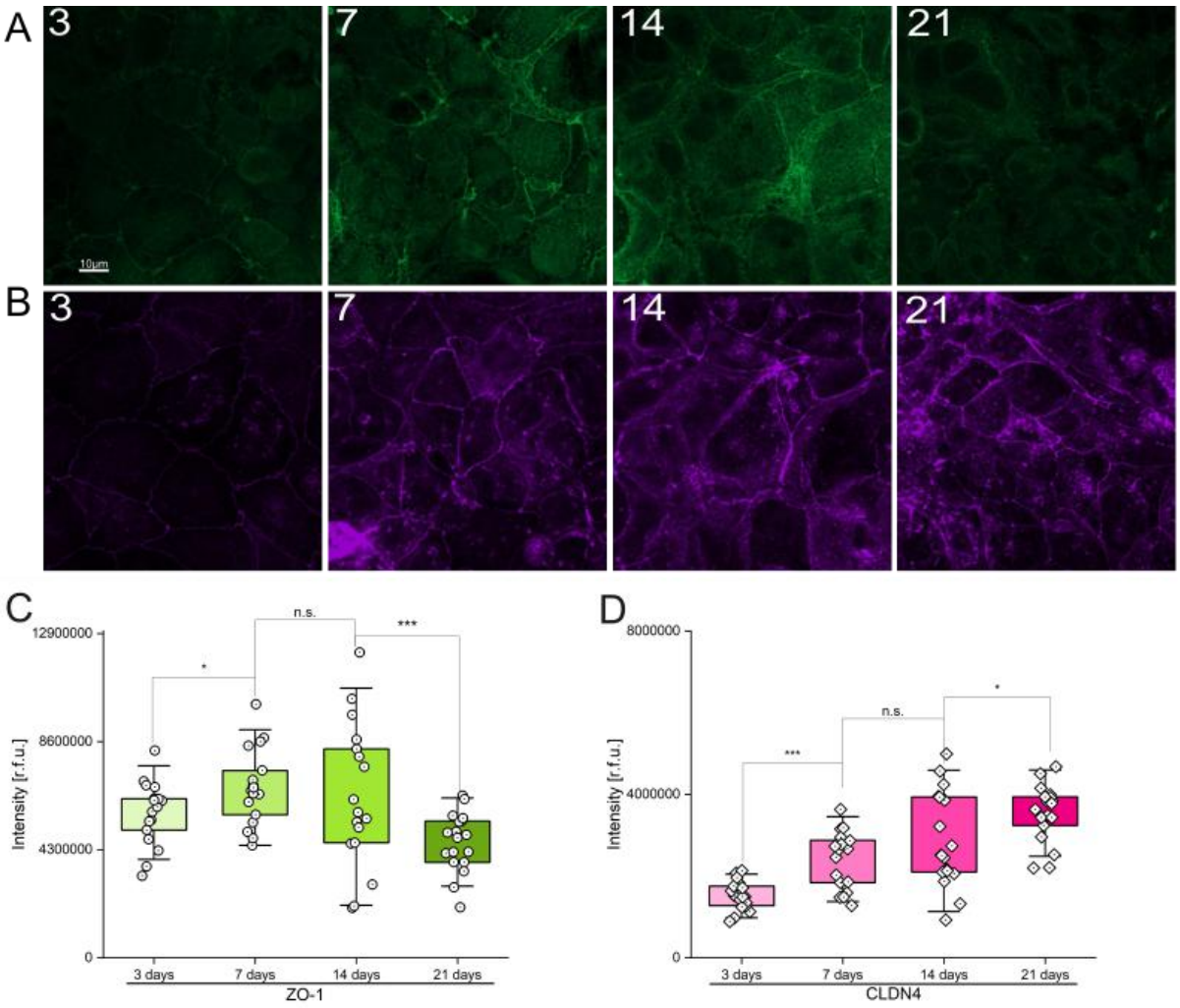

*Figure 12: Tight junction protein expression in Caco-2/HT29-MTX-E12 after 3, 7, 14 and 21 days. (A) Comparison of representative images of zonula occludens 1 (ZO-1, green) (B) Comparison of representative images of claudin 4 (CLDN4, pink) expressed after 3, 7, 14 and 21 days. Images were acquired with an LSM 800 (Zeiss) at X 63 magnification. (C) Quantification of expression of ZO-1 and (D) CLDN4 after 3, 7, 14 and 21 days of differentiation measured by intensity [r.f.u.] derived from 2D images. Scale bar 10 µm; ***p < 0.001, *p < 0.05, n.s. = no significance Students t-Test; Data derived n=18 images per condition from n=3 biological replicates in technical triplicates. Parts of this data have been published during the preparation of this master thesis in Bergen et al. 2025C,.*

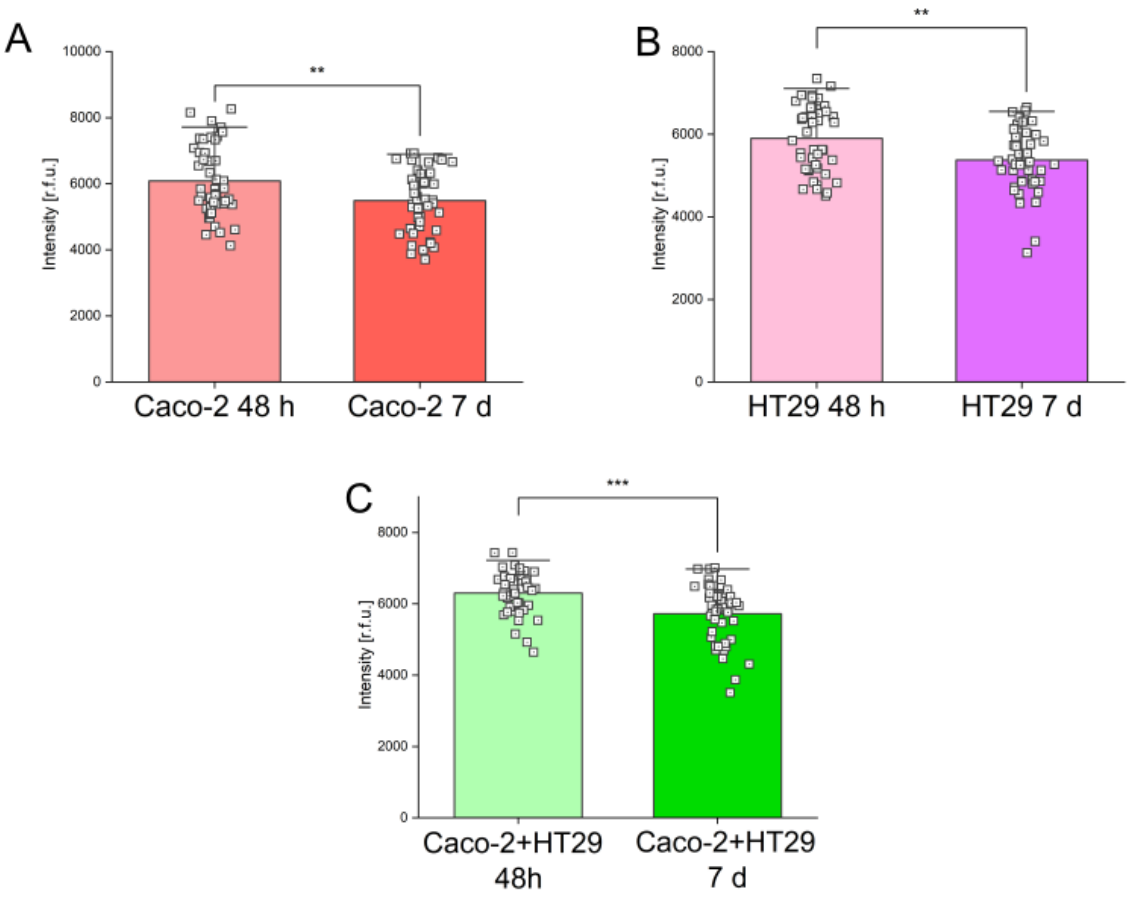

*Figure 13: Piezo1 intensity in intestinal cells after 48 h growth time compared to 7 days. (A) Piezo1 intensity [r.f.u.] in Caco-2 cells after 48 h and 7 days of differentiation. (B) Piezo1 intensity [r.f.u.] in HT29 cells after 48 h and 7 days of differentiation. (C) Piezo1 intensity [r.f.u.] in Caco-2/HT29 cells after 48 h and 7 days of differentiation. Nine 2D-images were analyzed for each condition from n=3 biological replicates. For each image 5 ROIs (region of interest) were randomly selected, with a total of 45 ROIs per condition. Significant differences are indicated with *p< 0,05, **p<0.01, ***p<0,001, Student's t-Test, Welch correction.*

4.1.3. Penetration depth and cell-cell-distance

To further proceed with the characterization of the model, coculture cell monolayer was used in combination of several silica-based rod-shaped mesoporous NPs. Materials used in this study were kindly provided by Prof. Kleitz and synthesized by Dr. Claudia Iriarte-Mesa. Two different sizes were applied: small rod-shaped NPs, with a size of 35x160 nm and bacteria-like NPs, with a size of 200x240 nm. Both kinds of NPs were FITC-labeled. The NPs implemented were either unfunctionalized, methylated or phosphonated based on previous works demonstrating different capacity to cross the mucus layer according to size and chemical surface modification.[18,19]

To further understand the interaction of the NPs and the Caco-2/HT29-MTX-E12 coculture on the nanoscale several experimental layouts were performed, including addition and incubation of these NPs on different long differentiated coculture, with mucus presence and reduction of mucus, resulting in the measurements of penetration depth and cell-cell-distance. The penetration depth and cell-cell-distance of NPs are illustrated in figure 14 and figure 15 respectively. These parameters were analyzed in a 7 or 21 day differentiated coculture (Caco-2/HT29-MTX-E12 9:1) model, as earlier described.

Figure 14 illustrates the results for the penetration depth; panel A shows the process of determining the penetration depth with representative pictures.

Panel B displays the penetration depth of the NPs in a 7 days differentiated coculture. Under mucus-producing conditions, both functionalized srNPs and non-functionalized srNPs exhibited similar, non-significant, penetration depths compared to each other. In mucus reduced conditions this trend was also seen, however the phosphonated srNPs penetrated significantly further than the non-functionalized ones but not compared to the methylated srNPs. In the 7-day differentiated culture the non-functionalized bacNPs still penetrated the least. In mucus and mucus reduced conditions the non-functionalized bacNPs had a significantly lower.

Panel C on the other hand demonstrates the penetration depth of the NPs in a 21-day differentiated coculture. Under mucus-producing conditions, both functionalized srNP variants exhibited similar penetration depths, though comparing them to each other resulted in no statistical significance. Unfunctionalized srNPs on the other hand penetrated less compared to functionalized NPs. In mucus reduced conditions this trend was similar, there were no statistically significant differences when comparing the functionalized NPs to each other,

however when comparing the functionalized with the non-functionalized a significant change could be observed. In contrast, unmodified bacNPs showed significantly reduced penetration compared to srNPs, functionalized srNPs and to the functionalized bacNPs in mucus and mucus reduced conditions.

Panel C displays the penetration depth of the NPs in a 21-day differentiated coculture. Under mucus-producing conditions, both functionalized srNP and non-functionalized srNPs exhibited similar, non-significant, penetration depths compared to each other. In mucus reduced conditions this trend was also seen, however the phosphonated srNPs penetrated significantly further than the non-functionalized ones but not compared to the methylated srNPs. In the 21-day differentiated culture the non-functionalized bacNPs still penetrated the least. In mucus and mucus reduced conditions the non-functionalized bacNPs had a significantly lower penetration depth compared to the functionalized NPs.

Figure 15 demonstrates the results for the cell-cell distance; panel A representative 20 X phase contrast images of the conditions after 6h incubation with the NPs, including a 1000 µm scale bar. The cell-cell distance in a 7-day differentiated coculture with (B) and with reduced (C) mucus was significantly increased when the coculture was incubated with most NPs. The only NP that decreased were the non-functionalized bacNPs. This same trend was also present in the 21-day differentiated coculture with (D) and with reduced (E) mucus. Only bacNPs decreased the cell-cell distance significantly, while the other NPs increased it.

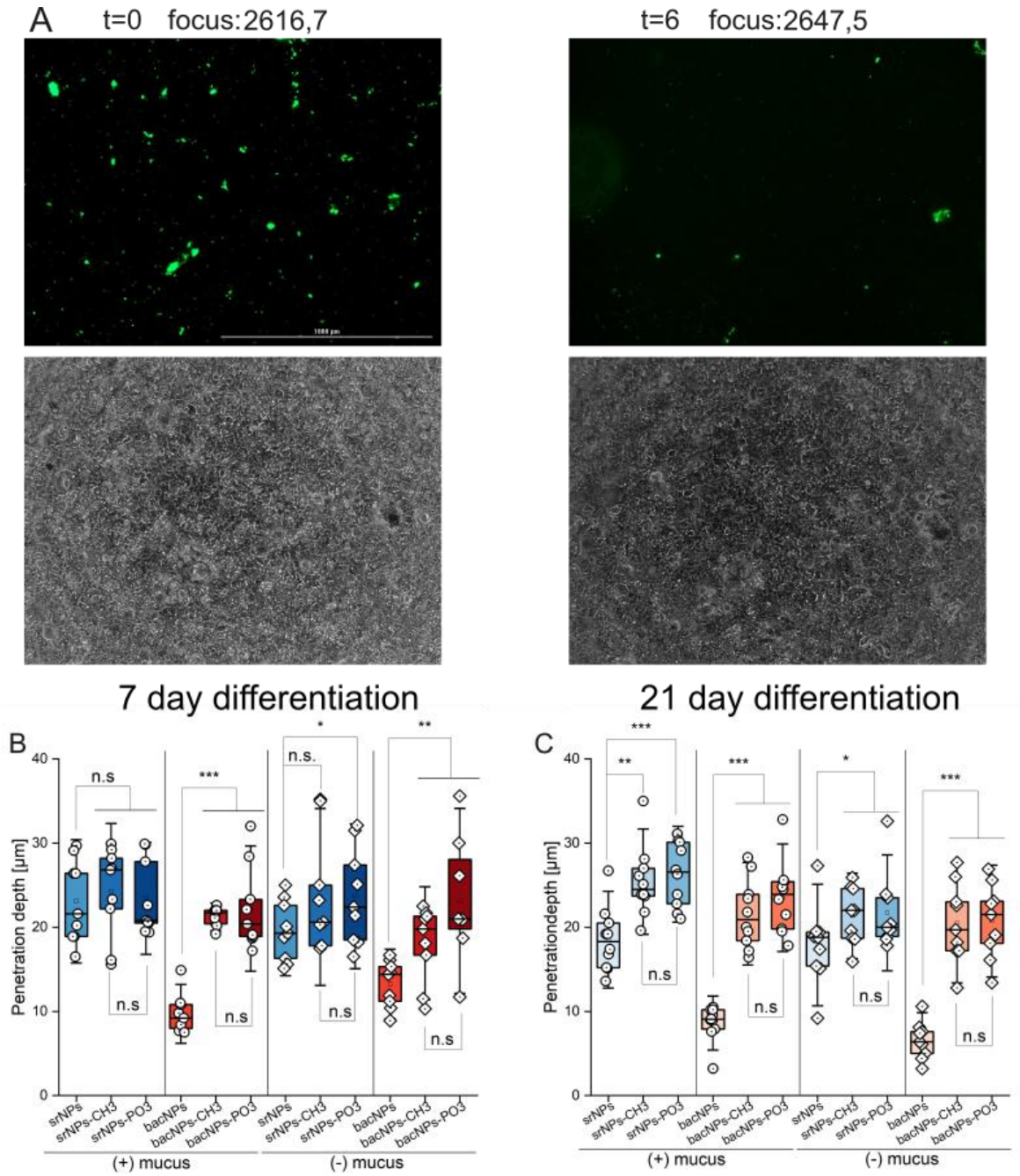

*Figure 14: Penetration depth of srNPs; srNPs-CH_3; srNPs-PO_3; bacNPs; bacNPs-CH_3 and bacNPs-PO_3 in a 7 or 21 day differentiated coculture (Caco-2/HT29-MTX-E12 9:1) model with (+) and without (-) mucus (A) 4 X phase contrast and GFP-channel images of representative nanoparticles in Caco-2/HT29-MTX-E12 coculture at 0 h and 6 h after addition of nanoparticles with them being in focus at t=0 and new focus at t=6. Scale bar 1000 µm. (B) Penetration depth [µm] of nanoparticles in a 7-day differentiated cocultured with mucus and with reduced mucus (C) Penetration depth [µm] of nanoparticles in a 21-day differentiated cocultured with and with reduced. In 3 2D-images the penetration depths were analyzed for each condition from n=3 biological replicates. Resulting in n=9 per condition. Significant differences are indicated with *p< 0,05, **p<0.01, ***p<0,001, Student's t-Test, Welch correction.*

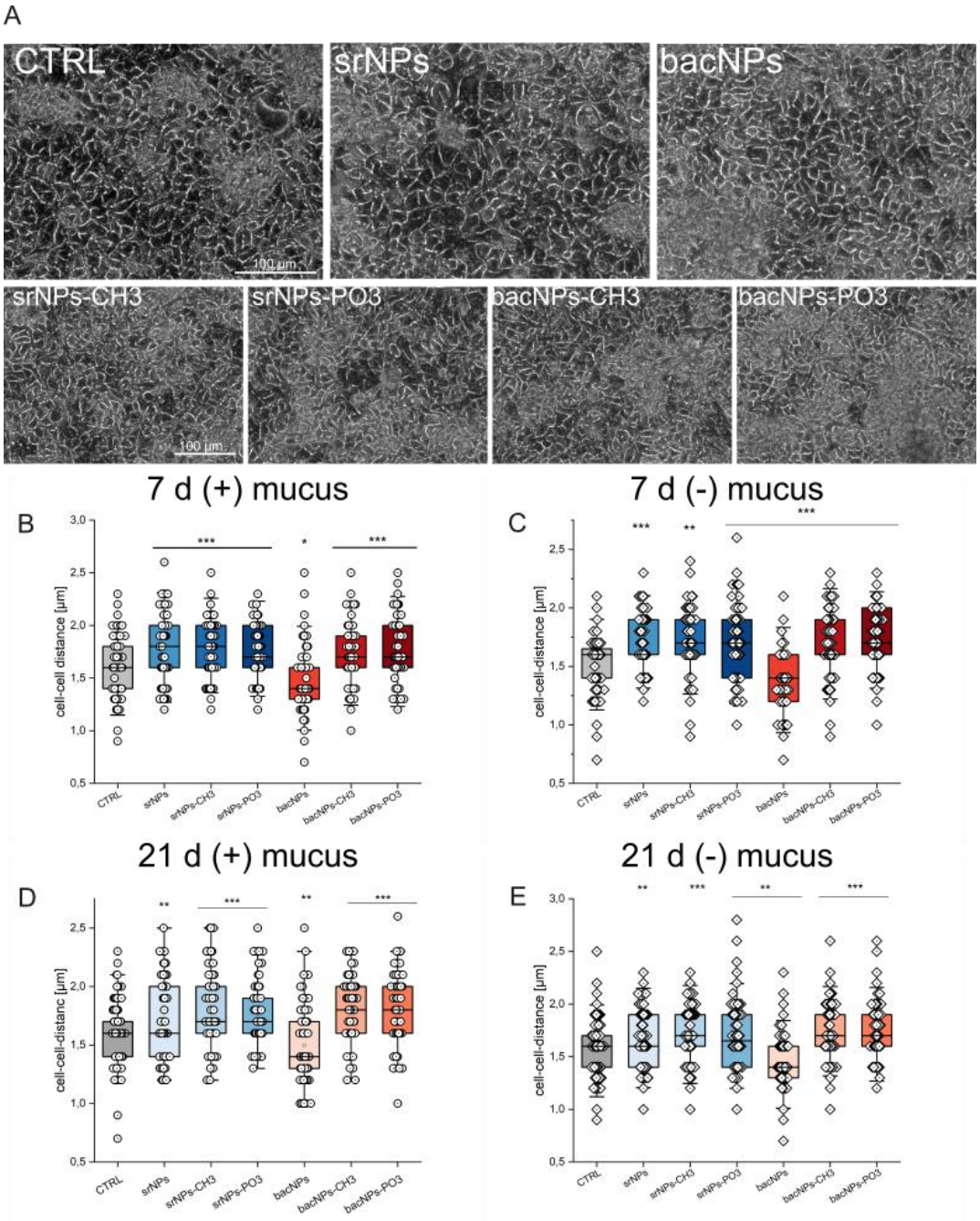

*Figure 15: Cell-cell distance after incubation with srNPs; srNPs-CH_3; srNPs-PO_3; bacNPs; bacNPs-CH_3 and bacNPs-PO_3 in a 7 or 21 day differentiated coculture (Caco-2/HT29-MTX-E12 9:1) model with (+) and without (-) mucus (A) 20 x images of representative nanoparticles in Caco-2/HT29-MTX-E12 co culture at 0 h and 6 h after addition of nanoparticles with them being in focus at t=0 , the old focus and new focus at t=6. Scale bar 100 µm. (B; C) intercellular distance [µm] of nanoparticles in a 7-day differentiated cocultured with (B) mucus and with reduced (C) mucus (D;E) intercellular distance [µm] of nanoparticles in a 21-day differentiated cocultured with (D) mucus and with reduced (E) mucus. In three 2D-images the penetration depths were analyzed for each condition from n=3 biological replicates in technical triplicates. Resulting in n=9 per condition. Significant differences are indicated with *p< 0,05, **p<0.01, ***p<0,001, Student's t-Test, Welch correction.*

4.2. Cytotoxicity

Cell viability was determined, to establish non-cytotoxic concentrations, that the actual effects of chosen substances and not cytotoxic effects would be observed in our further experimental work. Figure 16 shows the cell viability was assessed in Caco-2 or HT29 cells after 24 h attachment. The cells were treated with the substances for 24 h to a range of concentrations of the reference compounds AOH, BPF, BPA, DiDP and LNG. Viability was quantified relative to untreated controls as test over controls [%].

Panel A-E shows the cell viability as T/C [%] of HT29 after incubation with different concentrations of the tested compounds. There were no significant changes in viability in panel A and B, AOH and DiDP respectively. In panel C the exposure to LNG is illustrated, where multiple concentrations slightly reduced the cell viability. BPA and BPF, panel D and E, also did not affect the cell viability. For both compounds, all tested concentrations resulted in no statistical significance compared to the control.

The rest of the panels, F-K, show the cell viability as T/C [%] of Caco-2 cells, when treated with the same substances and concentration ranges. In contrast to the other panels there was no significant reduced or increased cell viability compared to the control. The only exception is in panel K, where 100 µM of BPF led to a moderate, albeit significant decrease in cell viability

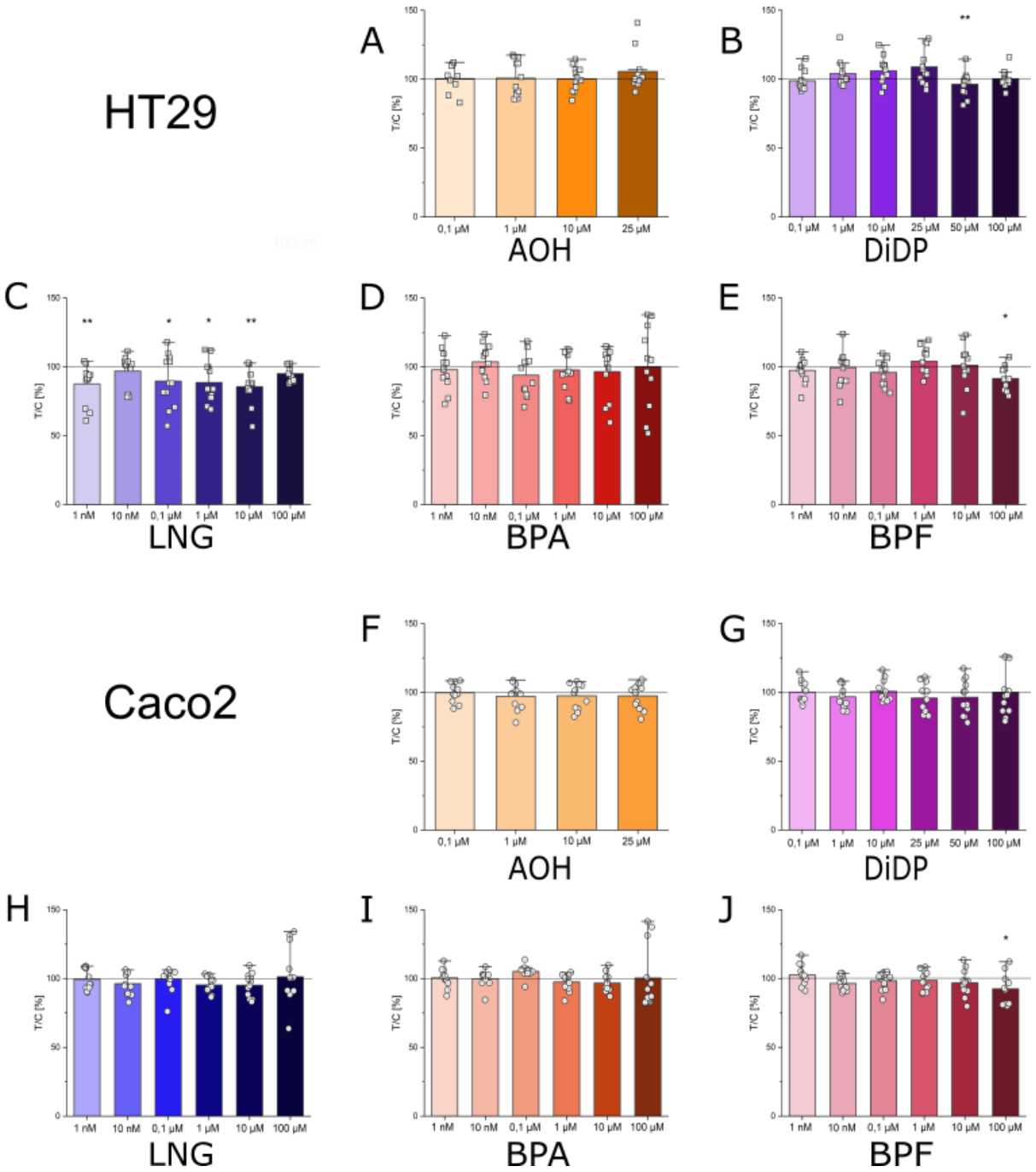

*Figure 16: Cytotoxic impact of endocrine disruptors on HT29 (A-E) and Caco-2 (F-J) cells. Alternariol (A); Diisodecyl phthalate (B), Levonorgestrel (C), BPA (D) and BPF (E) were tested in a concentration range from 0,1 µM to 100 µM in HT29 cells. Additionally Alternariol (F); Diisodecyl phthalate (G), Levonorgestrel (H), BPA (I) and BPF (J) were tested in a concentration range from 0,1 µM to 100 µM in Caco 2 cells. Significant differences to control cells are indicated with *p< 0,05, **p<0.01, ***p<0,001, ANOVA-Test, LSD-Fischer*

4.3. PBPK-model ICE-tool

PBPK models are silico prediction tools that allow to derive how exposure concentrations might result in relevant systemic concentrations.[34–36] Even if the results of the on-line tool have to be considered with caution, we decided to verify what concentration would be expected when assuming oral exposure to the compounds of interest as reported in the literature and use them as first reference to compare with the outcome of the cytotoxicity screening *in vitro*. Figure 17 illustrates the predicted c_{max} [mg/L] of various EDCs in different human tissues following oral intake. These predictions were calculated as modeled by physiologically based pharmacokinetic (PBPK) simulations. For each compound, the left panel displays the graph demonstrating the C_{Max} [mg/L] in the different compartments, while the right column illustrates the corresponding chemical structure of the EDCs.

Panel A depicts the results of the predicted C_{Max} of the simulated PBPK model for AOH (0,25 ng/kg body weight (bw) per day). The PBPK model predicts the highest tissue concentrations appearing in the liver and kidney, while the lower concentrations are predicted to be in plasma, brain, lung, and gut. The chemical structure of AOH is shown in panel B. Panel C illustrates the predicted results for DiDP (1 µg/kg bw per day). Here, the simulation forecasts the greatest accumulation in the liver and kidney, with moderate levels in the gut and lower concentrations in other tissues. The chemical structure of DiDP is presented in panel D. Panel E shows the predicted concentrations of BPA in the different compartments (1,5 µg/kg bw per day). BPA displays the highest simulated concentrations in the liver and kidney, followed by the gut, with minimal distribution to the brain and lungs. The chemical structure of BPA is presented in panel F. Panel G on the other hand displays the results for BPF (0,49 ng/kg bw per day). BPF demonstrates a similar distribution pattern as BPA, with the highest C_{max} in the liver and kidney, moderate levels in the gut, and lower concentrations in the plasma or the lung. The structure of BPF is shown in panel H. Panels I and J display LNG at two concentrations corresponding to its use as either contaminant or as contraceptive (0,7 ng/kg and 0,42 µg/kg bw per day, respectively). Both doses show the same trend, with the highest predicted concentrations being found in the liver and kidney. The chemical structure of LNG is presented in panel K.

The focus on these PBPK models was comparing the resulting C_{max} in the gut with the concentrations we used for the *in vitro* experiments. BPA and DiDP had the highest C_{max} in the gut, which also happened to match best to our used concentrations. The simulated C_{max}

for AOH was quite lower than the concentration used in our testing. As AOH occurs in natural products, there can be a strong variance in concentration in contaminated food, resulting in fluctuating exposure. BPFs C_{max} in the gut, also didn't match the used concentration for *in vitro* experiments. BPF has been replacing BPA for a while now to compare these we wanted to match concentrations for both bisphenols. In the moment there is not a lot of usage and exposure of BPF, through the banning of BPA in food contact material, it can be envisioned that exposure to BPF will increase. Calculated C_{max} gut of LNG in contaminated water or as a pill however is lower than our used concentration.

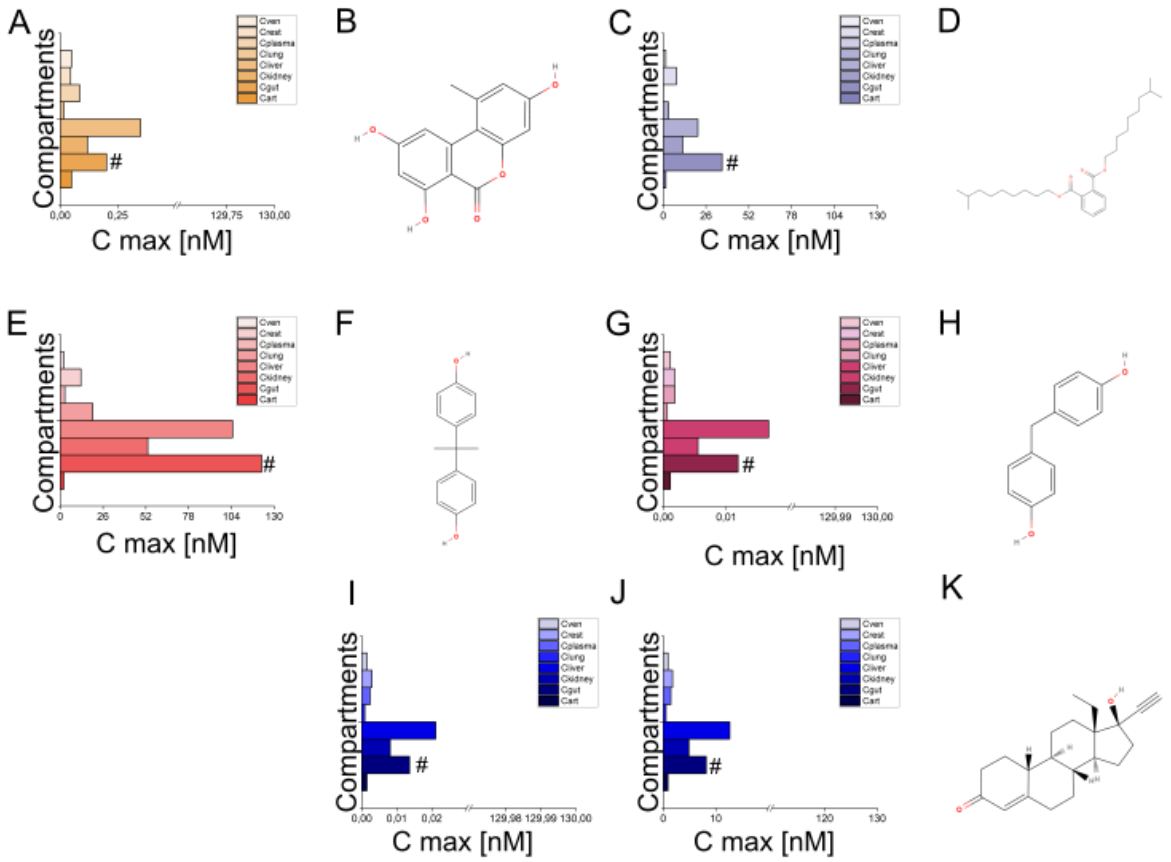

*Figure 17: C_{Max} [nM] of different endocrine disruptors at common exposure concentrations after simulating PBPK models via ICE-online-tool and their chemical structures, C_{Max}-gut is marked with **#**. (A) represents the C_{Max} in different compartments for a treatment of 25 ng/kg AOH for 70 kg bw per day oral intake. (B) shows the chemical structure of alternariol (C) represents the C_{Max} in different compartments for a treatment of 1 µg/kg DiDP for 70 kg bw per day oral intake (D) shows the chemical structure of Diisodecyl phthalate (E) represents the C_{Max} in different compartments for a treatment of 1,5 µg/kg BPA for 70 kg bw per day oral intake (F) shows the chemical structure of Bisphenol A (G) represents the C_{Max} in different compartments for a treatment of 0,49 ng/kg BPF for 70 kg bw per day oral intake (H) shows the chemical structure of BPF (I) represents the C_{Max} in different compartments for a treatment of 0,7 ng/kg LNG for 70 kg bw per day oral intake (J) represents the C_{Max} in different compartments for a treatment of 0,42 µg/kg LNG for 70 kg bw per day oral intake (K) shows the chemical structure of Levonorgestrel.*[117]

4.4. Nuclei analysis

The nuclei analysis was done to start evaluate morphological changes stemming from the endocrine active substances as it was previously described that their rearrangement correlates to changes in the architecture of the monolayer.[18] Here relative area, circularity, roundness, aspect ratio, and solidity were quantified. Figure 18 shows the results of the nuclei analysis in the Caco-2/HT29-MTX-E12 coculture, when mucus was present and figure 19 shows the same analysis, when mucus was reduced.

The substances did not impact the relative area a lot, in the mucus present conditions (A) only DiDP and BPA increased the relative area slightly. When mucus was reduced (B), DiDP and BPA did not influence the area, on the other hand relative area was decreased by AOH.

The circularity is a factor on how close a shape is to a true circle, with the true circle being 100%.[120,121] When mucus was present (C), all EDCs led to decreased circularity, while when mucus was reduced (D), only BPA and AOH changed the circularity, but leading to an increase as compared to the control.

Another shape factor we measured is the solidity, which is defined as the area of the object divided by the area of a convex hull drawn around the object.[121] A similar trend as in the marker circularity can be seen. When mucus was present (E) all EDCs decreased the solidity while when mucus was reduced (F) only BPA and AOH increased the solidity. This might be due to there being a correlation between solidity and circularity.

The roundness of a shape gives a value on how round the shape is. In mucus present conditions (G) AOH, BPA and LNG showed decreased roundness, while when mucus was reduced (H), BPA increased the roundness.

The aspect ratio is the ratio of an object's longer side to its shorter side. When mucus was present AOH, BPA and LNG increased the ratio, though only BPA reduced the aspect ratio when mucus was reduced (J).

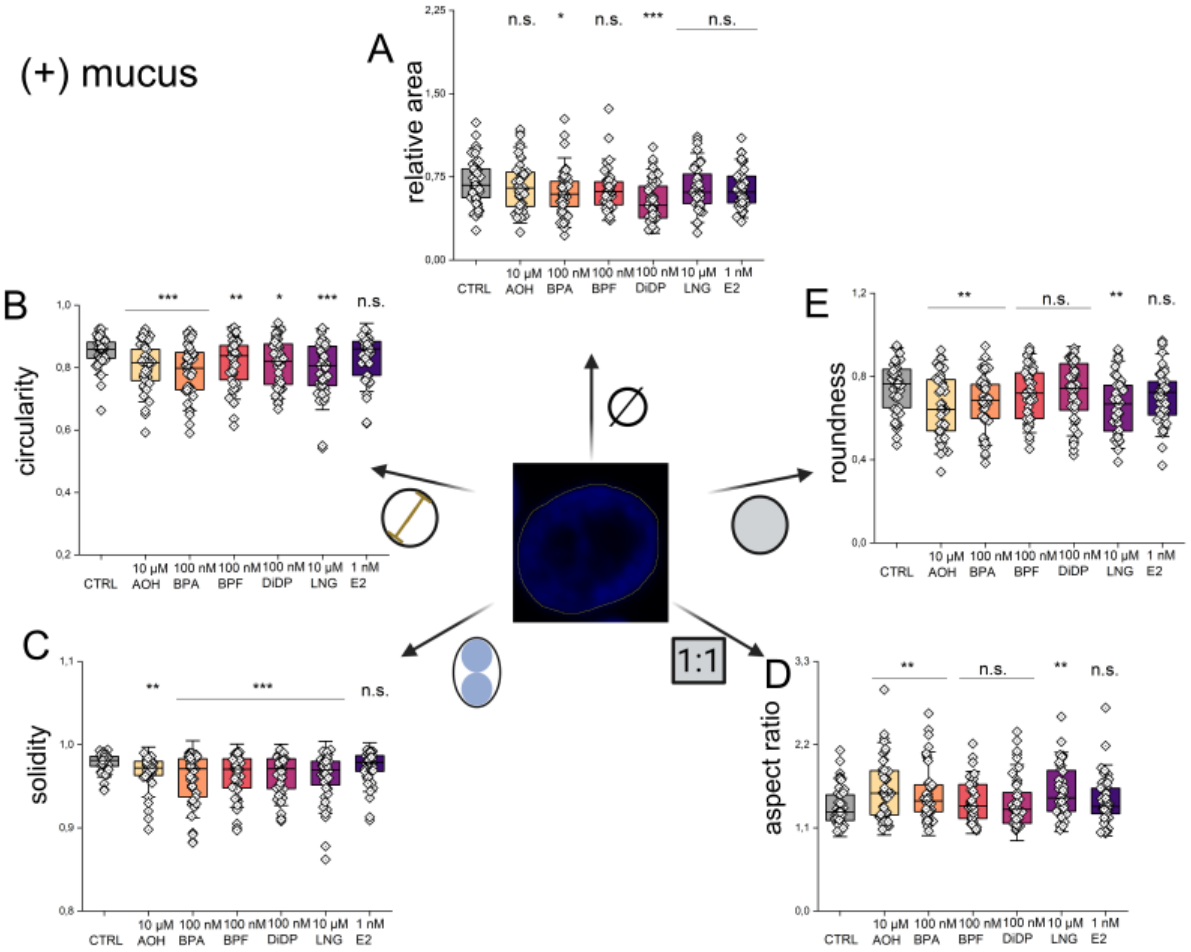

*Figure 18: Impact of EDCs and EACs on the coculture when analyzing the nuclei in CLDN4 stained images with mucus. (A) with mucus impact on relative nuclei area. (B) with mucus impact on relative circularity. (C) with mucus impact on solidity. (D) with mucus impact on nuclei roundness. (E) with mucus impact on aspect ratio. Nine 2D-images were analyzed for each condition from n=3 biological replicates. For each image five nuclei were chosen and outlined, then analyzed with FIJI, which were randomly selected, with a total of 45 nuclei per condition. Significant differences are indicated with *p< 0,05, **p<0.01, ***p<0,001, Student's t-Test, Welch correction.*

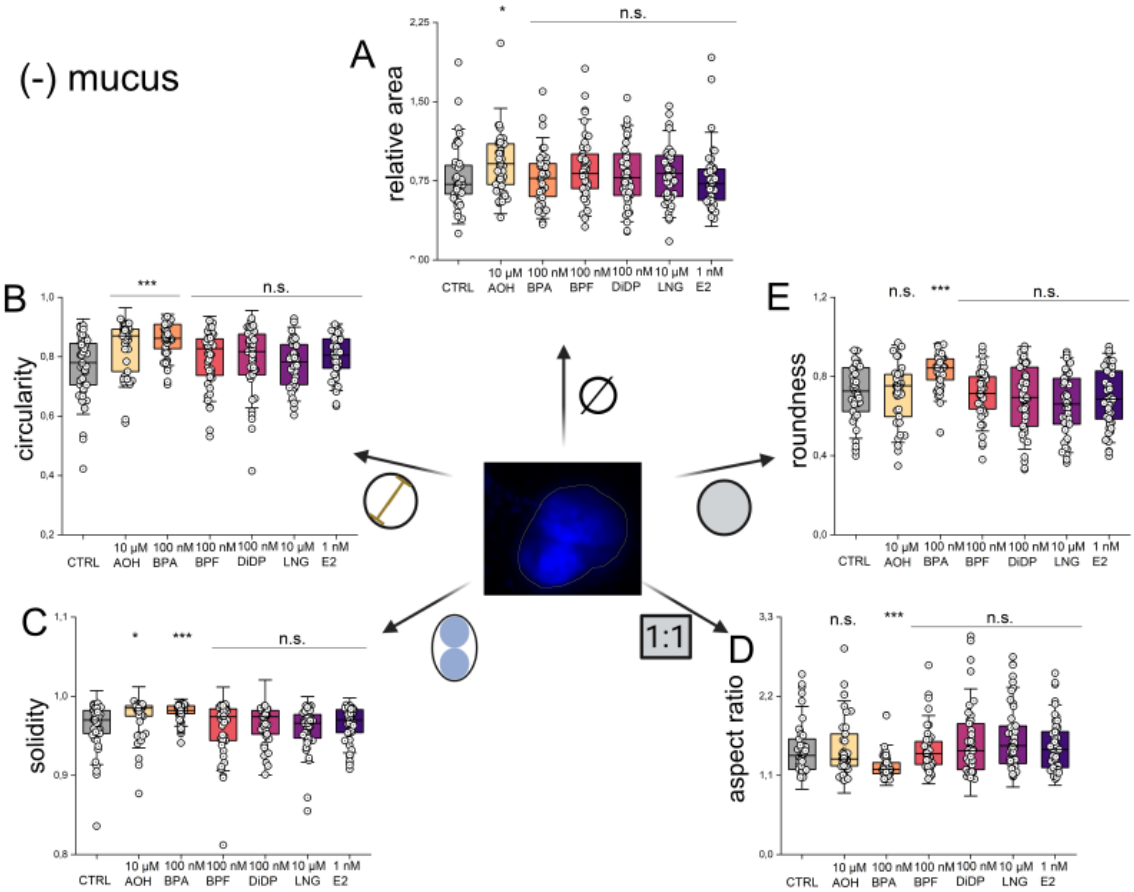

*Figure 19 Impact of EDCs and EACs on the coculture when analyzing the nuclei in CLDN4 stained images with reduced mucus. (A) with reduced mucus impact on relative nuclei area. (B) with reduced mucus impact on relative circularity. (C) with reduced mucus impact on solidity. (D) with reduced mucus impact on nuclei roundness. (E) with reduced mucus impact on aspect ratio. Nine 2D-images were analyzed for each condition from n=3 biological replicates. For each image five nuclei were chosen and outlined, then analyzed with FIJI, which were randomly selected, with a total of 45 nuclei per condition. Significant differences are indicated with *p< 0,05, **p<0.01, ***p<0,001, Student's t-Test, Welch correction.*

4.5. Immunostaining of CLDN4 and ZO-1

4.5.1. Tight junction thickness

The evaluation of immunostainings after treatments with the compounds of interest illustrates the impact and the changes of EDCs on epithelial cells and barrier function. These changes can be seen in TJ morphology. The results of the 2D TJs thickness analysis are presented in Figure 20 panel B-E. Here ZO-1 or CLDN4 were stained in mucus and mucus reduced conditions, after treatment with AOH, 10 µM, BPA, 100 nM, BPF, 100 nM, DiDP, 100 nM, LNG, 100 nM, and E2, 1 nM. Panel A shows representative images taken from slides with mucus present and different treatments.

Panel B-E illustrates the effect of the earlier mentioned EDCs on the thickness of TJs, ZO-1 and CLDN4, in presence of mucus or after the reduction of mucus in a Caco-2 and HT29-MTX-E12 coculture model. In panel B, with mucus, and C, without mucus, the results for the thickness of ZO-1 are shown. The EDCs decreased thickness in both conditions. A similar trend can be seen with the TJ CLDN4. In panel D, when mucus was present, TJ thickness did decrease, except when the cells were treated with BPF. Though when mucus was reduced, panel E, all TJ thicknesses decreased significantly by treating the cells with the EDCs.

4.5.2. Z-distance and height

To evaluate the impact of EDCs on TJs not only 2D images but also 3D images were taken. Figure 21 illustrates the impact of EDCs on the 3D morphology of the coculture. Panel A reports representative z-stacks.

Panels B-E show the results for the calculated z-distance from the z-stacks. This distance is the difference between the slice with the highest DAPI signal (nuclei) and the slice highest ZO-1/CLDN4 signal (TJs) was quantified to assess changes in epithelial monolayer architecture following exposure to earlier used EDCs, in the presence mucus and absence mucus of a mucus layer.

Panel B and C shows the z-distance of ZO-1, when mucus was present. The control z-distance of ZO-1 was around -1, a reduction of mucus also let this distance decrease. In mucus present

condition, panel B, all substances, except BPF, decreased the z-distance. This trend was not seen in panel C, where mucus reduced conditions for ZO-1. There only BPA and DiDP reduced the z-distance significantly to the control, while the other substances had similar values as the control. Evaluating the results from CLDN4, there the z-distance were only positive values. In panel D, under mucus present and panel E, reduced conditions the EDCs didn't change a lot. When mucus was present only E2 and AOH decreased the z-distance. In the mucus reduced conditions, the same substances and DiDP reduced the z-distance compared to the control.

The cell layer height illustrates how thick the cell layer in the z-axis is. This data is presented in panel F, with mucus and G, without mucus. When mucus was present, all EDCs except DiDP and LNG reduced the height significantly. Though a reduction in mucus changed this trend. There ever EDC, excluding BPF, reduced the height significantly.

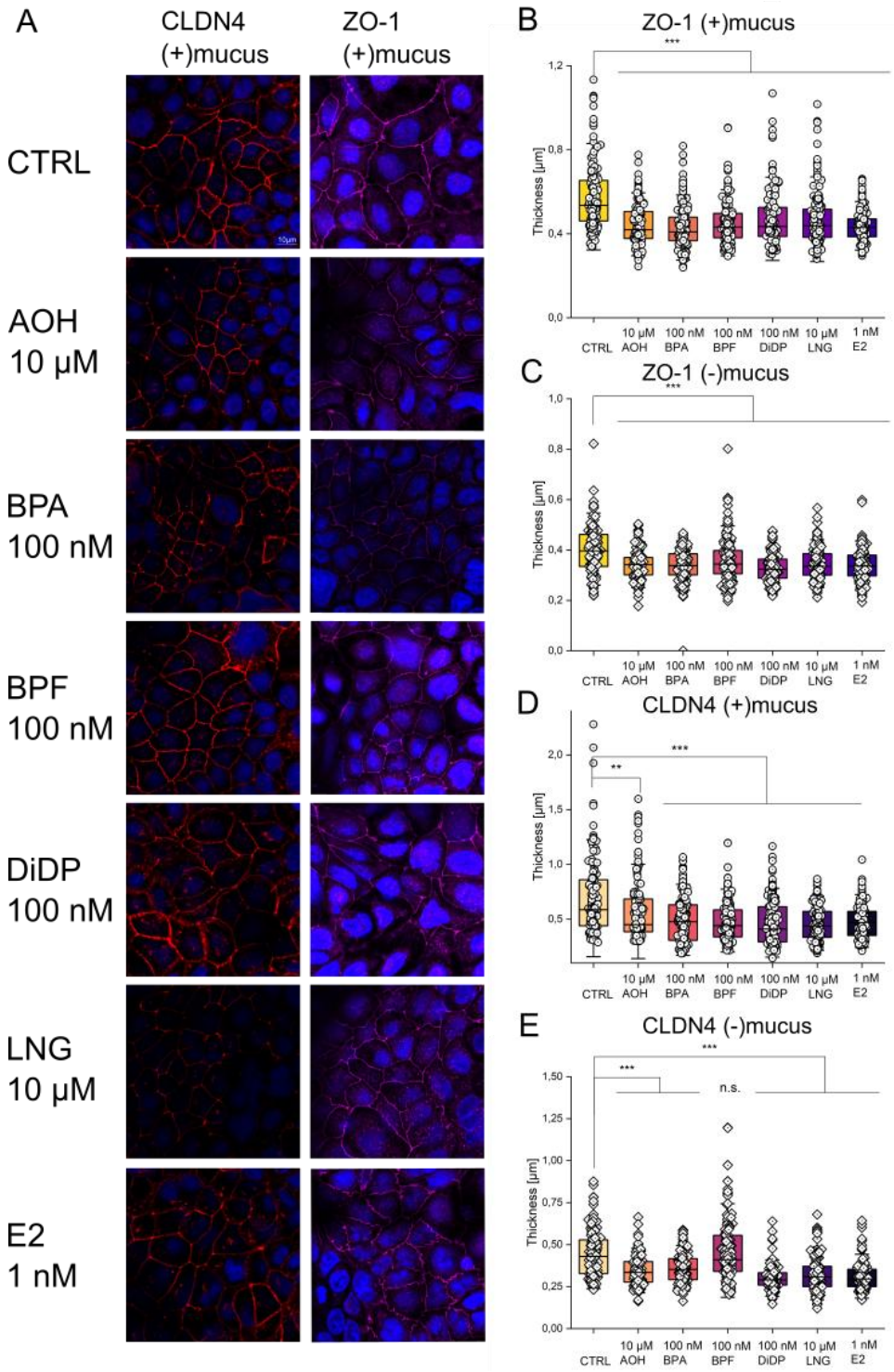

*Figure 20: Tight junction protein signal of ZO-1 and CLDN4 in Caco-2/HT29-MTX-E12 after treatment with several EDCs. (A) representative pictures of ZO-1 and CLDN4 with mucus. Scale bar 10 µm. (B-E) Quantification of tight junction thickness in ZO-1 with mucus (B) and without (C) and in CLDN4 with (D) and without (E) mucus. (G) Nine 2D-images were analyzed for each condition from n=3 biological replicates in technical triplicates. For B-E for each image five 15 tight junctions were randomly chosen, and the distance was measured with FIJI, with a total of 135 distances per condition. Significant differences are indicated with *p< 0,05, **p<0.01, ***p<0,001, Student's t-Test, Welch correction.*

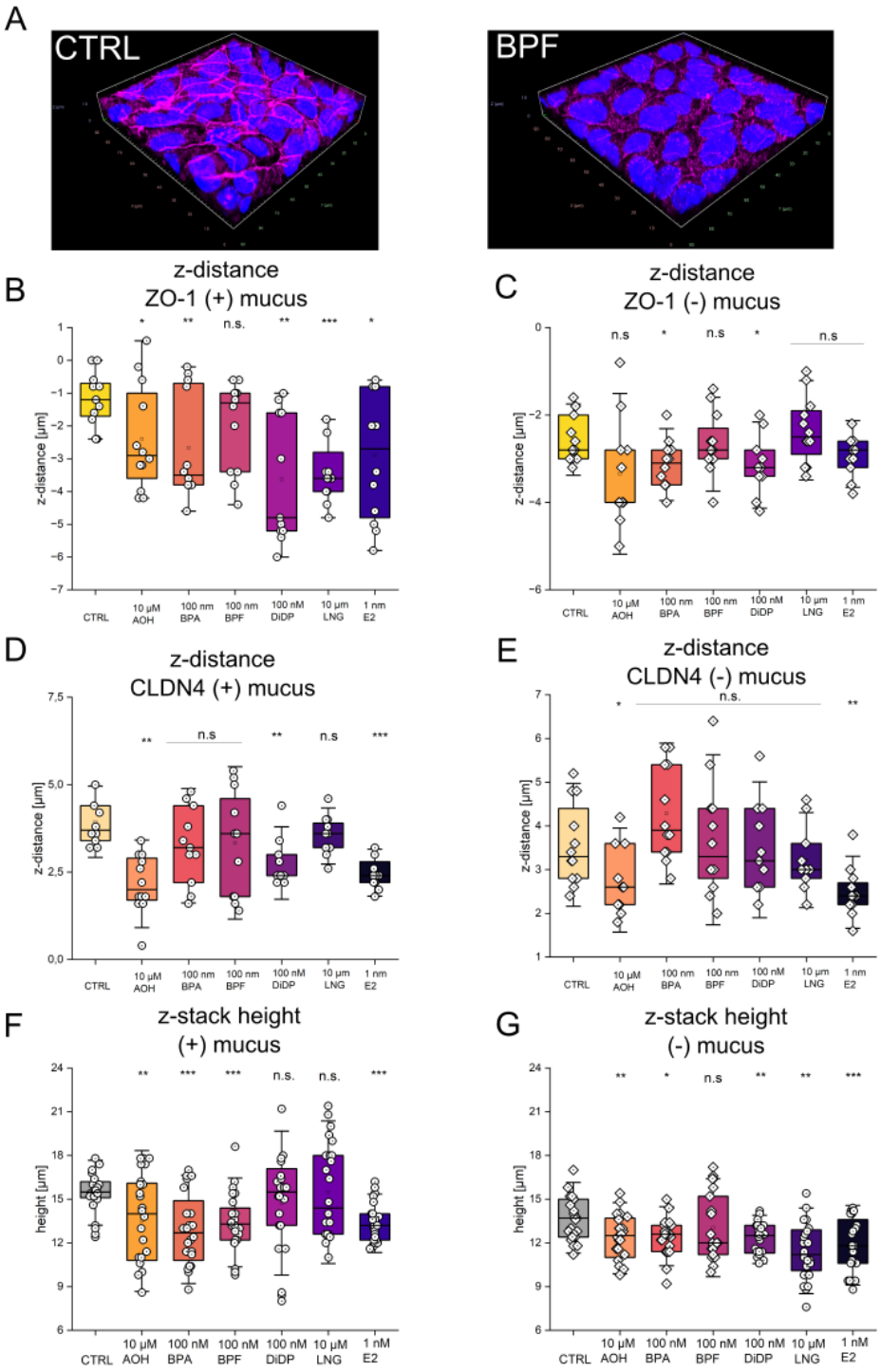

*Figure 21: Tight junction protein signal of ZO-1 and CLDN4 in Caco-2/HT29-MTX-E12 after treatment with several EDCs. (A) representative z-stacks of ZO-1 with mucus. (B-E) Quantification relative z-distance in ZO-1 with mucus (B) and without (C) and in CLDN4 with (D) and without (E) mucus. (F; G) Quantification of z-stack height with (F) and without (G) mucus. Three z-stacks were analyzed for each condition from n=3 biological replicates, for (F; G) ZO-1 and CLDN4 results were combined resulting in n=6. For B-E and F; G the z-stacks were quartered, resulting in 12 or 24 values per condition respectively. Significant differences are indicated with *p< 0,05, **p<0.01, ***p<0,001, Student's t-Test, Welch correction.*

4.5.3. Concentration dependency

To evaluate the concentration dependent effect of EDCs on TJ morphology we focused on one single substance BPF. We focused on BPF, due to two main reasons. Firstly, due to the ban on BPA in food contact materials,[43] BPF, as a substitute for BPA, will be used more in industry, leading to greater exposure, thereby gaining greater importance for toxicologists. Secondly BPF has not been impacting morphology of tight junctions as strongly as other EDCs or EACs. EDCs can show a non-monotonic effect, we wanted to elucidate if BPF could have such an impact, especially because BPA shows a non-monotonic endocrine disruptive response.[122]

These results are shown in figure 22, which illustrates the effects of BPF at different concentrations (1 nM, 10 nM, and 100 nM) on the Caco-2/HT29-MTX-E12 coculture assessed both in the presence and absence of mucus. Panel A displays representative pictures for the different concentrations in both conditions.

Panels B and C present the z-distance at the earlier mentioned treatments and mucus present, panel B, or mucus reduced, panel C, conditions. At 100 nM BPF, a significant increase in z-distance is evident compared to control and lower BPF concentrations in the absence of mucus and the presence of mucus. There is no effect at 10 nM and 1 nM BPF.

Panels D and E illustrate the measured thickness of the TJ marker. Both panels reveal a similar trend. While panel D shows the results of mucus conditions, panel E shows mucus reduced conditions. In mucus present and mucus reduced conditions the treatment reduced the thickness significantly. Except for the treatment with BPF 100 nM in mucus conditions, there no significance compared to the control is seen. Furthermore, the thickness of the TJs seems to decrease the lower concentrations are treated with. This can be seen due to the significant change comparing BPF 1 nM and BPF 10 nM to BPF 100 nM in mucus present and mucus reduced condition. Interestingly there was no significant change comparing 10 nM and 1 nM

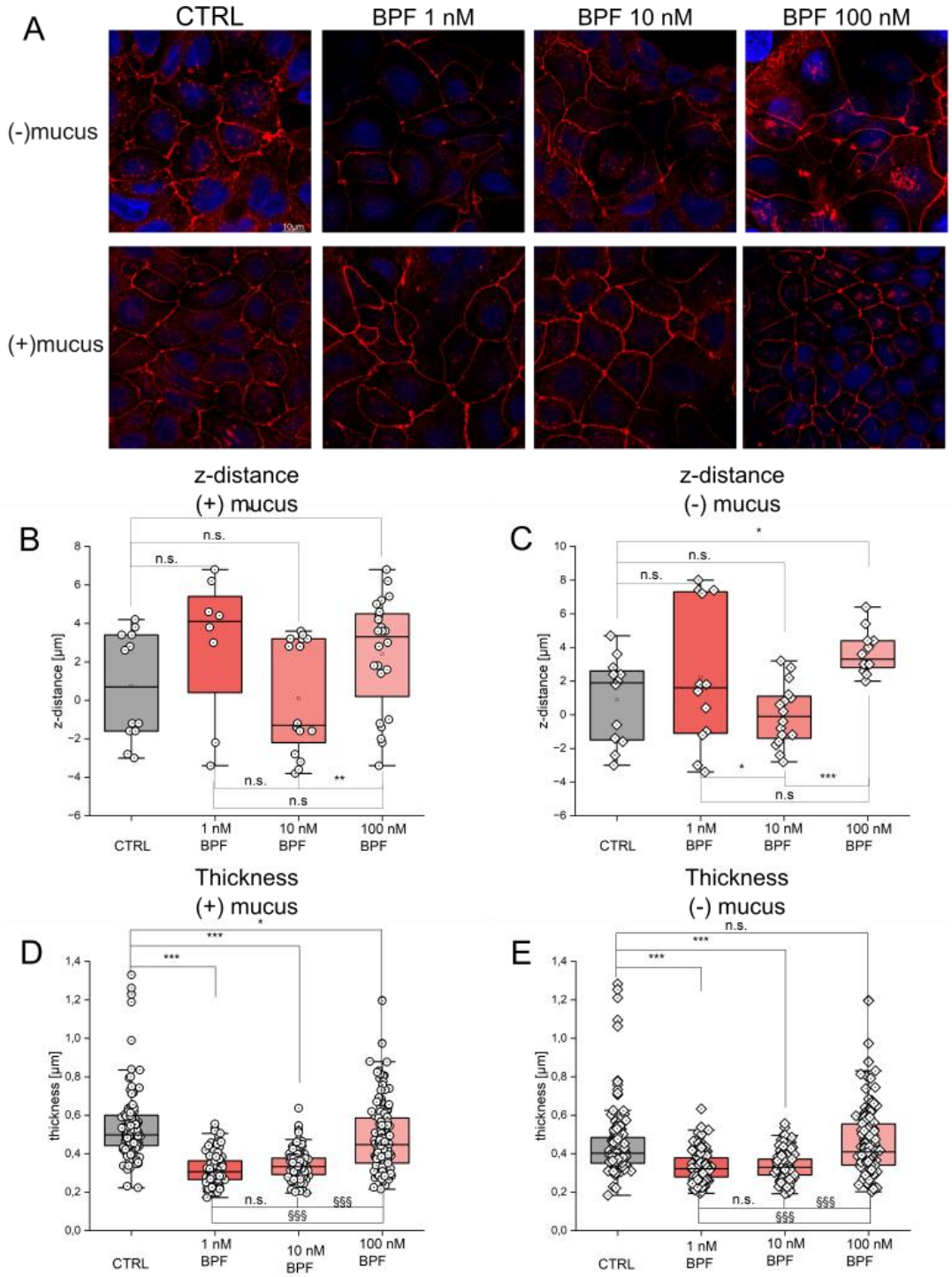

*Figure 22: Tight junction protein of CLDN4 in Caco-2/HT29-MTX-E12 after treatment with different concentrations of BPF. (A) (G) Representative 2D images CLDN4 with mucus. Scale bar 10 µm. (B; C) Quantification relative z-distance in CLDN4 with mucus (B) and without (C). (D; E) Quantification of tight junction thickness in CLDN4 with mucus (D) and without (E). Three z-stacks were analyzed for each condition from n=3 biological replicates. For B; C the z-stacks were quartered, resulting in 12 values per condition. Nine 2D-images were analyzed for each condition from n=3 biological replicates. For D; E for each image five 15 tight junctions were randomly chosen, and the distance was measured with FIJI, with a total of 135 distances per condition. Significant differences are indicated with *p< 0,05, **p<0.01, ***p<0,001, Student's t-Test, Welch correction.*

4.6. Lucifer-yellow assay

To determine the impact of selected bisphenols on permeability, we performed the Lucifer yellow assay. This was done to assess direct and indirect impacts of EDCs on permeability. During differentiation and before and after treatment with substances and NPs TEER-measurements were performed. The results of the Lucifer yellow assay and the TEER measurements are presented as test over control [%] values and are illustrated in figure 23.

Panel A-C displays T/C [%] TEER values before (A) the treatment with BPA or BPF, after (B) treatment with substances but before treatment with NPs and after (C) both treatments. Before any treatments were performed there was no significant change in TEER values compared to each other or compared to the control. After the treatment with the substances BPA 100 nM and BPF 10 nM decreased the T/C [%] values. After subsequent treatment with NPs BPF 10 nM and BPA 100 nM still had a significant T/C [%] value compared to the control. Interestingly only BPF 10 nM was significant compared to the NPs control, while BPA 100 nM was not. In general, there was a decreased T/C [%] value over this time frame, values started at 100 % T/C at d6 and averaged at 90 % at d7 t6.

Panel D displays the results of the Lucifer yellow assay, where all treatments did increase the T/C [%] values of permeability compared to the control. When no NPs were added, BPF 100 nM triggered the highest increase in permeability, being significantly higher as the lower concentration of 10 nM. However, the data presented high variability, and an even lower concentration of 1 nM was not significantly lower than 10 nM and even had a higher average value, then the higher concentration of 10 nM. The addition of NPs changed this trend. The average T/C [%] of permeability increased from control with NPs, with ascending BPF concentrations. BPF 10 and 100 nM were significantly higher compared to control, when NPs were added. For BPA 100 nM with NPs this was not the case. Interestingly to note is that BPF 10 nM with NPs have a significant stronger permeability, compared to BPF 10 nM, when no NPs was added.

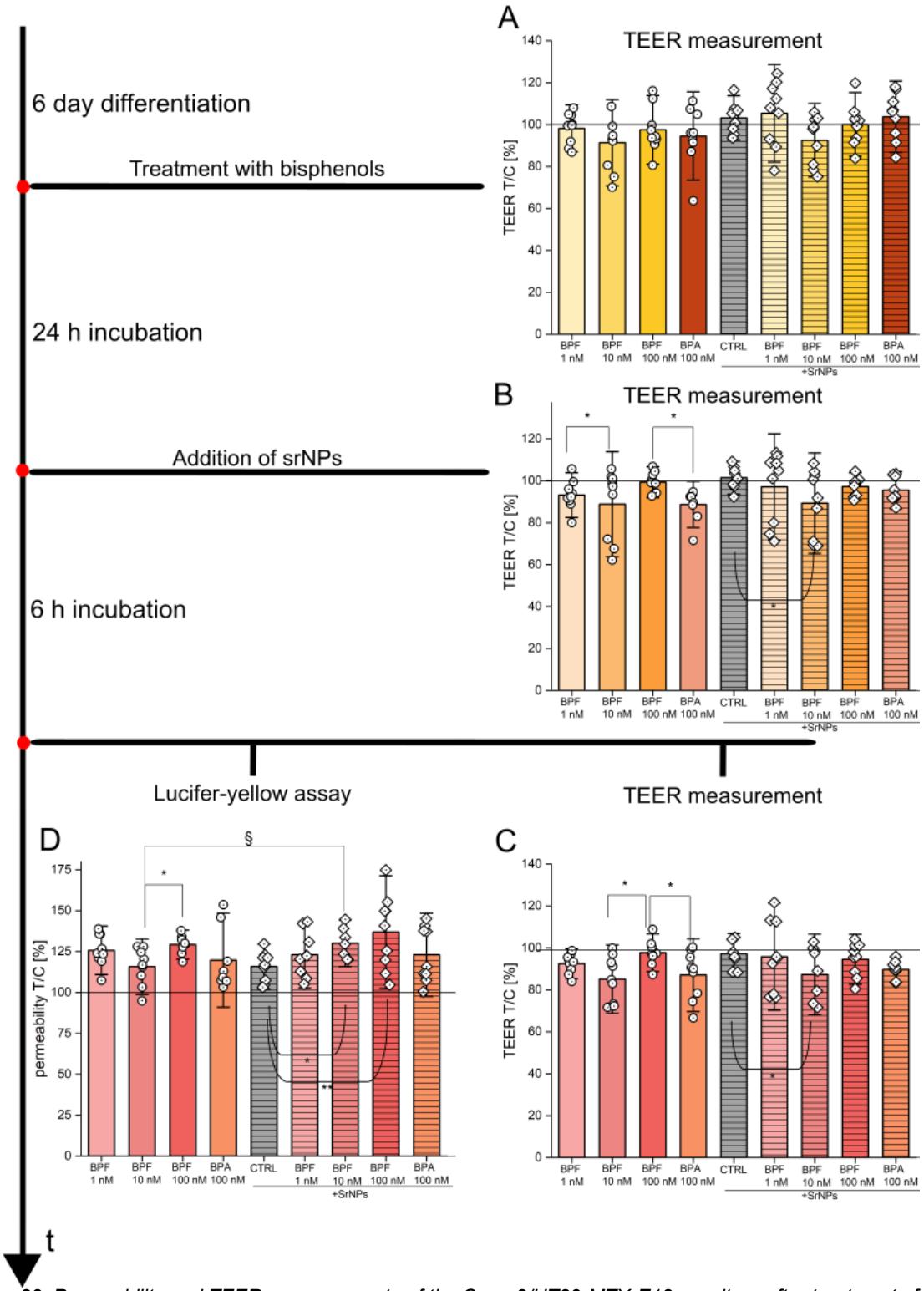

*Figure 23: Permeability and TEER measurements of the Caco-2/HT29-MTX-E12 coculture after treatment of BPF in different concentrations or BPA and subsequent incubation with srNPs. (A-C) TEER measurements before treatment (A), before srNPs addition (B) and after both (C). (D) T/C [%] of the permeability after prior incubation with BPA (100 µM) or BPF (1 µM, 10 µM; 100 µM) in the presence of mucus and for half successive incubation with srNPs for 6 h. All conditions in panel D were significant to the control. The experiment was done in three biological and technical replicates. *p< 0,05, **p<0.01, ***p<0,001, ***p < 0.001; Student's t-test (Welch correction).*

5. Discussion

EDCs and EACs can be of natural origin or manmade substances which pose a global problem. Exposure to these chemicals mainly occurs through ingestion, by inhalation or dermal contact. EDCs and EACs have been increasing as food contaminants and therefore oral exposure has become unavoidable. Hazard characterization is of utmost importance to better understand the underlying potential health outcomes upon exposure to these substances. The primary aim of this thesis was to investigate the impact of EACs of various origin on the morphology of intestinal cell monolayer with specific focus on the TJs distribution.

For Caco-2 monocultures differentiation can lead to establishment of absorption properties but also to creation of barrier function, depending on differentiation period.[18,123] A key role in every *in vitro* experiment is choosing the right cell line, seeding density and differentiation time. As part of the development of complex cell culture systems to be further explored in the context of new approach methodologies (NAMs), cell differentiation is an essential part of bringing *in vitro* models closer to reality. To better simulate the human gastrointestinal tract, we built on an established coculture model to enhance its features, verifying it throughout multiple experimental layouts to gain further insight on it.

Based on the data collected in this work it was possible to identify similarity and differences in the response profile after 7- and 21-days differentiation. Here the 7-day differentiation period for the Caco-2/HT29-MTX-E12 coculture model, which we already established in Bergen *et al*., 2025[18] resulted rather similar in the response profile to the conventional 21 day standard for Caco-2 monocultures.[124] Additionally we added HT29-MTX-E12 goblet cells, which produce mucus. This had multiple reasons, firstly as seen in figure 11 TJs do not necessarily increase with the differentiation time. For the scaffolding protein ZO-1, figure 11 panel C, the highest intensity was found in the 7 and 14 day differentiated cells, while a longer differentiation of 21 days decreased the expression signal. This trend was not continued by the other evaluated TJ protein CLDN4, figure 11 panel D, in which the signal intensity increased steadily, with prolonged differentiation period. Part of choosing the coculture over a Caco-2 monoculture was the findings of Béduneau *et al*. 2014[125], stating that a coculture mimics the permeability of the human gut better than a monoculture. Another important factor is the ratio of Caco-2 to HT29-MTX-E12 cells, where we chose a ratio of 9:1. While maintaining the versatility of the Caco-2 monolayer, the added feature of the mucus produced by HT29-

MTX-E12 cells, is essential to mimic the human gastrointestinal epithelial layer. Strugari *et al*. 2018[126] demonstrated the difference in models using 10:0, 7:3, 5:5 and 0:10 (Caco-2/HT29-MTX-E12) seeding ratios. Their results showed that a higher amount of HT29-MTX-E12 cells decreased TEER values, thereby resulting in weakened barrier function. Consequently, our choice of smaller amounts of HT29-MTX-E12 cells, was that larger amounts of Caco-2 cells would give us a greater amount of TJs and an increased barrier function, while not losing the additional protective dimension through the layer of mucus. Enhanced barrier function, due to a higher ratio of Caco-2 cells in the coculture was also proven by Hilgendorf, C. *et al.* 2000[127], where the higher ratio of Caco-2 cells leads to an increase of TEER values, which correlate negatively with the permeability. This adds to the view that there was also less permeability in the culture, when being compared to other cultures exhibiting higher amounts of goblet cells. Thus, the 7-day model, with a 9:1 ratio of cells, offers a pragmatic solution for evaluating mechanical and chemical induced barrier disruption.

To further understand the given coculture we looked at membrane proteins, focusing on mechanosensitive Piezo1 ion channels. Here the primary role as a mechanosensitive ion channel is transducing mechanical forces into biochemical signals.[128] For example, Piezo1 ion channels can effect claudin1 and ZO-1 expression, the first one through regulation of the ROCK1/2 pathway. This means activation of Piezo can induce epithelial dysfunction, resulting a negative correlation with TJ expression.[129,130] Differentiation of Caco-2 cells leads to increased TJ expression, applying this principle, it should lead to a decrease in Piezo 1 signal.[131] Similar results can be seen in figure 12, where a shorter differentiation time of the cultures lead to higher relative intensities, compared to the longer differentiated ones. This may be a sign that the Piezo1 ion channel enhances the differentiation process. In fully differentiated epithelial systems the Piezo1 ion channel exhibits a regulatory role, maintaining barrier function and cellular homeostasis. On this topic Jiang *et al.* 2021[132] found that the Piezo1 ion channel negatively regulates the barrier function by regulating the epithelial barrier function by affecting the expression of TJ proteins, such as claudin 1. Consequently, Piezo1 expression should decrease, the longer an epithelial cell line differentiates, coinciding with our results.

To further explore the extent of the Caco-2/HT29-MTX-E12 coculture model, we tested the barrier function with a variation of mesoporous silica-based NPs. This experiment was carried out to demonstrate the difference between a 7 day and a 21-day differentiated coculture and to compare results to figure 12, which showed that a prolonged differentiation time does not

necessarily correlate with increased TJ protein signal intensity and thereby does not necessarily increase barrier function. After application of the NPs, we observed the penetration depth of the NPs and measured the intercellular distances in 20x images. As seen in figure 14, all NPs, except the non-functionalized bacNPs, were able to penetrate toward the coculture very well. In the presence of mucus a broader distribution was present, this could be due to particle retention in the mucus layer.[133] The maturity of the culture did not change the trend, but led to some cases of increased penetration, which might be due to a longer time frame of mucus production. Additionally, it could be observed that the functionalized NPs (methylated; phosphonated) could penetrate better than the non-functionalized. In general data collected in this thesis align with the results in Bergen *et al.* 2025[18], where bacNPs penetrated significantly less than srNPs in the same coculture system. Though in their study, when mucus was reduced no significance between srNPs and bacNPs were found, when analyzing penetration depth. In this work the reduction of mucus did not change the finding that srNPs can penetrate deeper than bacNPs. With these results it can be concluded that the mucus protects the gut layer from solid particles as the bacterial shaped NPs, while smaller rodNPs and functionalized NPs can penetrate the mucus very well. Another aspect to consider is the size of NPs: 35 × 160 nm for srNPs and 200 × 450 nm for bacNPs. Cybulski *et al*. 2025[134] previously described that shape, size and charge play a big role in the penetration depth of NPs. They suggest that larger and neutral or positively charged NPs penetrate less than others. In our case the size of unfunctionalized particles mattered, where the bigger NPs penetrated less than smaller ones. Additionally it is known that 25-50 nm NPs penetrate similarly to each other, while bigger particles of the size 200 nm penetrate less.[135] Though Agarwal *et al*. 2015[136] found no distinct difference in spheroid penetration when comparing size. Another factor to consider is the charge and polarity of the NPs. The functionalization was achieved through methylated and phosphonated NPs, while the first increased the hydrophobic properties of the silica surface, the latter increased the colloidal stability of the particles, added a negative charge and increased hydrophilicity.[19] Interestingly, comparing data with Iriarte-Mesa *et al.* 2024[19] with the ones obtained from our experimental work, we had similar penetration depths in phosphonated NPs. We did not find a significant difference between the different functionalized small rod NPs. This difference could be due to Iriarte-Mesa et al. using differentially shaped NPs. Since our NPs were rod shaped and theirs spherical NPs, which also were bigger in size, when compared to the srNPs. This could lead to the conclusion that shape significantly impacts penetration depth in addition to functionalization. As we demonstrated NPs penetrated more strongly towards the Caco-2/HT29-MTX-E12 cells, when functionalized. Supportive of the coherence of the model, a

reduction of mucus leads to less penetration depth. We hypothesize this being due to there being more mucus to penetrate in total.

Additionally, intercellular distances were measured in 20x images, to determine if the NPs could jostle in between the cells and push them further apart after an incubation time of 6 h. The results can be seen in figure 15, where in all conditions, the NPs indeed increased the cell-cell distance, except the non-functionalized bacNPs, which decreased the cell-cell distance compared to the control. This supports the view that the bigger the particle, the harder it is to penetrate the protective layer of the mucus.[18,137] This data is supported by Bergen *et al*. 2025[18], where we also found that bacNPs penetrate less compared to srNPs. There it is tempting to hypothesize that the cells could decrease the intercellular space as resembling a mechanism to protect them from bacteria or bacteria-like NPs and therefore a decreased cell-cell distance arises. To conclude the work with NPs, our data supports the view that size and charge could help achieving penetration depth and tailored adjustment of the intercellular distance.

After characterizing the coculture model we moved on to elucidate the cytotoxic or proliferating effects of selected EDCs, as some hormonally active substances can have an impact on cell growth in specific cell lines, like ovarian cells.[138] The substances were tested in multiple concentration ranges derived from common *in vitro* concentrations. As seen in figure 16 no strong de- or increase can be observed in the CellTiter-Blue® Cell Viability Assay. The cell viability did decrease in HT29 cells in several different concentrations, but when carrying out the experiment in Caco-2 cells no significant change in cell viability can be seen. These results correspond with cytotoxicity data from the literature, while not matching the same cell lines, the same trend, no cytotoxicity at these concentrations was confirmed.[29,139,140] For the purpose of our study, it was essential to use non-cytotoxic concentrations in assays, to better assess the impact of potential functional impairment. With these considerations we chose the following concentrations for further experimental work: 10 µM AOH; 100 nM BPA; 100 nM BPF; 100 nM DiDP; 10 µM LNG and as an endogenous substance 1 nM E2.

To confirm the distribution of our substances in the human body, we applied the ICE_PBPK online tool. PBPK models are mathematical models that simulate the absorption, distribution, metabolism, and excretion of chemical substances including drugs, environmental contaminants, and hormones in living organisms. These models use detailed physiological

and biochemical parameters to represent the body as a series of interconnected compartments (such as liver, kidney, blood, fat, etc.), each with specific blood flows, volumes, and metabolic capacities.[141,142] As seen in figure 17 all the selected substances are relevant for this work as they have the capacity to locate to the gut.

After characterizing the intestinal model and investigating concentrations and distribution of the chosen substances, we continued to assess the morphology of ZO-1 and CLDN4 via immunofluorescence staining and confocal microscopy. In the acquired 2D images the nuclei shape markers were analyzed. This was done to ensure that no abnormalities are present, as nuclei features can provide information about age or disorders in cells.[59,143] These results can be seen in figure 18, with mucus, and figure 19, with reduced mucus. Most compounds had almost no impact on most nuclei shape markers, except solidity, where the EDCs decreased the marker. AOH and BPA were the only substances that changed the nuclei morphology constantly in multiple shape descriptors, both in the presence of mucus and when mucus was reduced.

It has been suggested that BPA could induce oxidative stress in diverse types of cells for a while.[144,145] This stress can lead to oxidative DNA and RNA damage, thereby inducing genotoxicity and DNA strand breaks.[146–148] We hypothesize that these morphological changes could possibly be linked to potential DNA damage. Though some data demonstrates that BPF has similar genotoxic and strand breaking effects.[149,150] However in our data set it is evident that only BPA and not BPF changed the nuclei shape markers in a constant manner. This might be due to BPAs hypothesized function of modulating the expression of nuclear receptors and thereby affecting morphology of nuclei,[151] however with regard to BPF further research needs to be conducted.

AOH also displays genotoxic properties, with some studies finding these properties in as low as 1 µM.[152,153] The mechanism behind that is mostly attributed to their ability of inhibiting the essential nuclei enzyme topoisomerase. Another important aspect could be the immunosuppressive factors of AOH, in which it targets the NF-κB pathway.[152,153] Here too, nuclei morphology changes could be sign for potential DNA damage.

The analysis of the 2D image resulted in the measured TJ thickness, as seen in figure 20 panel B-D, where EDCs reduced thickness in almost all conditions: the CLDN4 thickness of

cells treated with BPF in the presence of mucus were comparable to control cells. TJ thickness is correlated to many factors, like amount of strands, cell type, density and expression of TJs.[154,155] This correlation coincides with Zhou Z. *et al*. 2017[83] findings, who found that ZO-1 expression is reduced in Caco-2 cells after E2 treatment. The interaction between E2 and TJ is very complicated and not fully understood yet, especially if there is an interaction with the estrogen receptors or if there is a different binding opportunity for E2 and EDCs to interact with TJs themselves. As we observed that treatment with EDCs can reduce TJ thickness, it can be postulated that exposure to EDCs can also decrease expression of the TJ proteins, which is part of ongoing work.

After analyzing changes in nuclear morphology, we wanted to understand whether the selected EDCs and EACs could modulate the z-distance of the TJ signal, as seen in figure 21 panel B-E. A change in the z-distance can be attributed to a shift in the z-axis of the TJ signal. This can be due to many factors, for example treatment with NPs, which can impair barrier function.[19] In the presented work no EDC impacts the z-distance in all conditions (i.e. mucus/reduced mucus). However, AOH and E2 decreased the relative position significantly in most conditions (figure 21, panel B,D and E). To add to this, we analyzed the z-stack height, as seen in figure 21 panel F, with mucus, and G, with reduced mucus. DiDP and LNG didn't change height when mucus was present, while only BPF had no impact, when mucus was reduced. This could be hinting on a different mechanism in effecting TJ morphology.

After testing multiple EDCs with one concentration in presence or absence of mucus, we decided to focus on one EDC with multiple concentrations to establish a concentration dependent effect. BPF was chosen from the substances, due to several reasons. BPF is being used as a BPA substitute, it has been suggested, that it has not only similar structural but also endocrine disruptive features as BPA.[54] Our data has not shown this trend, the data illustrates, that BPF impact tight junction morphology differently than BPA. EDCs can have a non-monotonic effect, so does BPA. We wanted to test if a approach on testing different concentrations could elucidate more on the distinct relationship between BPF and TJ. Another factor is the recent ban on BPA in food contact material.[41] It is speculated that BPA-substitutes, like BPF will increase in usage through this and consequently exposure. The cells were prepared as before, then treated with 1 µM, 10 µM and 100 µM of BPF for 24 h. The findings are presented in figure 21 and show dose dependent impact of BPF on TJs. Interestingly lower concentrations did reduce TJ thickness compared to higher concentrations and compared to the control. Though lower concentrations did not change z-distance significantly when

comparing with the control. However, higher concentrations do change the z-distance significantly. Changes in z-distance can correlate to an impairment of barrier function, as demonstrated in Iriarte-Mesa *et al*. 2024[19]. However, they used physical means, NPs, to impair the barrier function, we on the other hand, used chemical means. Our results show that environmentally relevant concentrations of BPF can alter TJ distribution, reduce thickness and change the morphology in a concentration dependent manner. While the results for the z-distance showed a clear concentration-dependent effect, other results like the TJ thickness did not. BPFs impact on the TJ morphology is coherent with previous studies showing that bisphenol compounds can interfere with TJ protein expression and assembly, though they did not show concentration dependency.[156] Why a lower concentration reduced the thickness and a higher did not, leads to an indecisive conclusion regarding our data set, however, TJ thickness may be dependent on multiple factors as is stated in current literature.[154,155,157]

Furthermore, we performed an assay that measures barrier function via permeability of the monolayer with addition of NPs and prior incubation with BPF or BPA, to demonstrate whether NPs could enhance indirect changes to barrier integrity and to highlight these effects on the nanoscale. These results of the Lucifer-yellow assay and of the TEER measurements are shown in figure 23 panel D and A-C, respectively.

The addition of the NPs after incubation with EDCs enhanced the loss of barrier function and increased permeability of the coculture compared to the control. This might be due to the strength of the intestinal barrier function being strongly correlated to the expression of three big protein groups, TJs, adheres junctions and desmosomes.[158] We already established that an incubation with BPF or BPA leads to a decrease of TJ thickness as seen in figure 20 and exposure to EDCs can lead to a decrease in TJ expression as seen in the literature.[83] Another possibility to modulate barrier function could be the addition of NPs, which can increase the permeability through a monolayer as demonstrated previously .[19]

The goal of elucidating whether NPs enhance indirect changes to barrier function could not be demonstrated as hypothesized, since all substances had direct impact on the permeability. Still an increase in permeability can be seen when NPs are added to the coculture. This effect could be due to two different end points of weakening barrier function. While EDCs weaken the barrier function on chemical level, the NPs can push themselves between the epithelial cells, challenging the barrier integrity on a physical level.

6. Conclusion

This thesis investigated the effects of selected endocrine active chemicals potentially entering the body via the oral route such as AOH, BPA, BPF, DiDP, LNG and E2. Main point of the investigation was the evaluation of the intestinal barrier function, while focusing on the morphology of TJs. The results clearly demonstrate that in a non-cytotoxic range EDCs affect TJ morphology and can thereby affect barrier function.

First the coculture model was characterized, through staining of TJ proteins and mechanosensitive channels, to identify aspects of different differentiation times and finding an effective differentiation period. This helped us gain a better understanding of our coculture model.

We also explore technical aspects of barrier function disruption/modulation by applying *ad-hoc* synthesized NPs. Through this we further proved that shape, size and functionalization of NPs have a direct impact on their interaction with the chosen intestinal model. Additionally, we established that application of NPs after exposure to EDCs contributes to highlight impairment of the barrier function more than only an incubation with EDCs.

Furthermore, we tested the impact of various EDCs and EACs on the coculture model. The data demonstrates that AOH and BPA, in particular, induce significant changes in TJ morphology, as demonstrated by a decreased TJ thickness and changes in z-distance in multiple conditions. The findings for BPF, DiDP, and LNG further support the hypothesis that EACs from diverse chemical classes can affect barrier function and organization of TJ proteins. Even if the magnitude of the potential detrimental effects of EDCs on the gastro-intestinal tract remains to be elucidated, the results collected in this work, combined with the ongoing projects and the existing literature, suggest that non-cytotoxic concentrations of EDCs and EACs might have an impact on the morphology and functionality of the gut epithelium.

Supplementary

Supplementary Table 1: Consumables

Instrument	company	Cas/product number
8-well ibidi µ-slide	Ibidi	80826
Centrifugation tubes 15 ml	SARSTEDT	62.554.016
Centrifugation tubes 50 ml	SARSTEDT	72.691.001
Gloves; Nitrile, powder free, blue	Th. Geyer GmbH & Co. KG	7.696.900
Microtubes Transparent; brown Volume: 1 mL; 1.5 mL; 2 mL	SARSTEDT	72.706
Neubauer counting chamber	Paul Marienfeld GmbH & Co. KG, GER	640110
Pasteur pipette 150mm	SARSTEDT	15.310.965
Pipette tips 10-5000 µL	SARSTEDT	703.060
Sarstedt TC-Insert 12 well, Pore size 0.4 µm	SARSTEDT	833.931.041
Serological pipette, with tip, padded, 10 ml, sterile, pyrogen-free/endotoxin-free, non-cytotoxic	SARSTEDT	861.254.001
Solution basin 5 ml; 25 ml	Biologix Europe GmbH	25-1025/25-0051/ 25-1100
TC-Flask T175 Standard, Vent. Cap	SARSTEDT	833.911.002
TC-Flask T75 Standard, Vent. Cap	SARSTEDT	833.911.002
TC-Plate 12-well Standard, F	SARSTEDT	833.921
TC-Plate 24-well Standard, F	SARSTEDT	833.922.005
TC-Plate 96-well Standard, F	SARSTEDT	833.924
Transwell inserts; Tissue culture (TC)- inserts for 12-well plate	SARSTEDT	833.931.041

Supplementary Table 2: Software

Software	Version	Company
Excel	202505	Microsoft corporation
ImageJ (FIJI)	2.16.0	Wayne Rasband, National Institutes of Health
Olympus cellSens Entry	1.18	Olympus Corporation
OriginPro®,	2025 (learning edition)	OriginLab Corporation,
ZEN 2012 SP5 FP3 (black),	14.0.20.201	Carl Zeiss AG
ZEN (blue)		Carl Zeiss AG
Inkscape	1.2.1	Inkscape Community
Olympus cellSens Entry	1.18	Olympus Corporation
Gen 5	03.08	Biotek Instruments Inc

Supplementary Table 3: Instruments (WÄ: Währingerstr. 38 LMC faculty; Group Doris Marko; UZA2 Pharmazie Geozentrum LMC faculty; Group Giorgia Del Favero)

Instrument	Specification	Company
Centrifuge	Z 326 K	Hermle AG
Epithelial Voltohmmeter	EVOM2	World Precision Instruments
EVOM TEER electrode	STX 4	World Precision Instruments
Freezer	Temperature: -20°C	Liebherr-Hausgeräte GmbH
Fridge	Temperature: 4°C	Liebherr-Hausgeräte GmbH
Heating plate	MS-H-PRO+	DLAB Scientific Co
Incubator	Heracell 240i CO2	ThermoFischer
Laminar flow cabinet		
Microplate reader	BioTec Synergy H1	
Microscope		
Multichannel pipette	30-300 µL	Eppendorf SE
Pipettes	10; 20; 100; 200; 1000; 5000 µL	Eppendorf SE
Vortex shaker		

Water bath	GD100	Grant instruments Ltd.
Fridge	Temperature: 4°C	
Freezer	Temperature: -20°C	
Freezer	Temperature: -80°C	
Incubator		
Laminar flow cabinet		
LSM 800	ELYRA PS.1.5	Carl Zeiss AG
Zeiss LSM710	Elyra PS.1	Carl Zeiss AG

Supplementary Table 4: cell culture reagents and chemicals

Name	Supplier	Reference ID	Cas number	Additional Information
Triton-X 100	ROTH	270298309		
CellTiterBlue solution	SIGMA	514510		
PBS-A	Self-Prepared	ROTH 3904.1 VMR 26764.298 ROTH 0962.2 ROTH 4984.1		0.4 g KH2PO4 0.4 g KCl 16 g NaCl 4.4 g Na2HPO4 dissolve in autoclaved H2O (1L) adjust to pH 7.2 membrane-filter solution afterwards (Filtropur SARSTEDT 500ml 0.2 µm REF: 83.39.41.001)
Hank's Balanced Saline Solution (HBSS)	Self-Prepared			kindly provided by Dr. Claudia Iriarte-Mesa
Permeabilization Buffer	Self-Prepared			0.2 % Triton-X in PBS-A
Washing buffer	Self-Prepared			0.05 % Triton-X in PBS-A
ROTI Histofix Formaldehyd	ROTH	P087.4		4 % Formaldehyd, ready-to-use, phosphatgepuffert, pH 7
Roti-Mount Flourcare + DAPI	ROTH	HP 20.1		
Phalloidin-488 Oregon Green	Invitrogen	7466		
Dulbecco's Modified Eagle Medium	gibco	21063-029		
Donkey Serum	Sigma	D9663-10ML		
Fetal calf serum	gibco	10270-106		
Trypsin	gibco			

Antibodies				
Claudin 4 Monoclonal Antibody (3E2C1), Alexa Fluor™ 594	ThermoFischer	329494		
Anti-ZO1 tight junction protein antibody - C-terminal	ABclonal	A0659	5500044381	
Piezo1 monoclonal antibody (2-10)	invitrogen	ma5-32876		
Donkey anti-Rabbit IgG (H+L) Highly Cross-Adsorbed Secondary Antibody, Alexa Fluor™ 488	ThermoFischer	A-21206		
Donkey anti-Mouse IgG (H+L) Highly Cross-Adsorbed Secondary Antibody, Alexa Fluor™ 647	ThermoFischer	A31571		
Oregon Green™ 488 Phalloidin, Green, 496/520 nm	Invitrogen	O7466		
Treatments				
Alternariol	Szabo-Scandic	Charge: 0695083-2	641-83-8	
Bisphenol A	Sigma	239658-50G	80-05-7	
Bisphenol F (Bis(4-hydroxyphenyl)methane	Sigma	47006-19	620-92-8	
Levonorgestrel	ThermoFischer	461100010	797-63-7	
Diisodecyl Phthalate	Sigma	80135-10ML	26761-40-0	
17-beta-estradiol	Sigma	200-023-8		
N-Acetyl-L-cysteine aliquot	aliquot	aliquot		

Supplementary Table 5: cell culture

Cell line	Company	From
Caco-2 cells	Sigma-Aldrich Corporation (St. Louis, USA)	kindly provided by Prof. Marko
HT29-MTX-E12 cells	Sigma-Aldrich Corporation (St. Louis, USA)	kindly provided by Prof. Marko

HT29 cells	Sigma-Aldrich Corporation (St. Louis, USA)	kindly provided by Prof. Marko

Literature

(1) Combarnous, Y.; Nguyen, T. M. D. Comparative Overview of the Mechanisms of Action of Hormones and Endocrine Disruptor Compounds. *Toxics* **2019**, *7* (1), 5. https://doi.org/10.3390/toxics7010005.

(2) Stiefel, C.; Stintzing, F. Endocrine-Active and Endocrine-Disrupting Compounds in Food – Occurrence, Formation and Relevance. *NFS J.* **2023**, *31*, 57–92. https://doi.org/10.1016/j.nfs.2023.03.004.

(3) Ahn, C.; Jeung, E.-B. Endocrine-Disrupting Chemicals and Disease Endpoints. *Int. J. Mol. Sci.* **2023**, *24* (6), 5342. https://doi.org/10.3390/ijms24065342.

(4) Rosenfeld, C. S.; Cooke, P. S. Endocrine Disruption through Membrane Estrogen Receptors and Novel Pathways Leading to Rapid Toxicological and Epigenetic Effects. *J. Steroid Biochem. Mol. Biol.* **2019**, *187*, 106–117. https://doi.org/10.1016/j.jsbmb.2018.11.007.

(5) Effect of Chemicals on Plastics. In *Chemical Resistance of Engineering Thermoplastics*; Elsevier, 2016; pp xxvii–xli. https://doi.org/10.1016/b978-0-323-47357-6.00022-2.

(6) Van Hylckama Vlieg, A.; Helmerhorst, F. M.; Vandenbroucke, J. P.; Doggen, C. J. M.; Rosendaal, F. R. The Venous Thrombotic Risk of Oral Contraceptives, Effects of Oestrogen Dose and Progestogen Type: Results of the MEGA Case-Control Study. *BMJ* **2009**, *339* (aug13 2), b2921–b2921. https://doi.org/10.1136/bmj.b2921.

(7) Virtuoso, S.; Raggi, C.; Maugliani, A.; Baldi, F.; Gentili, D.; Narciso, L. Toxicological Effects of Naturally Occurring Endocrine Disruptors on Various Human Health Targets: A Rapid Review. *Toxics* **2024**, *12* (4), 256. https://doi.org/10.3390/toxics12040256.

(8) Kong, S.; Zhang, Y. H.; Zhang, W. Regulation of Intestinal Epithelial Cells Properties and Functions by Amino Acids. *BioMed Res. Int.* **2018**, *2018*, 1–10. https://doi.org/10.1155/2018/2819154.

(9) Bonis, V.; Rossell, C.; Gehart, H. The Intestinal Epithelium – Fluid Fate and Rigid Structure From Crypt Bottom to Villus Tip. *Front. Cell Dev. Biol.* **2021**, *9*, 661931. https://doi.org/10.3389/fcell.2021.661931.

(10) Clauss, W.; Clauss, C. *Humanbiologie kompakt*, 2. Auflage.; SpringerLink Bücher; Springer Spektrum: Berlin [Heidelberg], 2018. https://doi.org/10.1007/978-3-662-55850-8.

(11) Williams, J. M.; Duckworth, C. A.; Burkitt, M. D.; Watson, A. J. M.; Campbell, B. J.; Pritchard, D. M. Epithelial Cell Shedding and Barrier Function: A Matter of Life and Death at the Small Intestinal Villus Tip. *Vet. Pathol.* **2015**, *52* (3), 445–455. https://doi.org/10.1177/0300985814559404.

(12) Jany, B. H.; Gallup, M. W.; Yan, P. S.; Gum, J. R.; Kim, Y. S.; Basbaum, C. B. Human Bronchus and Intestine Express the Same Mucin Gene. *J. Clin. Invest.* **1991**, *87* (1), 77–82. https://doi.org/10.1172/jci115004.

(13) Chelakkot, C.; Ghim, J.; Ryu, S. H. Mechanisms Regulating Intestinal Barrier Integrity and Its Pathological Implications. *Exp. Mol. Med.* **2018**, *50* (8), 1–9. https://doi.org/10.1038/s12276-018-0126-x.

(14) Okumura, R.; Takeda, K. Roles of Intestinal Epithelial Cells in the Maintenance of Gut Homeostasis. *Exp. Mol. Med.* **2017**, *49* (5), e338–e338. https://doi.org/10.1038/emm.2017.20.

(15) Crudo, F.; Aichinger, G.; Dellafiora, L.; Kiss, E.; Mihajlovic, J.; Del Favero, G.; Berry, D.; Dall'Asta, C.; Marko, D. Persistence of the Antagonistic Effects of a Natural Mixture of Alternaria Mycotoxins on the Estrogen-like Activity of Human Feces after Anaerobic Incubation. *Toxicol. Lett.* **2022**, *358*, 88–99. https://doi.org/10.1016/j.toxlet.2022.01.015.
(16) Groestlinger, J.; Spindler, V.; Pahlke, G.; Rychlik, M.; Del Favero, G.; Marko, D. *Alternaria Alternata* Mycotoxins Activate the Aryl Hydrocarbon Receptor and Nrf2-ARE Pathway to Alter the Structure and Immune Response of Colon Epithelial Cells. *Chem. Res. Toxicol.* **2022**, *35* (5), 731–749. https://doi.org/10.1021/acs.chemrestox.1c00364.
(17) Del Favero, G.; Bergen, J.; Palm, L.; Fellinger, C.; Matlaeva, M.; Szabadi, A.; Fernandes, A. S.; Saraiva, N.; Schröder, C.; Marko, D. Short-Term Exposure to Foodborne Xenoestrogens Affects Breast Cancer Cell Morphology and Motility Relevant for Metastatic Behavior *In Vitro*. *Chem. Res. Toxicol.* **2024**, *37* (10), 1634–1650. https://doi.org/10.1021/acs.chemrestox.4c00061.
(18) Bergen, J.; Iriarte-Mesa, C.; Rieger, J.; Crudo, F.; Marko, D.; Kleitz, F.; Berthiller, F.; Del Favero, G. Integrating Physiologically-Inspired Nanoparticles with Intestinal Cell Co-Culture for Enhanced Activity Profiling of Food Constituents and Contaminants in Vitro. *Food Res. Int.* **2025**, *209*, 116206. https://doi.org/10.1016/j.foodres.2025.116206.
(19) Iriarte-Mesa, C.; Bergen, J.; Danielyan, K.; Crudo, F.; Marko, D.; Kählig, H.; Del Favero, G.; Kleitz, F. Functionalization of Silica Nanoparticles for Tailored Interactions with Intestinal Cells and Chemical Modulation of Paracellular Permeability. *Small Sci.* **2025**, *5* (1), 2400112. https://doi.org/10.1002/smsc.202400112.
(20) El-Sayed, R. A.; Jebur, A. B.; Kang, W.; El-Demerdash, F. M. An Overview on the Major Mycotoxins in Food Products: Characteristics, Toxicity, and Analysis. *J. Future Foods* **2022**, *2* (2), 91–102. https://doi.org/10.1016/j.jfutfo.2022.03.002.
(21) Fehr, M.; Pahlke, G.; Fritz, J.; Christensen, M. O.; Boege, F.; Altemöller, M.; Podlech, J.; Marko, D. Alternariol Acts as a Topoisomerase Poison, Preferentially Affecting the IIα Isoform. *Mol. Nutr. Food Res.* **2009**, *53* (4), 441–451. https://doi.org/10.1002/mnfr.200700379.
(22) Fleck, S. C.; Burkhardt, B.; Pfeiffer, E.; Metzler, M. Alternaria Toxins: Altertoxin II Is a Much Stronger Mutagen and DNA Strand Breaking Mycotoxin than Alternariol and Its Methyl Ether in Cultured Mammalian Cells. *Toxicol. Lett.* **2012**, *214* (1), 27–32. https://doi.org/10.1016/j.toxlet.2012.08.003.
(23) Solhaug, A.; Vines, L. L.; Ivanova, L.; Spilsberg, B.; Holme, J. A.; Pestka, J.; Collins, A.; Eriksen, G. S. Mechanisms Involved in Alternariol-Induced Cell Cycle Arrest. *Mutat. Res. Mol. Mech. Mutagen.* **2012**, *738–739*, 1–11. https://doi.org/10.1016/j.mrfmmm.2012.09.001.
(24) Scientific Opinion on the Risks for Animal and Public Health Related to the Presence of Alternaria Toxins in Feed and Food. *EFSA J.* No. 2011;9(11):2407. https://doi.org/10.2903/j.efsa.2011.2407.
(25) Saleh, I.; Zeidan, R.; Abu-Dieyeh, M. The Characteristics, Occurrence, and Toxicological Effects of Alternariol: A Mycotoxin. *Arch. Toxicol.* **2024**, *98* (6), 1659–1683. https://doi.org/10.1007/s00204-024-03743-0.
(26) Crudo, F.; Hong, C.; Varga, E.; Del Favero, G.; Marko, D. Genotoxic and Mutagenic Effects of the Alternaria Mycotoxin Alternariol in Combination with the Process Contaminant Acrylamide. *Toxins* **2023**, *15* (12), 670. https://doi.org/10.3390/toxins15120670.
(27) Solhaug, A.; Eriksen, G. S.; Holme, J. A. Mechanisms of Action and Toxicity of the Mycotoxin Alternariol: A Review. *Basic Clin. Pharmacol. Toxicol.* **2016**, *119* (6), 533–539. https://doi.org/10.1111/bcpt.12635.

(28) Aichinger, G.; Del Favero, G.; Warth, B.; Marko, D. *Alternaria* Toxins—Still Emerging? *Compr. Rev. Food Sci. Food Saf.* **2021**, *20* (5), 4390–4406. https://doi.org/10.1111/1541-4337.12803.
(29) Den Hollander, D.; Holvoet, C.; Demeyere, K.; De Zutter, N.; Audenaert, K.; Meyer, E.; Croubels, S. Cytotoxic Effects of Alternariol, Alternariol Monomethyl-Ether, and Tenuazonic Acid and Their Relevant Combined Mixtures on Human Enterocytes and Hepatocytes. *Front. Microbiol.* **2022**, *13*, 849243. https://doi.org/10.3389/fmicb.2022.849243.
(30) Crudo, F.; Hong, C.; Varga, E.; Del Favero, G.; Marko, D. Genotoxic and Mutagenic Effects of the Alternaria Mycotoxin Alternariol in Combination with the Process Contaminant Acrylamide. *Toxins* **2023**, *15* (12), 670. https://doi.org/10.3390/toxins15120670.
(31) Frizzell, C.; Ndossi, D.; Kalayou, S.; Eriksen, G. S.; Verhaegen, S.; Sørlie, M.; Elliott, C. T.; Ropstad, E.; Connolly, L. An in Vitro Investigation of Endocrine Disrupting Effects of the Mycotoxin Alternariol. *Toxicol. Appl. Pharmacol.* **2013**, *271* (1), 64–71. https://doi.org/10.1016/j.taap.2013.05.002.
(32) Louro, H.; Vettorazzi, A.; López De Cerain, A.; Spyropoulou, A.; Solhaug, A.; Straumfors, A.; Behr, A.-C.; Mertens, B.; Žegura, B.; Fæste, C. K.; Ndiaye, D.; Spilioti, E.; Varga, E.; Dubreil, E.; Borsos, E.; Crudo, F.; Eriksen, G. S.; Snapkow, I.; Henri, J.; Sanders, J.; Machera, K.; Gaté, L.; Le Hegarat, L.; Novak, M.; Smith, N. M.; Krapf, S.; Hager, S.; Fessard, V.; Kohl, Y.; Silva, M. J.; Dirven, H.; Dietrich, J.; Marko, D. Hazard Characterization of Alternaria Toxins to Identify Data Gaps and Improve Risk Assessment for Human Health. *Arch. Toxicol.* **2024**, *98* (2), 425–469. https://doi.org/10.1007/s00204-023-03636-8.
(33) Demaegdt, H.; Daminet, B.; Evrard, A.; Scippo, M.-L.; Muller, M.; Pussemier, L.; Callebaut, A.; Vandermeiren, K. Endocrine Activity of Mycotoxins and Mycotoxin Mixtures. *Food Chem. Toxicol.* **2016**, *96*, 107–116. https://doi.org/10.1016/j.fct.2016.07.033.
(34) Daina, A.; Michielin, O.; Zoete, V. SwissTargetPrediction: Updated Data and New Features for Efficient Prediction of Protein Targets of Small Molecules. *Nucleic Acids Res.* **2019**, *47* (W1), W357–W364. https://doi.org/10.1093/nar/gkz382.
(35) Gfeller, D.; Michielin, O.; Zoete, V. Shaping the Interaction Landscape of Bioactive Molecules. *Bioinformatics* **2013**, *29* (23), 3073–3079. https://doi.org/10.1093/bioinformatics/btt540.
(36) Daina, A.; Zoete, V. Testing the Predictive Power of Reverse Screening to Infer Drug Targets, with the Help of Machine Learning. *Commun. Chem.* **2024**, *7* (1), 105. https://doi.org/10.1038/s42004-024-01179-2.
(37) Scott, S. A.; Fu, J.; Chang, P. V. Microbial Tryptophan Metabolites Regulate Gut Barrier Function via the Aryl Hydrocarbon Receptor. *Proc. Natl. Acad. Sci.* **2020**, *117* (32), 19376–19387. https://doi.org/10.1073/pnas.2000047117.
(38) Groestlinger, J.; Seidl, C.; Varga, E.; Del Favero, G.; Marko, D. Combinatory Exposure to Urolithin A, Alternariol, and Deoxynivalenol Affects Colon Cancer Metabolism and Epithelial Barrier Integrity in Vitro. *Front. Nutr.* **2022**, *9*, 882222. https://doi.org/10.3389/fnut.2022.882222.
(39) *Https://Pubchem.Ncbi.Nlm.Nih.Gov/Compound/Alternariol Opened 05.08.25 at 18:50*.
(40) Manzoor, M. F.; Tariq, T.; Fatima, B.; Sahar, A.; Tariq, F.; Munir, S.; Khan, S.; Nawaz Ranjha, M. M. A.; Sameen, A.; Zeng, X.-A.; Ibrahim, S. A. An Insight into Bisphenol A, Food Exposure and Its Adverse Effects on Health: A Review. *Front. Nutr.* **2022**, *9*, 1047827. https://doi.org/10.3389/fnut.2022.1047827.
(41) *VERORDNUNG (EU) 2024/3190 DER KOMMISSION Vom 19. Dezember 2024 Über Die Verwendung von Bisphenol A (BPA) Und Anderen Bisphenolen Und Bisphenolderivaten, Die Aufgrund Spezifischer Gefährlicher Eigenschaften Eine*

Harmonisierte Einstufung Erhalten Haben, in Bestimmten Materialien Und Gegenständen, Die Dazu Bestimmt Sind, Mit Lebensmitteln in Berührung Zu Kommen, Zur Änderung Der Verordnung (EU) Nr. 10/2011 Und Zur Aufhebung Der Verordnung (EU) 2018/213.

(42) Mustieles, V.; D'Cruz, S. C.; Couderq, S.; Rodríguez-Carrillo, A.; Fini, J.-B.; Hofer, T.; Steffensen, I.-L.; Dirven, H.; Barouki, R.; Olea, N.; Fernández, M. F.; David, A. Bisphenol A and Its Analogues: A Comprehensive Review to Identify and Prioritize Effect Biomarkers for Human Biomonitoring. *Environ. Int.* **2020**, *144*, 105811. https://doi.org/10.1016/j.envint.2020.105811.

(43) *European Commission, 2024. Commission Regulation (EU) 2024/3190 of 19 December 2024 on the Use of Bisphenol A in Food Contact Materials. Official Journal of the European Union, L 338, Pp.31–45. Available at: Http://Data.Europa.Eu/Eli/Reg/2024/3190/Oj*.

(44) Opinion of the Scientific Panel on Food Additives, Flavourings, Processing Aids and Materials in Contact with Food (AFC) Related to 2,2-BIS(4-HYDROXYPHENYL)PROPANE. *EFSA J.* No. EFSA Journal. https://doi.org/10.2903/j.efsa.2007.428.

(45) Acconcia, F.; Pallottini, V.; Marino, M. Molecular Mechanisms of Action of BPA. *Dose-Response* **2015**, *13* (4), 1559325815610582. https://doi.org/10.1177/1559325815610582.

(46) Li, L.; Wang, Q.; Zhang, Y.; Niu, Y.; Yao, X.; Liu, H. The Molecular Mechanism of Bisphenol A (BPA) as an Endocrine Disruptor by Interacting with Nuclear Receptors: Insights from Molecular Dynamics (MD) Simulations. *PLOS ONE* **2015**, *10* (3), e0120330. https://doi.org/10.1371/journal.pone.0120330.

(47) Feng, L.; Chen, S.; Zhang, L.; Qu, W.; Chen, Z. Bisphenol A Increases Intestinal Permeability through Disrupting Intestinal Barrier Function in Mice. *Environ. Pollut.* **2019**, *254*, 112960. https://doi.org/10.1016/j.envpol.2019.112960.

(48) Wang, K.; Qiu, L.; Zhu, J.; Sun, Q.; Qu, W.; Yu, Y.; Zhao, Z.; Yu, Y.; Shao, G. Environmental Contaminant BPA Causes Intestinal Damage by Disrupting Cellular Repair and Injury Homeostasis in Vivo and in Vitro. *Biomed. Pharmacother.* **2021**, *137*, 111270. https://doi.org/10.1016/j.biopha.2021.111270.

(49) *Https://Pubchem.Ncbi.Nlm.Nih.Gov/Compound/Bisphenol-A Opened 05.08.25 at 20:12*.

(50) Rochester, J. R.; Bolden, A. L. Bisphenol S and F: A Systematic Review and Comparison of the Hormonal Activity of Bisphenol A Substitutes. *Environ. Health Perspect.* **2015**, *123* (7), 643–650. https://doi.org/10.1289/ehp.1408989.

(51) Erdal, İ.; Yıldız, Y.; Yalçın, S. S.; Yirün, A.; Demirel, G.; Erkekoğlu, P. Evaluation of Exposure to Bisphenol A, Bisphenol F, and Phthalates in Patients with Phenylketonuria and Its Differences According to Dietary Status. *Nutrients* **2024**, *16* (18), 3213. https://doi.org/10.3390/nu16183213.

(52) Wiklund, L.; Beronius, A. Systematic Evaluation of the Evidence for Identification of Endocrine Disrupting Properties of Bisphenol F. *Toxicology* **2022**, *476*, 153255. https://doi.org/10.1016/j.tox.2022.153255.

(53) Zhang, J.; Yao, K.; Yin, J.; Lyu, B.; Zhao, Y.; Li, J.; Shao, B.; Wu, Y. Exposure to Bisphenolic Analogues in the Sixth Total Diet Study - China, 2016-2019. *China CDC Wkly.* **2022**, *4* (9), 180–184. https://doi.org/10.46234/ccdcw2022.044.

(54) Wiklund, L.; Beronius, A. Systematic Evaluation of the Evidence for Identification of Endocrine Disrupting Properties of Bisphenol F. *Toxicology* **2022**, *476*, 153255. https://doi.org/10.1016/j.tox.2022.153255.

(55) *Https://Pubchem.Ncbi.Nlm.Nih.Gov/Compound/Bisphenol-F Opened 05.08.25 at 20:12*.

(56) Wormuth, M.; Scheringer, M.; Vollenweider, M.; Hungerbühler, K. What Are the Sources of Exposure to Eight Frequently Used Phthalic Acid Esters in Europeans? *Risk Anal.* **2006**, *26* (3), 803–824. https://doi.org/10.1111/j.1539-6924.2006.00770.x.
(57) Przybylińska, P. A.; Wyszkowski, M. Environmental Contamination with Phthalates and Its Impact on Living Organisms. *Ecol. Chem. Eng. S* **2016**, *23* (2), 347–356. https://doi.org/10.1515/eces-2016-0024.
(58) Kransler, K. M.; Bachman, A. N.; McKee, R. H. Estimates of Daily Di-Isodecyl Phthalate (DIDP) Intake Calculated from Urinary Biomonitoring Data. *Regul. Toxicol. Pharmacol.* **2013**, *65* (1), 29–33. https://doi.org/10.1016/j.yrtph.2012.11.004.
(59) Lee, H.; Lee, J.; Choi, K.; Kim, K.-T. Comparative Analysis of Endocrine Disrupting Effects of Major Phthalates in Employed Two Cell Lines (MVLN and H295R) and Embryonic Zebrafish Assay. *Environ. Res.* **2019**, *172*, 319–325. https://doi.org/10.1016/j.envres.2019.02.033.
(60) *Lake BG, Cook WM, Worrell NR, Cunningham ME, Evans JG, Price RJ, Young PJ & Carpanini F (1991) Dose-Response Relationships for Induction of Hepatic Peroxisome Proliferation and Testicular Atrophy by Phthalate Esters in the Rat. Human Exp. Toxicol., 10:67-68.*
(61) *BIBRA (1986) A 21 Day Feeding Study of Diisodecyl Phthalate to Rats: Effects on the Liver and Liver Lipids. British Industrial Biological Research Association (BIBRA), Project No 3.0495.5, Report No 0495/5/85 Submitted to the Chemical Manufacturers Association (CMA).*
(62) Hushka, L. J.; Waterman, S. J.; Keller, L. H.; Trimmer, G. W.; Freeman, J. J.; Ambroso, J. L.; Nicolich, M.; McKee, R. H. Two-Generation Reproduction Studies in Rats Fed Di-Isodecyl Phthalate. *Reprod. Toxicol.* **2001**, *15* (2), 153–169. https://doi.org/10.1016/S0890-6238(01)00109-5.
(63) Zhang, Y.; Wang, J.; Yang, H.; Guan, Y. The Potential Mechanisms Underlying Phthalate-Induced Hypospadias: A Systematic Review of Rodent Model Studies. *Front. Endocrinol.* **2024**, *15*, 1490011. https://doi.org/10.3389/fendo.2024.1490011.
(64) Zhou, Y.; Huang, F.; Liu, Y.; Li, D.; Zhou, Y.; Shen, L.; Long, C.; Liu, X.; Wei, G. TGF-B1 Relieves Epithelial–Mesenchymal Transition Reduction in Hypospadias Induced by DEHP in Rats. *Pediatr. Res.* **2020**, *87* (4), 639–646. https://doi.org/10.1038/s41390-019-0622-2.
(65) Zhou, X.; Zhang, X.; Zhou, X.; Abulimiti, G.; Wang, Y.; Zhang, Q.; Cong, R.; Ji, C.; Luan, J.; Yao, L.; Yang, J.; Song, N. Identification of Endocrine-Disrupting Chemicals Targeting the Genes and Pathways of Genital Anomalies in Males. *Ecotoxicol. Environ. Saf.* **2022**, *247*, 114241. https://doi.org/10.1016/j.ecoenv.2022.114241.
(66) *Https://Pubchem.Ncbi.Nlm.Nih.Gov/Compound/Diisodecyl_phthalate Opened 05.08.25 at 20:15*.
(67) Camp, S. L.; Wilkerson, D. S.; Raine, T. R. The Benefits and Risks of Over-the-Counter Availability of Levonorgestrel Emergency Contraception. *Contraception* **2003**, *68* (5), 309–317. https://doi.org/10.1016/j.contraception.2003.08.011.
(68) Gemzell-Danielsson, K.; Berger, C.; P.G.L., L. Emergency Contraception — Mechanisms of Action. *Contraception* **2013**, *87* (3), 300–308. https://doi.org/10.1016/j.contraception.2012.08.021.
(69) Narváez, J. F.; Grant, H.; Gil, V. C.; Porras, J.; Bueno Sanchez, J. C.; Ocampo Duque, L. F.; Sossa, R. R.; Quintana-Castillo, J. C. Assessment of Endocrine Disruptor Effects of Levonorgestrel and Its Photoproducts: Environmental Implications of Released Fractions after Their Photocatalytic Removal. *J. Hazard. Mater.* **2019**, *371*, 273–279. https://doi.org/10.1016/j.jhazmat.2019.02.095.
(70) Oropesa, A. L.; Guimarães, L. Occurrence of Levonorgestrel in Water Systems and Its Effects on Aquatic Organisms: A Review. In *Reviews of Environmental Contamination and Toxicology Volume 254*; De Voogt, P., Ed.; Reviews of Environmental

Contamination and Toxicology; Springer International Publishing: Cham, 2020; Vol. 254, pp 57–84. https://doi.org/10.1007/398_2020_44.
(71) Graham, S.; Fraser, I. S. The Progestogen-Only Mini-Pill. *Contraception* **1982**, *26* (4), 373–388. https://doi.org/10.1016/0010-7824(82)90104-4.
(72) Oropesa, A. L.; Guimarães, L. Occurrence of Levonorgestrel in Water Systems and Its Effects on Aquatic Organisms: A Review. In *Reviews of Environmental Contamination and Toxicology Volume 254*; De Voogt, P., Ed.; Reviews of Environmental Contamination and Toxicology; Springer International Publishing: Cham, 2020; Vol. 254, pp 57–84. https://doi.org/10.1007/398_2020_44.
(73) Watanabe, A.; Myosho, T.; Ishibashi, A.; Yamamoto, J.; Toda, M.; Onishi, Y.; Kobayashi, T. Levonorgestrel Causes Feminization and Dose-Dependent Masculinization in Medaka Fish (Oryzias Latipes): Endocrine-Disruption Activity and Its Correlation with Sex Reversal. *Sci. Total Environ.* **2023**, *876*, 162740. https://doi.org/10.1016/j.scitotenv.2023.162740.
(74) Quispe Calla, N. E.; Vicetti Miguel, R. D.; Boyaka, P. N.; Hall-Stoodley, L.; Kaur, B.; Trout, W.; Pavelko, S. D.; Cherpes, T. L. Medroxyprogesterone Acetate and Levonorgestrel Increase Genital Mucosal Permeability and Enhance Susceptibility to Genital Herpes Simplex Virus Type 2 Infection. *Mucosal Immunol.* **2016**, *9* (6), 1571–1583. https://doi.org/10.1038/mi.2016.22.
(75) Zim, A.; Bommareddy, A. Estrogen-Gut-Brain Axis: Examining the Role of Combined Oral Contraceptives on Mental Health Through Their Impact on the Gut Microbiome. *Cureus* **2025**. https://doi.org/10.7759/cureus.81354.
(76) Siddiqui, R.; Makhlouf, Z.; Alharbi, A. M.; Alfahemi, H.; Khan, N. A. The Gut Microbiome and Female Health. *Biology* **2022**, *11* (11), 1683. https://doi.org/10.3390/biology11111683.
(77) Flores, R.; Shi, J.; Fuhrman, B.; Xu, X.; Veenstra, T. D.; Gail, M. H.; Gajer, P.; Ravel, J.; Goedert, J. J. Fecal Microbial Determinants of Fecal and Systemic Estrogens and Estrogen Metabolites: A Cross-Sectional Study. *J. Transl. Med.* **2012**, *10* (1), 253. https://doi.org/10.1186/1479-5876-10-253.
(78) *Https://Pubchem.Ncbi.Nlm.Nih.Gov/Compound/13109 Opened 05.08.25 at 20:16*.
(79) Mahmoodzadeh, S.; Dworatzek, E. The Role of 17β-Estradiol and Estrogen Receptors in Regulation of Ca2+ Channels and Mitochondrial Function in Cardiomyocytes. *Front. Endocrinol.* **2019**, *10*, 310. https://doi.org/10.3389/fendo.2019.00310.
(80) Prokai-Tatrai, K.; Prokai, L. The Impact of 17β-Estradiol on the Estrogen-Deficient Female Brain: From Mechanisms to Therapy with Hot Flushes as Target Symptoms. *Front. Endocrinol.* **2024**, *14*, 1310432. https://doi.org/10.3389/fendo.2023.1310432.
(81) Yaşar, P.; Ayaz, G.; User, S. D.; Güpür, G.; Muyan, M. Molecular Mechanism of Estrogen–Estrogen Receptor Signaling. *Reprod. Med. Biol.* **2017**, *16* (1), 4–20. https://doi.org/10.1002/rmb2.12006.
(82) Björnström, L.; Sjöberg, M. Mechanisms of Estrogen Receptor Signaling: Convergence of Genomic and Nongenomic Actions on Target Genes. *Mol. Endocrinol.* **2005**, *19* (4), 833–842. https://doi.org/10.1210/me.2004-0486.
(83) Zhou, Z.; Zhang, L.; Ding, M.; Luo, Z.; Yuan, S.; Bansal, M. B.; Gilkeson, G.; Lang, R.; Jiang, W. Estrogen Decreases Tight Junction Protein ZO-1 Expression in Human Primary Gut Tissues. *Clin. Immunol.* **2017**, *183*, 174–180. https://doi.org/10.1016/j.clim.2017.08.019.
(84) Choi, Y. S.; Baek, K.; Choi, Y. Estrogen Reinforces Barrier Formation and Protects against Tumor Necrosis Factor Alpha-Induced Barrier Dysfunction in Oral Epithelial Cells. *J. Periodontal Implant Sci.* **2018**, *48* (5), 284. https://doi.org/10.5051/jpis.2018.48.5.284.
(85) *Https://Pubchem.Ncbi.Nlm.Nih.Gov/Compound/Estradiol Opened 05.08.25 at 20:18*.

(86) Otani, T.; Furuse, M. Tight Junction Structure and Function Revisited. *Trends Cell Biol.* **2020**, *30* (10), 805–817. https://doi.org/10.1016/j.tcb.2020.08.004.
(87) *Van Itallie CM, Anderson JM. Claudin Interactions in and out of the Tight Junction. Tissue Barriers. 2013;1(3):E25247*.
(88) *Fanning AS, Jameson BJ, Jesaitis LA, Anderson JM. The Tight Junction Protein ZO-1 Establishes a Link between the Transmembrane Protein Occludin and the Actin Cytoskeleton. J Biol Chem. 1998;273(45):29745–29753.*
(89) *Raleigh DR, Boe DM, Yu D, Weber CR, Marchiando AM, Bradford EM, et al. Occludin S408 Phosphorylation Regulates Tight Junction Protein Interactions and Barrier Function. J Cell Biol. 2011;193(3):565–582*.
(90) *Mandell KJ, Parkos CA. The JAM Family of Proteins. Adv Drug Deliv Rev. 2005;57(6):857–867.*
(91) *Alberts, B., Johnson, A., Lewis, J., Raff, M., Roberts, K., & Walter, P. (2015). Molecular Biology of the Cell (6th Ed.). Garland Science.*
(92) Stevenson, B. R.; Siliciano, J. D.; Mooseker, M. S.; Goodenough, D. A. Identification of ZO-1: A High Molecular Weight Polypeptide Associated with the Tight Junction (Zonula Occludens) in a Variety of Epithelia. *J. Cell Biol.* **1986**, *103* (3), 755–766. https://doi.org/10.1083/jcb.103.3.755.
(93) González-Mariscal, L.; Betanzos, A.; Ávila-Flores, A. MAGUK Proteins: Structure and Role in the Tight Junction. *Semin. Cell Dev. Biol.* **2000**, *11* (4), 315–324. https://doi.org/10.1006/scdb.2000.0178.
(94) McNeil, E.; Capaldo, C. T.; Macara, I. G. Zonula Occludens-1 Function in the Assembly of Tight Junctions in Madin-Darby Canine Kidney Epithelial Cells. *Mol. Biol. Cell* **2006**, *17* (4), 1922–1932. https://doi.org/10.1091/mbc.e05-07-0650.
(95) Kuo, W.-T.; Zuo, L.; Odenwald, M. A.; Madha, S.; Singh, G.; Gurniak, C. B.; Abraham, C.; Turner, J. R. The Tight Junction Protein ZO-1 Is Dispensable for Barrier Function but Critical for Effective Mucosal Repair. *Gastroenterology* **2021**, *161* (6), 1924–1939. https://doi.org/10.1053/j.gastro.2021.08.047.
(96) Van Itallie, C. M.; Anderson, J. M. CLAUDINS AND EPITHELIAL PARACELLULAR TRANSPORT. *Annu. Rev. Physiol.* **2006**, *68* (1), 403–429. https://doi.org/10.1146/annurev.physiol.68.040104.131404.
(97) Capaldo, C. T.; Nusrat, A. Claudin Switching: Physiological Plasticity of the Tight Junction. *Semin. Cell Dev. Biol.* **2015**, *42*, 22–29. https://doi.org/10.1016/j.semcdb.2015.04.003.
(98) Luis Negri, A. Role of Claudins in Renal Calcium Handling. *Nefrol. Engl. Ed.* **2015**, *35* (4), 347–352. https://doi.org/10.1016/j.nefroe.2015.09.006.
(99) *Physiology of the Gastrointestinal Tract*; Elsevier, 2006. https://doi.org/10.1016/B978-0-12-088394-3.X5000-4.
(100) Erramilli, S. K.; Dominik, P. K.; Ogbu, C. P.; Kossiakoff, A. A.; Vecchio, A. J. Structural and Biophysical Insights into Targeting of Claudin-4 by a Synthetic Antibody Fragment. *Commun. Biol.* **2024**, *7* (1), 733. https://doi.org/10.1038/s42003-024-06437-6.
(101) Shashikanth, N.; France, M. M.; Xiao, R.; Haest, X.; Rizzo, H. E.; Yeste, J.; Reiner, J.; Turner, J. R. Tight Junction Channel Regulation by Interclaudin Interference. *Nat. Commun.* **2022**, *13* (1), 3780. https://doi.org/10.1038/s41467-022-31587-8.
(102) Günzel, D.; Yu, A. S. L. Claudins and the Modulation of Tight Junction Permeability. *Physiol. Rev.* **2013**, *93* (2), 525–569. https://doi.org/10.1152/physrev.00019.2012.
(103) Zihni, C.; Mills, C.; Matter, K.; Balda, M. S. Tight Junctions: From Simple Barriers to Multifunctional Molecular Gates. *Nat. Rev. Mol. Cell Biol.* **2016**, *17* (9), 564–580. https://doi.org/10.1038/nrm.2016.80.
(104) Otani, T.; Furuse, M. Tight Junction Structure and Function Revisited. *Trends Cell Biol.* **2020**, *30* (10), 805–817. https://doi.org/10.1016/j.tcb.2020.08.004.

(105) Luissint, A.-C.; Parkos, C. A.; Nusrat, A. Inflammation and the Intestinal Barrier: Leukocyte–Epithelial Cell Interactions, Cell Junction Remodeling, and Mucosal Repair. *Gastroenterology* **2016**, *151* (4), 616–632. https://doi.org/10.1053/j.gastro.2016.07.008.
(106) *Https://Www.Thermofisher.Com/at/En/Home/References/Gibco-Cell-Culture-Basics/Cell-Culture-Protocols/Counting-Cells-in-a-Hemacytometer.Html?ef_id=Cj0KCQjwlrvBBhDnARIsAHEQgOT3AneFK5NFomPveGOxprTPt54MY17ryrWVFiJqLrWO9BOHGCBP6lEaAky5EALw_wcB:G:s&s_kwcid=AL!3652!3!530416915609!!!G!!!382790548!125487008778&cid=bid_clb_cce_r01_co_cp0000_pjt0000_bid00000_0se_gaw_dy_pur_con&s_kwcid=AL!3652!3!530416915609!!!G!!&gad_source=1&gad_campaignid=382790548&gbraid=0AAAADxi_GQ3k_XxSQcAAQoKpmv0mSF8Y&gclid=Cj0KCQjwlrvBBhDnARIsAHEQgOT3AneFK5NFomPveGOxprTPt54MY17ryrWVFiJqLrWO9BOHGCBP6lEaAky5EALw_wcB Aufgerufen Am 22.05.25 Um 11:51*.
(107) *Gstraunthaler, G., Lindl, T. (2021). Bestimmung Allgemeiner Wachstumsparameter. In: Zell- Und Gewebekultur. Springer Spektrum, Berlin, Heidelberg. Https://Doi.Org/10.1007/978-3-662-62606-1_12*.
(108) *CellTiter-Blue ® Cell Viability Assay Instructions for Use of Products G8080, G8081 and G8082, n.d. Www.Promega.Com.*
(109) Behrens, I.; Pena, A. I. V.; Alonso, M. J.; Kissel, T. [No Title Found]. *Pharm. Res.* **2002**, *19* (8), 1185–1193. https://doi.org/10.1023/A:1019854327540.
(110) Yu, M.; Wang, J.; Yang, Y.; Zhu, C.; Su, Q.; Guo, S.; Sun, J.; Gan, Y.; Shi, X.; Gao, H. Rotation-Facilitated Rapid Transport of Nanorods in Mucosal Tissues. *Nano Lett.* **2016**, *16* (11), 7176–7182. https://doi.org/10.1021/acs.nanolett.6b03515.
(111) Hohagen, M.; Guggenberger, P.; Kiss, E.; Kählig, H.; Marko, D.; Del Favero, G.; Kleitz, F. TANNylation of Mesoporous Silica Nanoparticles and Bioactivity Profiling in Intestinal Cells. *J. Colloid Interface Sci.* **2022**, *623*, 962–973. https://doi.org/10.1016/j.jcis.2022.05.035.
(112) *Https://Moldraw.Com/ Opened 01.08.25 at 18:23 Oclock*.
(113) Beisl, J.; Varga, E.; Braun, D.; Warth, B.; Ehling-Schulz, M.; Del Favero, G.; Marko, D. Assessing Mixture Effects of Cereulide and Deoxynivalenol on Intestinal Barrier Integrity and Uptake in Differentiated Human Caco-2 Cells. *Toxins* **2021**, *13* (3), 189. https://doi.org/10.3390/toxins13030189.
(114) Srinivasan, B.; Kolli, A. R.; Esch, M. B.; Abaci, H. E.; Shuler, M. L.; Hickman, J. J. TEER Measurement Techniques for In Vitro Barrier Model Systems. *SLAS Technol.* **2015**, *20* (2), 107–126. https://doi.org/10.1177/2211068214561025.
(115) Del Favero, G.; Mayer, R. M.; Dellafiora, L.; Janker, L.; Niederstaetter, L.; Dall'Asta, C.; Gerner, C.; Marko, D. Structural Similarity with Cholesterol Reveals Crucial Insights into Mechanisms Sustaining the Immunomodulatory Activity of the Mycotoxin Alternariol. *Cells* **2020**, *9* (4), 847. https://doi.org/10.3390/cells9040847.
(116) Iriarte-Mesa, C.; Jobst, M.; Bergen, J.; Kiss, E.; Ryoo, R.; Kim, J.-C.; Crudo, F.; Marko, D.; Kleitz, F.; Del Favero, G. Morphology-Dependent Interaction of Silica Nanoparticles with Intestinal Cells: Connecting Shape to Barrier Function. *Nano Lett.* **2023**, *23* (16), 7758–7766. https://doi.org/10.1021/acs.nanolett.3c00835.
(117) *Analysis Conducted Using the PBPK Tool from the National Toxicology Program's Integrated Chemical Environment Version 4.0, Released March 2023 (Https://Ice.Ntp.Niehs.Nih.Gov/) on 6th August 2025*.
(118) He, H.; Zhou, J.; Xu, X.; Zhou, P.; Zhong, H.; Liu, M. Piezo Channels in the Intestinal Tract. *Front. Physiol.* **2024**, *15*, 1356317. https://doi.org/10.3389/fphys.2024.1356317.
(119) Swain, S. M.; Liddle, R. A. Mechanosensing Piezo Channels in Gastrointestinal Disorders. *J. Clin. Invest.* **2023**, *133* (19), e171955. https://doi.org/10.1172/JCI171955.
(120) Grace, J. R.; Ebneyamini, A. Connecting Particle Sphericity and Circularity. *Particuology* **2021**, *54*, 1–4. https://doi.org/10.1016/j.partic.2020.09.006.

(121) Zdilla, M. J.; Hatfield, S. A.; McLean, K. A.; Cyrus, L. M.; Laslo, J. M.; Lambert, H. W. Circularity, Solidity, Axes of a Best Fit Ellipse, Aspect Ratio, and Roundness of the Foramen Ovale: A Morphometric Analysis With Neurosurgical Considerations. *J. Craniofac. Surg.* **2016**, *27* (1), 222–228. https://doi.org/10.1097/SCS.0000000000002285.
(122) Vandenberg, L. N. Non-Monotonic Dose Responses in Studies of Endocrine Disrupting Chemicals: Bisphenol a as a Case Study. *Dose-Response Publ. Int. Hormesis Soc.* **2014**, *12* (2), 259–276. https://doi.org/10.2203/dose-response.13-020.Vandenberg.
(123) Delie, F.; Rubas, W. A Human Colonic Cell Line Sharing Similarities With Enterocytes as a Model to Examine Oral Absorption: Advantages and Limitations of the Caco-2 Model. *Crit. Rev. Ther. Drug Carrier Syst.* **1997**, *14* (3), 66. https://doi.org/10.1615/CritRevTherDrugCarrierSyst.v14.i3.20.
(124) *HIDALGO IJ, RAUB TJ, BORCHARDT RT: Characterization of the Human Colon Carcinoma Cell Line (Caco-2) as a Model System for Intestinal Epithelial Permeability. Gastroenterology (1989) 96:736-749.*
(125) Béduneau, A.; Tempesta, C.; Fimbel, S.; Pellequer, Y.; Jannin, V.; Demarne, F.; Lamprecht, A. A Tunable Caco-2/HT29-MTX Co-Culture Model Mimicking Variable Permeabilities of the Human Intestine Obtained by an Original Seeding Procedure. *Eur. J. Pharm. Biopharm.* **2014**, *87* (2), 290–298. https://doi.org/10.1016/j.ejpb.2014.03.017.
(126) Strugari, A. F. G.; Stan, M. S.; Gharbia, S.; Hermenean, A.; Dinischiotu, A. Characterization of Nanoparticle Intestinal Transport Using an In Vitro Co-Culture Model. *Nanomaterials* **2018**, *9* (1), 5. https://doi.org/10.3390/nano9010005.
(127) Hilgendorf, C.; Spahn-Langguth, H.; Regårdh, C. G.; Lipka, E.; Amidon, G. L.; Langguth, P. Caco-2 versus Caco-2/HT29-MTX Co-cultured Cell Lines: Permeabilities Via Diffusion, Inside- and Outside-Directed Carrier-Mediated Transport. *J. Pharm. Sci.* **2000**, *89* (1), 63–75. https://doi.org/10.1002/(SICI)1520-6017(200001)89:1<63::AID-JPS7>3.0.CO;2-6.
(128) Tian, C.; Lyu, T.; Zhao, X.; Wang, R.; Wu, Y.; Yang, D. Piezo1 Channel: A Global Bibliometric Analysis from 2010 to 2024. *Channels* **2024**, *18* (1), 2396354. https://doi.org/10.1080/19336950.2024.2396354.
(129) Jiang, Y.; Song, J.; Xu, Y.; Liu, C.; Qian, W.; Bai, T.; Hou, X. Piezo1 Regulates Intestinal Epithelial Function by Affecting the Tight Junction Protein Claudin-1 via the ROCK Pathway. *Life Sci.* **2021**, *275*, 119254. https://doi.org/10.1016/j.lfs.2021.119254.
(130) Guo, J.; Li, L.; Chen, F.; Fu, M.; Cheng, C.; Wang, M.; Hu, J.; Pei, L.; Sun, J. Forces Bless You: Mechanosensitive Piezo Channels in Gastrointestinal Physiology and Pathology. *Biomolecules* **2024**, *14* (7), 804. https://doi.org/10.3390/biom14070804.
(131) Donetti, E.; Bendinelli, P.; Correnti, M.; Gammella, E.; Recalcati, S.; Ferraretto, A. Caco2/HT-29 In Vitro Cell Co-Culture: Barrier Integrity, Permeability, and Tight Junctions' Composition During Progressive Passages of Parental Cells. *Biology* **2025**, *14* (3), 267. https://doi.org/10.3390/biology14030267.
(132) Jiang, Y.; Song, J.; Xu, Y.; Liu, C.; Qian, W.; Bai, T.; Hou, X. Piezo1 Regulates Intestinal Epithelial Function by Affecting the Tight Junction Protein Claudin-1 via the ROCK Pathway. *Life Sci.* **2021**, *275*, 119254. https://doi.org/10.1016/j.lfs.2021.119254.
(133) Iriarte-Mesa, C.; Jobst, M.; Bergen, J.; Kiss, E.; Ryoo, R.; Kim, J.-C.; Crudo, F.; Marko, D.; Kleitz, F.; Del Favero, G. Morphology-Dependent Interaction of Silica Nanoparticles with Intestinal Cells: Connecting Shape to Barrier Function. *Nano Lett.* **2023**, *23* (16), 7758–7766. https://doi.org/10.1021/acs.nanolett.3c00835.
(134) Cybulski, P.; Bravo, M.; Chen, J. J.-K.; Van Zundert, I.; Krzyzowska, S.; Taemaitree, F.; Uji-i, H.; Hofkens, J.; Rocha, S.; Fortuni, B. Nanoparticle Accumulation and Penetration in 3D Tumor Models: The Effect of Size, Shape, and Surface Charge. *Front. Cell Dev. Biol.* **2025**, *12*, 1520078. https://doi.org/10.3389/fcell.2024.1520078.

(135) Pratiwi, F. W.; Peng, C.-C.; Wu, S.-H.; Kuo, C. W.; Mou, C.-Y.; Tung, Y.-C.; Chen, P. Evaluation of Nanoparticle Penetration in the Tumor Spheroid Using Two-Photon Microscopy. *Biomedicines* **2020**, *9* (1), 10. https://doi.org/10.3390/biomedicines9010010.
(136) Agarwal, R.; Jurney, P.; Raythatha, M.; Singh, V.; Sreenivasan, Sidlgata. V.; Shi, L.; Roy, K. Effect of Shape, Size, and Aspect Ratio on Nanoparticle Penetration and Distribution inside Solid Tissues Using 3D Spheroid Models. *Adv. Healthc. Mater.* **2015**, *4* (15), 2269–2280. https://doi.org/10.1002/adhm.201500441.
(137) Song, K.; Dai, L.; Long, X.; Wang, W.; Di, W. Follicle-Stimulating Hormone Promotes the Proliferation of Epithelial Ovarian Cancer Cells by Activating Sphingosine Kinase. *Sci. Rep.* **2020**, *10* (1), 13834. https://doi.org/10.1038/s41598-020-70896-0.
(138) Song, K.; Dai, L.; Long, X.; Wang, W.; Di, W. Follicle-Stimulating Hormone Promotes the Proliferation of Epithelial Ovarian Cancer Cells by Activating Sphingosine Kinase. *Sci. Rep.* **2020**, *10* (1), 13834. https://doi.org/10.1038/s41598-020-70896-0.
(139) Caglayan, M.; Ozden, S. Potential Impacts of Bisphenols on Prostate Cells: An Overview of Cytotoxicity, Proliferation, Oxidative Stress, Apoptosis, and ER-Stress Response Activation. *Food Chem. Toxicol.* **2024**, *184*, 114416. https://doi.org/10.1016/j.fct.2023.114416.
(140) İPek, S.; İYiGündoğdu, İ.; Üstündağ, A.; Duydu, Y. Evaluation of the Cytotoxic Effect of Bisphenol A and Its Analogs in MCF-7 and HSeC Cell Lines in Vitro. *Fabad J. Pharm. Sci.* **2022**, 13–22. https://doi.org/10.55262/fabadeczacilik.1078759.
(141) Khalil, F.; Läer, S. Physiologically Based Pharmacokinetic Modeling: Methodology, Applications, and Limitations with a Focus on Its Role in Pediatric Drug Development. *BioMed Res. Int.* **2011**, *2011* (1), 907461. https://doi.org/10.1155/2011/907461.
(142) Hartmanshenn, C.; Scherholz, M.; Androulakis, I. P. Physiologically-Based Pharmacokinetic Models: Approaches for Enabling Personalized Medicine. *J. Pharmacokinet. Pharmacodyn.* **2016**, *43* (5), 481–504. https://doi.org/10.1007/s10928-016-9492-y.
(143) Caicedo, J. C.; Goodman, A.; Karhohs, K. W.; Cimini, B. A.; Ackerman, J.; Haghighi, M.; Heng, C.; Becker, T.; Doan, M.; McQuin, C.; Rohban, M.; Singh, S.; Carpenter, A. E. Nucleus Segmentation across Imaging Experiments: The 2018 Data Science Bowl. *Nat. Methods* **2019**, *16* (12), 1247–1253. https://doi.org/10.1038/s41592-019-0612-7.
(144) Yuan, J.; Kong, Y.; Ommati, M. M.; Tang, Z.; Li, H.; Li, L.; Zhao, C.; Shi, Z.; Wang, J. Bisphenol A-Induced Apoptosis, Oxidative Stress and DNA Damage in Cultured Rhesus Monkey Embryo Renal Epithelial Marc-145 Cells. *Chemosphere* **2019**, *234*, 682–689. https://doi.org/10.1016/j.chemosphere.2019.06.125.
(145) Akram, R.; Iqbal, R.; Hussain, R.; Jabeen, F.; Ali, M. Evaluation of Oxidative Stress, Antioxidant Enzymes and Genotoxic Potential of Bisphenol A in Fresh Water Bighead Carp (Aristichthys Nobils) Fish at Low Concentrations. *Environ. Pollut.* **2021**, *268*, 115896. https://doi.org/10.1016/j.envpol.2020.115896.
(146) Zhou, Y.; Yao, Y.; Shao, Y.; Qu, W.; Chen, Y.; Jiang, Q. Urinary Bisphenol Analogues Concentrations and Biomarkers of Oxidative DNA and RNA Damage in Chinese School Children in East China: A Repeated Measures Study. *Environ. Pollut.* **2019**, *254*, 112921. https://doi.org/10.1016/j.envpol.2019.07.089.
(147) Hercog, K.; Maisanaba, S.; Filipič, M.; Sollner-Dolenc, M.; Kač, L.; Žegura, B. Genotoxic Activity of Bisphenol A and Its Analogues Bisphenol S, Bisphenol F and Bisphenol AF and Their Mixtures in Human Hepatocellular Carcinoma (HepG2) Cells. *Sci. Total Environ.* **2019**, *687*, 267–276. https://doi.org/10.1016/j.scitotenv.2019.05.486.
(148) Yuan, J.; Kong, Y.; Ommati, M. M.; Tang, Z.; Li, H.; Li, L.; Zhao, C.; Shi, Z.; Wang, J. Bisphenol A-Induced Apoptosis, Oxidative Stress and DNA Damage in Cultured Rhesus Monkey Embryo Renal Epithelial Marc-145 Cells. *Chemosphere* **2019**, *234*, 682–689. https://doi.org/10.1016/j.chemosphere.2019.06.125.

(149) Kose, O.; Rachidi, W.; Beal, D.; Erkekoglu, P.; Fayyad-Kazan, H.; Kocer Gumusel, B. The Effects of Different Bisphenol Derivatives on Oxidative Stress, DNA Damage and DNA Repair in RWPE-1 Cells: A Comparative Study. *J. Appl. Toxicol.* **2020**, *40* (5), 643–654. https://doi.org/10.1002/jat.3934.
(150) Huang, M.; Liu, S.; Fu, L.; Jiang, X.; Yang, M. Bisphenol A and Its Analogues Bisphenol S, Bisphenol F and Bisphenol AF Induce Oxidative Stress and Biomacromolecular Damage in Human Granulosa KGN Cells. *Chemosphere* **2020**, *253*, 126707. https://doi.org/10.1016/j.chemosphere.2020.126707.
(151) Mlynarcikova, A. B.; Scsukova, S. Effect of Selected Bisphenol Derivatives on Nuclear Receptor Expression in Ovarian Cell Line COV434. *Endocr. Regul.* **2020**, *54* (4), 275–283. https://doi.org/10.2478/enr-2020-0031.
(152) Pfeiffer, E.; Eschbach, S.; Metzler, M. Alternaria Toxins: DNA Strand-Breaking Activity in Mammalian Cellsin Vitro. *Mycotoxin Res.* **2007**, *23* (3), 152–157. https://doi.org/10.1007/bf02951512.
(153) Fehr, M.; Pahlke, G.; Fritz, J.; Christensen, M. O.; Boege, F.; Altemöller, M.; Podlech, J.; Marko, D. Alternariol Acts as a Topoisomerase Poison, Preferentially Affecting the IIα Isoform. *Mol. Nutr. Food Res.* **2009**, *53* (4), 441–451. https://doi.org/10.1002/mnfr.200700379.
(154) Moonwiriyakit, A.; Pathomthongtaweechai, N.; Steinhagen, P. R.; Chantawichitwong, P.; Satianrapapong, W.; Pongkorpsakol, P. Tight Junctions: From Molecules to Gastrointestinal Diseases. *Tissue Barriers* **2023**, *11* (2), 2077620. https://doi.org/10.1080/21688370.2022.2077620.
(155) Vermette, D.; Hu, P.; Canarie, M. F.; Funaro, M.; Glover, J.; Pierce, R. W. Tight Junction Structure, Function, and Assessment in the Critically Ill: A Systematic Review. *Intensive Care Med. Exp.* **2018**, *6* (1), 37. https://doi.org/10.1186/s40635-018-0203-4.
(156) Malaisé, Y.; Lencina, C.; Cartier, C.; Olier, M.; Ménard, S.; Guzylack-Piriou, L. Perinatal Oral Exposure to Low Doses of Bisphenol A, S or F Impairs Immune Functions at Intestinal and Systemic Levels in Female Offspring Mice. *Environ. Health Glob. Access Sci. Source* **2020**, *19* (1), 93. https://doi.org/10.1186/s12940-020-00614-w.
(157) Malaisé, Y.; Lencina, C.; Cartier, C.; Olier, M.; Ménard, S.; Guzylack-Piriou, L. Perinatal Oral Exposure to Low Doses of Bisphenol A, S or F Impairs Immune Functions at Intestinal and Systemic Levels in Female Offspring Mice. *Environ. Health* **2020**, *19* (1), 93. https://doi.org/10.1186/s12940-020-00614-w.
(158) Camilleri, M.; Madsen, K.; Spiller, R.; Van Meerveld, B. G.; Verne, G. N. Intestinal Barrier Function in Health and Gastrointestinal Disease. *Neurogastroenterol. Motil.* **2012**, *24* (6), 503–512. https://doi.org/10.1111/j.1365-2982.2012.01921.x.